Quantum groundstates of the spin-$\frac{1}{2}$ XXZ model on a fully-frustrated honeycomb lattice

by

Stephen Inglis

A thesis
presented to the University of Waterloo
in fulfillment of the
thesis requirement for the degree of
Master of Science
in
Physics

Waterloo, Ontario, Canada, 2010

I hereby declare that I am the sole author of this thesis. This is a true copy of the thesis, including any required final revisions, as accepted by my examiners.

I understand that my thesis may be made electronically available to the public.

Abstract

In this thesis we present results from quantum Monte Carlo for the fully-frustrated honeycomb lattice. The XXZ model is of interest in the classical limit, as there is a mapping between the classical fully-frustrated honeycomb Ising model groundstates and the classical hard-core dimer model groundstate. The aim of this work is to explore the effect of quantum fluctuations on the fully-frustrated honeycomb model to see what sort of interesting physics arises. One might expect unusual physics due to the quantum hard-core dimer model, where interesting physics are known to exist. This is because there is a duality mapping between the classical dimer model and the classical fully-frustrated honeycomb Ising model. Indeed, by studying the fully-frustrated honeycomb XXZ model we find that in some cases the system orders into crystal-like structures, a case of order-by-disorder. The most interesting case, when the frustrating bonds are chosen randomly, reveals to us a novel state without any discernible order while at the same time avoiding the freezing one would expect of a glass. This state is a featureless system lacking low temperature magnetic susceptibility—a candidate "quantum spin liquid". Future work that might more easily measure quantum spin liquid criteria is suggested.

Acknowledgements

I would like to thank the Quantum Matters group at the University of Waterloo. The professors always had time and organized opportunities for me to meet many important and relevant people in the field. I must especially thank my supervisor Roger Melko. Through no small effort he has found me opportunities in physics that I did not even know existed.

Dedication

This is dedicated to my love, my wife Tiffany. Her dedication and genuine curiosity in her own work has always inspired and driven me to do better in my own.

Contents

List of Figures

Chapter 1

Introduction

1.1 Overview

A quantum spin liquid describes a zero temperature paramagnet-like state in which the quantum correlations give rise to strange physics. In some of the known theoretical examples, the state manifests as a featureless ground state which is an overlap of all possible singlet coverings on the lattice [1]. These strange states have no classical analogue and we are only beginning to find compounds which may possess the necessary structure to realize and analyze these strange systems in real materials [1].

Quantum spin liquids are interesting because they permit strange excitations that may fractionalize quantum numbers. One property all quantum spin liquids must have is deconfined spinon excitations [1]. This means that the spin quantum number becomes dissociated with the charge quantum number of the electron. Such splitting of the electron's quantum numbers is thought to be another mechanism by which we can create superconductivity [2]. Experimental search for quantum spin liquids in materials is ongoing, with new candidates appearing in many classes of materials, such as organic compounds [3].

In this thesis we explore the effect of quantum perturbations on the fully-frustrated honeycomb model. These perturbations are explored by examining the XXZ model in the limit where the quantum perturbations are small, the quantum term is 1/3 of the classical term. We use the XXZ model to study an interesting case of the effect of quantum perturbations of a classical manifold, similar to previous work along these lines carried out by Moessner and Sondhi [4]. In their study they used a transverse field to generate a quantum perturbation—our case uses in-plane coupling between nearest neighbors, and produces different results.

The quantum XXZ model on the honeycomb lattice is interesting to study because of the close relation to spin liquids this system may have. The reason we expect there may be

a relation to quantum spin liquids is two-fold. First, there is a duality mapping between the classical groundstates of the fully-frustrated honeycomb lattice Ising model and classical dimers on the triangular lattice. This alone is not interesting, but the quantum dimer model on the triangular lattice is known to have an extended Resonating Valence Bond phase, also called a quantum spin liquid [5]. Adding quantum fluctuations to the fully-frustrated honeycomb model may then let us approach the quantum dimer model through this duality mapping. As a second point, frustrated systems under quantum perturbation are themselves good candidates for quantum spin liquids [1], and so such systems are promising candidates for finding quantum spin liquids.

The thesis is organized as follows. We start with a brief introduction to magnetic systems including the Ising model and classical and quantum Heisenberg models. The Monte Carlo formalism for classical simulation is presented, followed by the concepts behind Stochastic Series Expansion quantum Monte Carlo (SSE QMC). This is followed by sections on observables in SSE QMC and specific details about what we measure during simulation. Visualization techniques for data analysis are presented along with a short proof relating hopping in the quantum model to the existence of singlets. Frustrated magnetic systems and their defining characteristics are discussed.

In Chapter 2 we treat the classical Ising spin model in mean-field theory and then examine the quantum model in spin-wave theory, showing the magnetization reduction and spin stiffness in the XY model. We follow by detailing the important results of the classical fully-frustrated honeycomb Ising model. It describes the way in which we satisfy the fully-frustrated requirement and follows with results from the interaction matrix approximation. Results from classical Monte Carlo show the extensive entropy in the groundstate. Analytical results that allowed exact calculations of the extensive entropy using combinatorics are also presented.

Chapter 3 describes the quantum Hamiltonian and the specific observables that are measured in the simulations. We then go on to show that results from SSE QMC agree with an exact diagonalization method, and present results from the three gauges we studied, the Discrete Translationally Symmetric (DTS) gauge, the Discrete Rotationally Symmetric (DRS) gauge and the random gauge. We show that the first two groundstate phases are locally fluctuating solid phases, while the third appears to be a featureless liquid phase. The perturbation theory explaining these gauges is also covered in this chapter.

In the Conclusions, we re-emphasize the nature of the groundstates of these quantum systems and examine how well they fit into the paradigm of quantum spin liquids. The first two phases do not fit the description of quantum spin liquids, and rather appear to be cases of order-by-disorder where the quantum fluctuations have ordered the classically degenerate manifold. In the case of the random gauge, when most bonds are antiferromagnetic, the system is featureless in the spin sector, but analysis of spinon excitations are needed to verify the system as a quantum spin liquid. For this reason the system remains a candidate

quantum spin liquid.

The candidate's contributions specific to this thesis include all material following the introduction except where old material is referenced. The classical work on the fully-frustrated honeycomb lattice Ising model was performed by Shawn Andrews, Hans De Sterck, Roger Melko and the candidate, with measurement and analysis of the extensive entropy carried out by the candidate. Specific contributions include all the modifications of the SSE QMC code necessary to simulate the DRS and random gauges. The analytical interaction matrix approach as well as the spin-wave theory were performed to assist in fundamental understanding of the groundstate phase. The visualization material, although brief, represents a large body of work that was necessary to produce the detailed images of the lattice presented in later sections.

1.2 Magnetic systems

In the field of condensed matter physics, one way in which the study of magnetic systems arises is examining the Hubbard model. The Hubbard model is a very general model that describes electrons on a lattice that interact by "hopping" around the lattice and costing an energy U when two electrons share the same site. The fermionic nature of the electrons combined with their spin lead to a nearest neighbor spin-spin interaction of the electrons as the low energy physics effective model, specifically in the large U limit. There are also more direct examples of magnetic systems, such as lattices that have large magnetic ions that interact with their neighbors. When each of these models is broken down, our fundamental unit is that of a magnetic moment, usually fixed in size, that interacts with its neighbors through some effective interaction, mediated by hopping, the dipole field, or any number of other terms. The moment may be pinned to an axis, a plane, or allowed to freely rotate. The spin may be effectively classical, or may be small enough that we must consider them fully quantum mechanically. In any case, the field of magnetism is rich in models, methods and materials, and it is within this broad umbrella that we have decided to examine the fully-frustrated honeycomb lattice. The XXZ model is an effective Hamiltonian for the Hubbard model in the large U limit, and the frustration of the system is thought to be a crucial ingredient in the search for spin liquids [1]. On a fully-frustrated honeycomb lattice the known mapping of the groundstate to that of the triangular lattice dimer model, the quantum triangular lattice dimer model groundstate being one of the prototypical 2d quantum spin liquids [1], makes it more interesting as a candidate for unusual physics.

To discuss much of the work on the honeycomb model, it helps to know some standard results from well known magnetic systems. The most simple model of a magnetic system, both in concept and computation, is the Ising model. As a note, in addition to magnetic

systems, the Ising model is general enough that it can be mapped to a host of other problems and in the most general case is NP-Complete [6]. The Ising model is simple, relates to real systems and in the worst case is not solvable in polynomial time, and this alone is enough reason to want to understand its complexities and the state of the art methods that are pushing our understanding of this class of problems.

To build some intuition, we will start by discussing the classical Ising ferromagnet in various spatial dimensions. The Hamiltonian for the Ising model takes the form

$$H = \sum_{\langle i,j \rangle} \sigma_i \sigma_j, \tag{1.1}$$

where $\langle i, j \rangle$ denotes nearest neighbors, and σ_i denotes the spin at site i, taking values of plus or minus 1. In one spatial dimension, where $\langle i, j \rangle \to \{i, i+1\}$, Ising showed [7] that there is no ordering all the way down to absolute zero. In two dimensions and above there is a critical temperature after which the systems undergoes a process known as spontaneous symmetry breaking and the spins align parallel or anti-parallel to their neighbors. That the Hamiltonian for such a system does not break Z_2 symmetry while the groundstate does is the very reason why such systems tend to be interesting, and the ways in which symmetry is broken can become very different in more complex systems.

1.3 Heisenberg model

There are two versions of the Heisenberg models one can consider, the classical and quantum version. In the classical version the Heisenberg model is simply a set of classical three-dimensional vectors that have an interaction energy proportional to their dot product,

$$H = \sum_{\langle i,j \rangle} J_{ij} \mathbf{S}_i \cdot \mathbf{S}_j. \tag{1.2}$$

The quantum version of the Hamiltonian replaces the classical spins with quantum mechanical spins. Quantum mechanical spins have the peculiar property that measuring the spin in one axis forces the spin to an eigenstate of the operator along that axis. Eigenstates of different axis do not commute—measuring the spin in one axis will affect the measurement we get when we measure the spin in a different axis. For this reason, we write out the dot product explicitly and then transform it to a more convenient form where the non-commuting properties of the operators is most clear. In this spin-$\frac{1}{2}$ case the Hamiltonian

is re-written as

$$\begin{aligned} H &= \sum_{\langle i,j \rangle} J_{ij} \left(S_i^z S_j^z + S_i^x S_j^x + S_i^y S_j^y \right) \\ &= \sum_{\langle i,j \rangle} J_{ij} \left(S_i^z S_j^z + \frac{1}{2}(S_i^+ S_j^- + S_i^- S_j^+) \right). \end{aligned} \tag{1.3}$$

Much like the Ising model, the classical Heisenberg ferromagnet and antiferromagnet do not order in one dimension [8], but do permit a finite temperature transition to a long range ordered state in three dimensions or higher. The Heisenberg model differs from the Ising model in that for two dimensions, it remains disordered in the thermodynamic limit all the way down to $T = 0$.

In the classical version the energy can be minimized by having every pair of spins parallel (or antiparallel, assuming the system is not frustrated), but things are slightly more complicated in the quantum case. For the quantum ferromagnet, the state of all spins aligned is still an eigenstate of the Hamiltonian, and so the classical picture is at least plausible as a groundstate for the quantum ferromagnet. We can see this by examining the only part of the Hamiltonian that takes us to a different state, the term $(S_i^+ S_j^- + S_i^- S_j^+)$. On the fully polarized state, each of these terms would annihilate the state, as both include the product of one lowering or raising operator, and one of these would annihilate either the fully down or fully up polarized state, respectively. This means the only remaining term would be the diagonal one, which does not change the state, and in this way the state is diagonal with respect to the Hamiltonian. The quantum antiferromagnet however is much different, as the classical groundstate where neighboring spins are antiparallel is no longer even an eigenstate of this new Hamiltonian. Consider the act of $(S_i^+ S_j^- + S_i^- S_j^+)$ as one that flips neighboring spins and then gives back that modified state. If we imagine the classical antiferromagnet, all neighboring spins are antiparallel, and any action of this operator would give contributions to different states than the ones we started with. That the action of the Hamiltonian produces a different state than we started with is the very definition of the state not being diagonal with respect to the Hamiltonian. In the following we will present various analytical methods that give us some insight on the basic concepts of phase transitions from a disordered to ordered state, and how the quantum system is different than the classical system.

1.4 Monte Carlo simulations

Monte Carlo methods today describe a wide range of techniques that at their core use a pseudo-random process, usually random number generation, to gain information about

some problem that is too difficult or impossible to solve exactly. A crude numerical integration algorithm can be made in this fashion by taking a finite region that a function is bounded within, and generating random points in the bounded region. By counting the number of points under the function to the total number of points generated in the region, one has the ratio of the functions volume to the bounded region's volume, or an estimate of the function's integral on the domain chosen. The approximation is quite crude, and it is obvious from the construction that depending how the bounding domain is chosen, it may take a large number of points to get a good approximation for the integral.

If we want to learn about some large thermodynamic system, we can imagine examining that system in the canonical ensemble, for a lattice system this would correspond to a fixed number of sites of the lattice. In that language, and quantity we want to figure out can be measured as

$$\langle A \rangle = \frac{\sum_i A_i e^{-\beta E_i}}{\sum_i e^{-\beta E_i}}, \tag{1.4}$$

where the sum over i includes all possible microstates in the system. If you imagine a spin system with N spins, then naively the number of states scales as 2^N and becomes impossible to calculate for a large system. This is where Monte Carlo can be useful through something called importance sampling. Importance sampling is the idea that there are a subset of states within the distribution that contribute more to the expectation value than others, due to them having a larger "weight" (where the $e^{-\beta E_i}$ factor is the weight). If we sample all the configurations with a frequency proportional to their weight, then the expectation of some operator is simply the average value observed over the sampling. This can be easily seen by rewriting the above as

$$\begin{aligned} \langle A \rangle =& \frac{\sum_i A_i W_i N_{tot}}{\sum_i W_i N_{tot}} = \frac{\sum_i A_i W_i N_{tot}}{N_{tot}}, \\ W_i =& \frac{e^{-\beta E_i}}{\sum_j e^{-\beta E_j}}, \end{aligned} \tag{1.5}$$

where W_i is the normalized weight of a state, such that the sum of all weights adds to one. From the above it should also be obvious that there is a discretization error as N_{tot} and $W_i N_{tot}$ must both be integers. A necessary condition for this being accurate is that we actually sample configurations proportional to their weight (a condition satisfied by having *balance*) and that our algorithm is capable of sampling every configuration of relevance (a condition known as *ergodicity*).

A class of Monte Carlo that efficiently achieves balance and ergodicity is the Metropolis condition Markov chain Monte Carlo [9]. This type of Monte Carlo works by starting from an arbitrary state with some known energy, and then moving to a *nearby* state. In this

case nearby usually refers to the fact that we generate the new state by some small change to the original state, and this new state is expected to have a similar weight. We then accept or reject moving to that state with some probability, takes measurements (even if the move is rejected) and continue the process. The probability that we accept a move is given by

$$\frac{P(A \to B)}{P(B \to A)} = \frac{W(B)}{W(A)}. \tag{1.6}$$

For the canonical distribution the weights can be determined from the energy, and the above reduces to

$$\frac{P(A \to B)}{P(B \to A)} = e^{\beta(E_A - E_B)}. \tag{1.7}$$

There are two parts in the transition from a state A to a state B. The first is our update scheme has a certain probability of choosing to *try* to go from state A to state B. The second is that we have some probability of accepting this move after that. For simplicity, often a condition know as *detailed balance* is used instead of the balance condition, but the former satisfies the latter. The condition for detailed balance can then be written as

$$\frac{P_{choose}(B, A)P_{accept}(B, A)}{P_{choose}(A, B)P_{accept}(A, B)} = e^{\beta(E_A - E_B)}. \tag{1.8}$$

In the simplest methods, from every state we randomly select one of the nearby states with some flat probability distribution. An example of this is taking some initial spin configuration, and randomly choosing one of the spins to flip. In this example, the probability of choosing state B from state A and vice-versa are both $1/N_{spin}$. Due to this symmetry the first part of Equation (1.8) can be removed from the top and bottom of the fraction, and we are only left with acceptance probabilities.

One choice of acceptance probabilities that satisfies the above is

$$P_{accept}(B, A) = \min[K, Ke^{\beta(E_A - E_B)}], \qquad K \in (0, 1]. \tag{1.9}$$

Often to ensure that the system changes as much as possible, often resulting in faster convergence, K is chosen to be 1. With the above information one already knows enough to construct a Monte Carlo simulation of the classical Ising model any number of dimensions that is capable of measuring quantities like the Néel ordering temperature or the correlation function at any finite temperature. The main difficulty that arises from this point forward is that at even though the simulation is fully ergodic, because the Markov chain only ever moves a small distance in configuration space, if there are two or more regions in phase space that both give large contributions to the partition function but are separated by a

large energy barrier in configuration space, the simulation may not be able to sample both of these regions efficiently. This breakdown in the Monte Carlo sampling is referred to as a critical slowdown (or loss of ergodicity), and it is usually most problematic around a phase transition or when trying to sample different symmetry-broken states.

Near a phase transition there are often a host of states that the simulation should be sampling in order to properly describe the system. This means that if the Monte Carlo algorithm gets stuck, it will often only sample a small region in configuration space, as opposed to sampling all the relevant configurations. One of the most direct resolutions to this problem is to design update schemes that are more complex than simply flipping a single site, such as the Wolff algorithm, that builds large clusters of spins and flips all of them at the same time [10, 11]. Methods of this sort restore ergodicity by ensuring that the sampling taken truly represent the set of weights for the partition function at a given temperature. Specific problems may even require specialized algorithms, such as the loop move for the fully-frustrated honeycomb lattice [12].

1.5 Quantum Monte Carlo

In the preceding Monte Carlo discussed, the systems of study were always treated as classical. The primary difference between quantum and classical systems is the nature of the Hamiltonian. In a classical system, all elements of the Hamiltonian commute with one another, meaning that there is a simple basis where the Hamiltonian is exactly diagonal and eigenstates of the system have exact product-state like representation in that basis. A good example is the classical Heisenberg system, where the x-,y- and z-component of the spin can all be simultaneously known, and specifying each component fully describes each spin.

In quantum systems the operators of the Hamiltonian do not necessarily commute with one another, making it much harder to make clear and simple statements about the groundstate like the classical case. For instance, for the spin $\frac{1}{2}$ Heisenberg antiferromagnet the magnetization in the z-axis is a good quantum number for the system, but as the Hamiltonian in Equation (1.3) clearly shows, there are elements that are off diagonal with respect to this basis. This means, in general, that a state defined by the z-axis magnetization on each site will not be an eigenstate of the Hamiltonian. Since the states form a complete basis, we are guaranteed that some (possibly complex) linear combination of the z-axis magnetization states will be able to represent any eigenstate of the system.

The class of quantum Monte Carlo algorithms is quite broad. In a continuous real-space problem, one may try to minimize the energy over a set of variational wave functions [13]. If the wave functions are good, the result is expected to be a good approximation to the groundstate wave function and from this perspective many of the properties of the system

can be extracted from the variational wave function. The class of methods we use use direct samplings of the partition function itself, in a similar way to classical Monte Carlo. Specifically, we use a method known as Stochastic Series Expansion Quantum Monte Carlo (SSE QMC) which is an exact, unbiased method for quantum systems as long as the basic updates remain ergodic [14, 15, 16].

As before, we have a partition function for our system. Writing it out explicitly, it takes the form

$$Z = \mathrm{Tr}[e^{-\beta H}] = \sum_{\alpha_0} \langle \alpha_0 | \, e^{-\beta H} \, | \alpha_0 \rangle \,, \tag{1.10}$$

which is so far exact. We then expand the exponential as its Taylor series and insert the identity operator between each power of H, in a formulation known as the Stochastic Series Expansion, to get

$$\begin{aligned} \sum_{\alpha_0} \langle \alpha_0 | \, e^{-\beta H} \, | \alpha_0 \rangle &= \sum_{\alpha_0} \langle \alpha_0 | \sum_{n=0}^{\infty} \frac{-\beta}{n!} H^n \, | \alpha_0 \rangle \,, \\ &= \sum_{\{\alpha_i\}} \sum_{n=0}^{\infty} \frac{(-1)^n (\beta)^n}{n!} \prod_{i=0}^{n} \langle \alpha_i | \, H \, | \alpha_{i+1} \rangle \,, \end{aligned} \tag{1.11}$$

where we must demand that $|\alpha_0\rangle = |\alpha_{n+1}\rangle$ to be consistent with the expansion representing the trace. The difference between classical and quantum Monte Carlo is where in the first we could sample the different basis states of the system to learn about the partition function, here we must sample different sets of expansions of the system $\{\alpha_i\}$. Building the Monte Carlo for this system amounts to finding a way to do importance sampling on the sets $\{\alpha_i\}$.

Before we move on, it is important to note the $(-1)^n$ factor in the partition function, suggesting that it may be possible to get negative weights in our sampling, a difficulty known as the sign problem. As shown in the classical Monte Carlo section, the condition of detailed balance only makes sense if all the weights are positive. The best way to remedy this problem is to ensure that the expansion of the Hamiltonian in Equation (1.11) precisely cancels the $(-1)^n$ factor. If all the terms in the Hamiltonian can be modified to have a negative sign in front of them, then this will solve the problem directly. For diagonal elements of the Hamiltonian, we can simply add a constant to all of them to ensure that they are negative. If we have positive off diagonal terms then we can only simulate a bipartite lattice. The reason for this is that to transform the basis to its original state will always require an even number of off diagonal operators, and hence we are guaranteed that the expectation of any expansion $\{\alpha_i\}$ is positive. In practice this tends to mean that frustrated systems, such as the Heisenberg antiferromagnet on a triangular lattice, cannot be simulated efficiently in this framework.

The next step in the procedure is to break up the Hamiltonian into it is most elementary interactions

$$H = -\sum_t \sum_a H_{t,a}, \tag{1.12}$$

where t and a specify the nature of the operator (diagonal, off-diagonal, etc..) and the location on the lattice that the operator occurs at, for instance a bond index for a two site operator. With this change, we now write the SSE as

$$Z = \sum_\alpha \sum_{n=0}^{\infty} \sum_{S_n} \frac{\beta^n}{n!} \langle\alpha| \prod_{i=0}^{n} H_{t_i,a_i} |\alpha\rangle , \tag{1.13}$$

where S_n now denotes a set of $\{t_i, a_i\}$ signifying a particular element by element product of H^n that we must sample now in addition to the basis states $|\alpha\rangle$ to do the Monte Carlo simulation.

Finally, we may truncate this sampling at some finite value of $n = M$. If we look at the contributions to the partition function as a function of n, we find that it is typically peaked at some finite value of n with an exponentially decaying tail [16]. Using equilibration we can determine how large an M is needed to ensure that we are sampling all of the relevant region. One can achieve this by having the original list and adding "filler" operators, conventionally labeled $H_{0,0} = I$ which do not change the basis or contribute to the value of a particular expansion of operators. What these filler operators do change is the number of permutations of an instance of the list S_n, which must be accounted for by dividing the weight of each element of the partition function by the number of ways we can insert blank elements into the list, which is $M!/(M-n)!n!$. With this, the final expression for our partition function can be written as

$$Z = \sum_\alpha \sum_{S_M} \frac{\beta^n (M-n)!}{M!} \langle\alpha| \prod_{i=0}^{M} H_{t_i,a_i} |\alpha\rangle . \tag{1.14}$$

As we originally wrote, this method involves the trace over all basis states, meaning that the first and last state must be the same, or $|\alpha_0\rangle = |\alpha_M\rangle$. This puts a high constraint on the off diagonal operators in the list S_M, since if they are chosen incorrectly one could imagine generating expansions with zero contribution to the trace—a waste of computational effort. With this in mind, the fundamental moves in the SSE are designed such that they are both ergodic but only sample states with non-zero contribution to the trace. To do this requires two types of updates in simulation: the diagonal update and the off-diagonal update.

In the diagonal update, we fluctuate the number n by swapping "filler" identity operators, $H_{0,0}$, with diagonal operators. Since diagonal operators do not change the configuration of any of the states $|\alpha\rangle$, we can add them anywhere without ruining the boundary

conditions of the system. To perform the update, we move through the list of operators and wherever we find an identity operator, we randomly choose a diagonal element of the Hamiltonian and calculate the ratio of the weight of the old weight to the new weight to determine whether to accept the move. Since all the matrix elements are multiplied to calculate the weight of a state, when we add a single operator we only need to look at the weight of that state compared to the weight before, plus any prefactors that have changed. Writing it in a general form using the notation that $H_{1,i}$ refers to the diagonal operator and assuming n is the number of operators in the list S_M excluding the the one we are looking at, then

$$\frac{W(H_{1,i})}{W(H_{0,0})} = \frac{\langle \alpha_j | \, H_{1,i} \, | \alpha_j + 1 \rangle \, \beta}{(M-n)}. \tag{1.15}$$

Since $H_{1,i}$ will in general only act on a small number of spins of the system, all the possible matrix elements of $\langle \alpha_i | \, H_{1,i} \, | \alpha_j \rangle$ can be calculated before running the simulation. In this way, the Monte Carlo update remains a local procedure, requiring a fixed amount of information independent of the lattice size for the diagonal update scheme.

The off-diagonal update is slightly more complicated, as we have to ensure that we design it in such a way that the boundary conditions are always satisfied. The first step in this process is constructing a linked list of vertices involved in operators in the list S_M as shown in Figure 1.1.

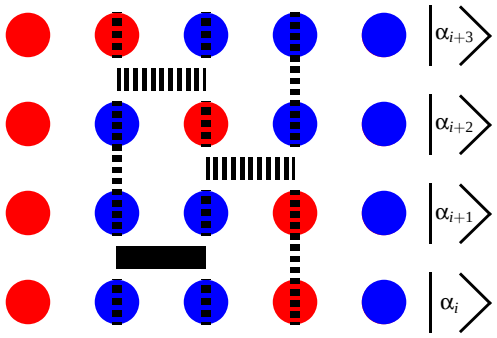

Figure 1.1: Cartoon of the operator list S_M and extracted vertex list. Operators (bars) connect spins at different layers, $|\alpha_i\rangle$. If we look up in the list and connect spins only where they are involved in operators, then we can create the linked list needed for the off-diagonal update. Blue dots represent up spins, while red dots represent down spins, and the dashed bars represent operators that have off-diagonal overlap.

First, we will define a vertex as any of the spins connected to an operator. In our case, every operator has 4 associated vertices, two for the spin that it acts on in $|\alpha_i\rangle$ and two

for the spins it "produces" in $|\alpha_{i+1}\rangle$. Diagonal operators do not change the orientation of these spins, but they are still the four spins of relevance to each operator. Vertices are also connected to other vertices. Vertices "above" an operator in the operator list connect to the next vertex "below" an operator that acts on the same spin, and vice versa. Starting on a random vertex of an operator in the list, we enter an operator through a spin and choose a spin to exit through. After exiting the operator, the loop continues to the vertex connected to the one it just left. The loop repeats this procedure, flipping all the spins it passes through until it reaches the starting location. Once the loop reaches its starting location, it finishes and all the spins it has flipped and operators it has changed result in a new state. Although we could construct a random loop and use the metropolis condition to compare the initial and final state, this would likely result in states with vastly different weights, and hence be inefficient. Instead a slightly different condition known as time-reversal symmetry is used

$$W(s)T(s, e \to s', x) = W(s')T(s', x \to s, e), \tag{1.16}$$

where s is the local configuration around a particular operator, $\langle\alpha_k|$ and $|\alpha_{k+1}\rangle$, and $W(s)$ is the weight of those states around an operator. The state s is the initial state when the loop enters from vertex e, and s' the state when the loop exits by vertex x. Keep in mind that in our construction of the operators $H_{t,a}$, for a particular choice of s there is only one operator (that is not the identity) that will have a non-zero expectation value, so by changing the local configuration we explicitly change the contribution to the weight from that state. This transition looks very similar to the condition for detailed balance in Equation (1.8), and indeed if we use the time reversal symmetry condition we can recover detailed balance, the proof for such presented in [14].

The other condition that is required is

$$\sum_x T(s, e \to s', x) = 1, \tag{1.17}$$

or any loop that enters a vertex must exit the vertex with probability one. Using time-reversal symmetry, the above condition and the weights of the matrix elements (given by the Hamiltonian) result in an under-constrained set of equations for all the possible transition probabilities. Often one adds additional constraints, such as insisting that the loop bounce infrequently, to make the set of transition probabilities deterministic. Once the transition probabilities are determined we have all physics necessary to construct a SSE QMC simulation of a system.

Observables in SSE QMC are measured just as you would expect from the framework. For a generic quantum Hamiltonian, the expectation of some operator A takes the form

$$\langle A\rangle = \mathrm{Tr}[Ae^{-\beta H}]. \tag{1.18}$$

If we insert this in to Equation (1.14) then we get something of the form

$$\langle A \rangle = \sum_{\alpha} \sum_{S_M} \frac{\beta^n (M-n)!}{M!} \langle \alpha | A \prod_{i=0}^{M} H_{t_i,a_i} | \alpha \rangle . \tag{1.19}$$

Since A may not be diagonal in the set of $|\alpha\rangle$ we have chosen, or even commute with the Hamiltonian, measuring it may represent another challenge. If it is diagonal with respect to our basis, we can measure it directly in each Monte Carlo step as

$$\langle A \rangle = \frac{1}{M} \sum_{i=0}^{M} \langle \alpha_i | A | \alpha_i \rangle , \tag{1.20}$$

where the α_i are the different basis elements generated by the application of operators in the list S_M. If we imagine off-diagonal operators that can be represented by an element of our Hamiltonian H_{t_k,a_k}, then we can easily measure it by plugging the element into Equation (1.14) which then becomes

$$\langle H_{t_k,a_k} \rangle = \sum_{\alpha} \sum_{S_M} \frac{\beta^n (M-n)!}{M!} \langle \alpha | H_{t_k,a_k} \prod_{i=0}^{M} H_{t_i,a_i} | \alpha \rangle . \tag{1.21}$$

But we can easily relate the list of length M times an element of the Hamiltonian to a list of length $M+1$ that begins with H_{t_k,a_k} by rewriting it as the weight of some configuration $W(H_{t_k,a_k}, \alpha, S_M)$

$$\begin{aligned} W(H_{t_k,a_k}, \alpha, S_M) &= \frac{\beta^{n+1}((M+1)-(n+1))!}{(M+1)!} \langle \alpha | H_{t_k,a_k} \prod_{i=0}^{M} H_{t_i,a_i} | \alpha \rangle , \\ &= \frac{\beta}{M+1} \frac{\beta^n (M-n)!}{M!} \langle \alpha | H_{t_k,a_k} \prod_{i=0}^{M} H_{t_i,a_i} | \alpha \rangle , \\ \langle H_{t_k,a_k} \rangle &= \begin{cases} \frac{M+1}{\beta} & \text{if } S_{M+1} \text{ begins in } H_{t_k,a_k} \\ 0 & \text{otherwise} \end{cases} . \end{aligned} \tag{1.22}$$

We can easily replace $M+1$ with M (since it is arbitrary in this case) and average over all permutations of S_M to finally get

$$\begin{aligned} \langle H_{t_k,a_k} \rangle &= \frac{M}{\beta} \frac{1}{M} \langle N[t_k, a_k] \rangle , \\ &= \frac{\langle N[t_k, a_k] \rangle}{\beta}, \end{aligned} \tag{1.23}$$

where $\langle N[t_k, a_k]\rangle$ is the number of operators of type H_{t_k,a_k} in the list S_M. In this way we find that if we measure the average number of occurrences of a particular operator over the Monte Carlo simulation, we find the expectation value of that particular operator times β.

If we have an operator that is represented as a product of m elements of the Hamiltonian, then using the same method as above we can calculate the expectation of the product of those two operators. We use the same argument as before, except now we consider a list of length S_{M-m} with the exact product of relevant operators tacked on the end. The equation we get in this case is

$$\begin{aligned} W\left(\prod_{k=1}^{m} H_{t_k,a_k}, \alpha, S_M\right) &= \frac{\beta^{n+m}((M+m)-(n+m))!}{(M+m)!} \langle\alpha| \prod_{k=1}^{m} H_{t_k,a_k} \prod_{i=0}^{M} H_{t_i,a_i} |\alpha\rangle , \\ &= \frac{\beta^m M!}{(M+m)!} \frac{\beta^n (M-n)!}{M!} \langle\alpha| \prod_{k=1}^{m} H_{t_k,a_k} \prod_{i=0}^{M} H_{t_i,a_i} |\alpha\rangle , \qquad (1.24) \\ \left\langle \prod_{k=1}^{m} H_{t_k,a_k} \right\rangle &= \begin{cases} \frac{(M+m)!}{\beta^m M!} & \text{if } S_{M+m} \text{begins in } \prod_{k=1}^{m} H_{t_k,a_k} \\ 0 & \text{otherwise} \end{cases} . \end{aligned}$$

Again, $M+m$ is simply the length of the appended list. Averaging over all the permutations of the list we get something similar to the form before

$$\left\langle \prod_{k=1}^{m} H_{t_k,a_k} \right\rangle = \frac{1}{\beta^m} \left\langle \frac{(M-1)!}{(M-m)!} N[t_{k1}, a_{k1}, ..., t_{km}, a_{km}] \right\rangle , \qquad (1.25)$$

where $N[t_{k1}, a_{k1}, ..., t_{km}, a_{km}]$ represents the number of times the subsequence of operators representing the one of interest occur in the list. In general due to the infrequency of specific orders of operators occurring in the list, statistics of products of operators take much longer to converge than that of single operators. We can speed up the process by ignoring the identity operators in the list, since inserting the identity in the list of $\prod_{k=1}^{m} H_{t_k,a_k}$ does not change it. We then get the form

$$\left\langle \prod_{k=1}^{m} H_{t_k,a_k} \right\rangle = \frac{1}{\beta^m} \left\langle \frac{(n-1)!}{(n-m)!} N[t_{k1}, a_{k1}, ..., t_{km}, a_{km}] \right\rangle . \qquad (1.26)$$

This time $N[t_{k1}, a_{k1}, ..., t_{km}, a_{km}]$ represents the number of times the sublist occurs in the operator list ignoring the identity operators in S_M. The above converges faster than the previous form, but should converge to the same value in the limit of large Monte Carlo sampling.

1.6 Observables in quantum Monte Carlo

The choice of basis in the SSE QMC makes certain variables very easy to measure while some require more complicated procedures to extract the relevant information. For instance, any information relating to the spins themselves can be extracted from the base layer, $|\alpha_0\rangle$, of the Stochastic Series Expansion. If we wish to calculate the spin-spin correlation function, we can simply extract it by iterating over the spins in the base layer at each Monte Carlo step. The reason we do not integrate over the entire Stochastic Series Expansion to calculate the spin-spin correlation is that each layer is only modified if it has an off-diagonal operator between them, and even then it is only changed by the swapping of two spins. In this way, adjacent layers of the SSE are highly correlated, and collecting such data would be a large time investment for a limited increase in accuracy. From the base layer we also extract the single spin expectation value as well as bulk properties like the sublattice and full lattice magnetization.

Formally, the diagonal quantities we regularly measure are

$$\langle S_i^z \rangle = \frac{1}{N_M} \sum_M \langle \alpha_0 | \, S_i^z \, | \alpha_0 \rangle \,, \tag{1.27}$$

$$\left\langle S_i^z S_j^z \right\rangle = \frac{1}{N_M} \sum_M \langle \alpha_0 | \, S_i^z S_j^z \, | \alpha_0 \rangle \,, \tag{1.28}$$

$$\langle m \rangle = \frac{1}{N_M} \sum_M \left(\frac{1}{N_s} \sum_i \langle \alpha_0 | \, S_i^z \, | \alpha_0 \rangle \right), \tag{1.29}$$

$$\left\langle m^2 \right\rangle = \frac{1}{N_M} \sum_M \left(\frac{1}{N_s} \sum_i \langle \alpha_0 | \, S_i^z \, | \alpha_0 \rangle \right)^2, \tag{1.30}$$

where N_M is the number of Monte Carlo steps, and the sum is performed after each step of the Monte Carlo simulation. The first two quantities are the single site expectation, showing the average orientation of a particular spin over the simulation, and the spin-spin correlation function, showing the relative orientation of all pairs over the simulation. N_s in the above is the number of spins in the simulation, making the last two quantities the magnetization and magnetization squared per spin, useful in calculating the susceptibility.

From the above quantities we can calculate further quantities of interest to analyze the simulation. One can imagine that for some conditions the simulation may be ergodic in such a way that the single spin expectation was zero for every site—due to spin inversion symmetry—but the groundstate was some symmetry breaking groundstate, such as the antiferromagnet. One generic method for detecting spatial ordering is the Fourier transform of the spin-spin correlation function, often referred to as the structure factor. It is defined

as

$$S(\mathbf{q}) = \frac{1}{N_s} \sum_{i,j} e^{i\mathbf{r}_{ij}\cdot\mathbf{q}} \left\langle S_i^z S_j^z \right\rangle . \tag{1.31}$$

For strong ordering, Bragg peaks develop in this function that scale with N_s. We can also examine the "connected" correlation function, defined as

$$S(\mathbf{q}) = \frac{1}{N_s} \sum_{i,j} e^{i\mathbf{r}_{ij}\cdot\mathbf{q}} \left(\left\langle S_i^z S_j^z \right\rangle - \left\langle S_i^z \right\rangle \left\langle S_j^z \right\rangle \right) . \tag{1.32}$$

This measure subtracts off any static structure in the groundstate, and only shows how fluctuations out of the ordered state are correlated. A flat spectrum in the thermodynamic limit, in either of the above would imply that the groundstate, or groundstate fluctuation correlation, lacks long range order.

From the magnetization we can derive the spin susceptibility of the system. The uniform spin susceptibility is defined as

$$\chi = \frac{\beta(\langle m^2 \rangle - \langle m \rangle^2)}{N}. \tag{1.33}$$

This quantity can have important features that describe the low energy physics of the system. If there is a temperature at which the magnetic susceptibility drops to zero, this signifies the energy scale at which density fluctuations are frozen out. If such a regime exists at low temperature, we would say that the system is gapped to single spin excitations at low temperature. These types of descriptors help build intuitive pictures of the system by describing bulk properties that are easier to interpret than the raw microscopic data.

The spin variables are simple to extract, but other variables require a more careful examination of the SSE formalism to relate quantities in the simulation to parameters from our original model. As described in Section 1.5, off diagonal operators can be measured easily if they exist in the Hamiltonian by looking for their occurrences in the operator list.

The most common operator expectation value to measure is $\left\langle S_i^+ S_j^- + S_i^- S_j^+ \right\rangle$, or the local kinetic energy density. For every bond of the lattice, we count the number of occurrences of the operator in the operator list. Doing simulations at a fixed β and using the equations given before, we find that the expectation of any bond operator is given by

$$\left\langle S_i^+ S_j^- + S_i^- S_j^+ \right\rangle = \frac{\langle N_{2,ij} \rangle}{\beta} \tag{1.34}$$

Where $N_{2,ij}$ represents the number of times the relevant operator occurs in the operator list, and this number is averaged over all Monte Carlo steps.

Similarly, if we define

$$b_{ij} = S_i^+ S_j^- + S_i^- S_j^+ \tag{1.35}$$

then we can examine $\langle b_{ij} b_{kl} \rangle$ and its Fourier transform to see if there is a pattern in the bond structure of the lattice. The equations are the same as Equation (1.31) and (1.32) except we replace the spin-spin correlation with the new bond-bond correlation function, and again we expect scaling proportional to N_s for strong order.

There is a special case of an operator measurement that is both diagonal and off diagonal—the energy. Using the definition in Section 1.5 the energy is a special case of Equation (1.21) which can be written as

$$\langle H \rangle = \sum_{\alpha} \sum_{S_M} \frac{\beta^n (M-n)!}{M!} \langle \alpha | H \prod_{i=0}^{M} H_{t_i,a_i} | \alpha \rangle . \tag{1.36}$$

As before, we find that the expectation of the operator is matched to the number of occurrences of the operator in the list. The Hamiltonian is a special case as the operators that we count are all the non-identity operators in the operator list. In this way the energy becomes

$$E = -\frac{\langle n \rangle}{\beta}. \tag{1.37}$$

The energy of the system is useful in that you expect it to converge to some stable value for low enough temperature—that of the groundstate energy. By also measuring the energy fluctuations we can calculate the specific heat by the equation

$$c_v = \left\langle n^2 \right\rangle - \langle n \rangle^2 - \langle n \rangle , \tag{1.38}$$

which one can derive this by taking the derivative of the energy equation with respect to temperature. The specific heat lets us measure certain important characteristics of the system. As we mentioned before, Equation (2.34) shows how we can calculate entropy from specific heat. For the typical systems we deal with the entropy at infinite temperature is finite. For any Ising system with N spins, this maximal entropy is $N k_B \ln(2)$. Using the known maximal entropy, we can calculate what the entropy is at zero temperature using the above method. Spikes in the specific heat in the above context signify a large change in entropy over a small temperature change, something that can signify a phase transition or the suppression of a class of excitation.

1.7 Visualization and interpretation

For many of the observables the formalism of their derivation means that looking at a single number should contain all the relevant information to make a classification of the

underlying groundstate. This is an approach that is unambiguous—as long as the observable is well defined in terms of this number, there is little to interpret. Such methods tend to be less informative when the groundstate is not as well understood, perhaps leading to incorrect applications of methods that may have underlying assumptions.

As mentioned in the description of observables, the structure factor is expected to have peaks that scale with N_s if there is strong ordering, but the interpretation of these peaks then comes in to play. Since the structure factor is really just the Fourier transform of the spatial two site correlation function, whether of spins or bonds, then if you think comfortably in this space perhaps the answer is easy, but here I will use a few examples from known groundstates and their transforms to build intuition. Also, to further simplify things we will always distort our lattice so that it is a square lattice with a basis. This simplifies things greatly, as the results for the square lattice carry very little ambiguity, and since the entire point of this transform is to make the results as simple as possible, nothing is lost by doing so.

For the structure factor of a finite lattice n-dimensional cubic lattice with lattice spacing of unity, the allowed vectors take the form

$$\mathbf{q} = \sum_i \frac{2\pi}{L_i} n_i \hat{i}, \qquad n_i \in [-L_i/2, L_i/2]. \tag{1.39}$$

Where L_i is the length of the system in the dimension labeled by i, and $\hat{i}$ is the unit vector in the basis vector for that dimension. The above is well defined when all of the dimensions have an even length and periodic boundary conditions. There is some redundancy in the above representation as well—technically there should only be as many valid $\mathbf{q}$-vectors as points in the lattice, but the redundant representation makes interpretation easier.

If we imagine the square lattice ferromagnet groundstate, then we expect to only find a peak for the vector $\mathbf{q} = (0, 0)$. This is because for all other choices of $\mathbf{q}$-vector the contributions, for the fully polarized state $\langle S_i^z S_j^z \rangle = 1/4$ for all i and j, the phase factors exactly cancel. The graphical representation can be seen in Figure 1.2, showing the uniform order transform into a central peak. In this way, the central peak of the structure factor only gives properties regarding the bulk expectation of the property one is interested in. For this reason, the correlation function is sometimes constructed to have an explicit zero mean, by shifting all values by a constant, so that other more subtle effects than the central peak may be observed.

Another common state that is detectable by this method is the square lattice antiferromagnetic state. For the classical groundstate of the square lattice antiferromagnet, one expects to find peaks for the value $\mathbf{q} = (\pm\pi, \pm\pi)$. The lattice pattern and structure factor for this case are shown in Figure 1.3.

To give one last example, we present a state with columnar order and the resulting structure factor. Figure 1.4 shows the columnar ordering and the structure factor that

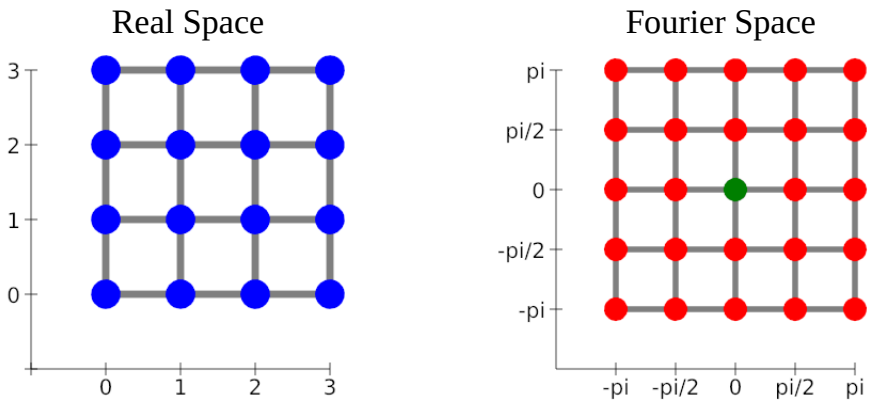

Figure 1.2: A typical ferromagnetic pattern (left) and the structure factor generated (right). Blue circles represent +1 while red circles represent 0, green circles represent large positive values.

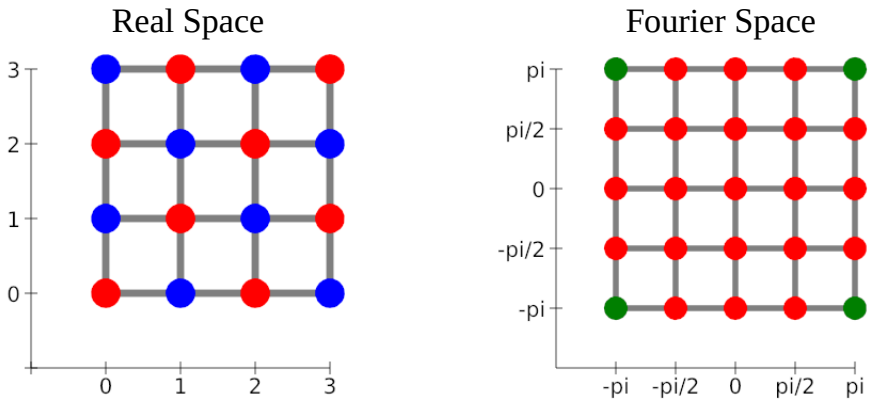

Figure 1.3: A typical antiferromagnetic pattern (left) and the structure factor generated (right). Notice that there are four peaks this time—this is due to the "repeated-zone" representation that is often used for structure factors. Normally there should only be as many points as the original lattice, but more are often shown for symmetry and clarity. Blue circles represent +1 while red circles represent 0, green circles represent large positive values.

results from it. In general, the structure factor is able to detect any ordering that has a unit cell and repeats in some direction. Since we are dealing with crystals to start with such ordering is quite common, and hence the reason that this method is often used to

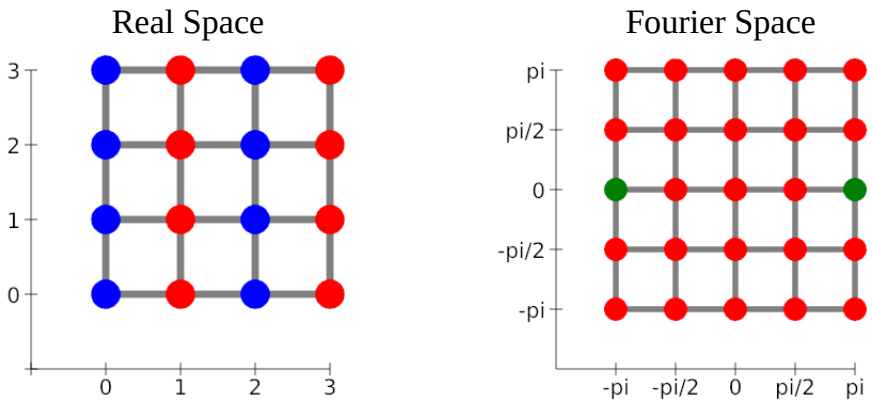

Figure 1.4: Striped order in a system, most simply seen in models that have an x/y asymmetry. If we imagine rotating the striped order (in a way that was commensurate with the lattice size) the structure factor points would similarly rotate, with the distance from the origin inversely proportional to the distance between layers. In this way, the antiferromagnet can be seen as diagonal layers separated by the smallest possible distance, as the **q**-vectors are the farthest possible distance from the origin. Blue circles represent $+1$ while red circles represent 0, green circles represent large positive values.

characterize materials. Beyond that, scattering experiment results are often in the form of structure factors, so relating to physical measurements is another reason this result is calculated for any simulated systems that might be realizable in physical systems.

Another scenario that arises in some systems is that of a mix of correlated spins and uncorrelated spins, perhaps on one of the sublattices and another. In this case, the ordered sublattice contributes to the structure factor, and the uncorrelated sublattice should give a zero contribution for all q-vectors in the thermodynamic limit. This ability of the structure factor to detect partial orders makes it useful for analyzing a variety of phases.

If the structure factor shows that the spins are ordered in some long range configuration, the phase is considered to be long range ordered, and hence referred to as a crystalline phase. If the structure factor shows peaks that do not scale with the number of spins, this implies there is no long range order in the system—but it says nothing about the short range correlations in the system. This is because if each spin is only correlated with a finite set of other spins in the lattice, then each spin only contributes a fixed amount to the structure factor. Multiplying this fixed contribution by the number of spins gives us a value that scales with N_s before multiplying by the prefactor of $1/N_s$, giving a constant value as opposed to one that diverges in the thermodynamic limit. In either case the structure factor describes if the system has any sort of order, but it takes further intuition to extract

the groundstate configuration from this method. Since we had access to the full single site and two site correlation function, it is possible to visualize the data directly using a color mapping and the original lattice geometry. This method was first developed to assist in interpreting the structure factors, but eventually became one of the primary methods of interpretation in this thesis, although as we will see it has limitations as well.

For a two dimensional lattice, you can assign every site an x and y coordinate, usually chosen as the real lattice parameters for simplicity. At each of these sites we then draw a circle to represent the spin that has a quality, usually color, representing $\langle S_i^z \rangle$ for that site. If the we are in a disordered (non-symmetry breaking) phase then we would expect every spin would be colored the same, namely the color representing $\langle S_i^z \rangle = 0$. For a highly ordered phase such as the antiferromagnet, one will see the typical checkerboard pattern in the coloring of the sites, and distinguishing this would again be fairly easy. In our fully-frustrated honeycomb XXZ model some of the groundstates involve some of the spins strongly ordering, and some of the spins highly fluctuating. Using the structure factor we find a peak that scale with N_s but at a lower value than if all the spins were collectively correlated. Although the structure factor is able to detect even very weak order very well, the real space pictures allow us to precisely describe that order in terms of the original lattice. The difficulty with real space is that the representation is in some ways less precise—it is easy to distinguish patterns in color, but only if the colors are distinguishable. In this way the data must have significant numerical differentiation or be prepared in such a way so that the color scale has enough contrast to be easily interpreted. If the simulation were fully ergodic and lacked an explicit symmetry breaking terms like an external field, one would expect the pattern of colors to show nothing at all—a uniform average of zero.

The second use of real space pictures is choosing a site (or bond) of the lattice and using the spin-spin (bond-bond) correlation function to generate the remaining sites of the lattice. By using different sites as a basis we can examine the local environment of spins and bonds from any point on the lattice. In this way we can directly visualize whether the correlations are long range or short range, if they system undergoes a dimensional reduction to correlated one dimensional chains, or any other number of exotic behaviors. The main difficulty again lies in processing the data in a way that will show the qualities of interest, but this can be overcome by a smart choice of coloring scheme.

The last method of analyzing the data is using histograms. Suppose instead of measuring the bulk magnetization we bin the average magnetization of each site. Using only the bulk magnetization we are unable to differentiate a state where every spin equally fluctuates or half of the spins freeze into a spin up configuration and half into the spin down configuration. By examining the histogram of each spins average magnetization, these configurations look like a distribution with a single peak and a doubly-peaked distribution, respectively. This is also useful in the examination of order parameters near a phase transition. Imagine near a phase transition that the system fluctuates between

an ordered phase where the order parameter takes a value of $O_1 = A_0$ and $O_2 = 0$ and a second ordered phase where a different order parameter takes the value $O_2 = B_0$ and $O_1 = 0$. In Monte Carlo averaging we would interpret this as a phase with the first order parameter of $O_1 = A_0/2$ and the second order parameter at $O_2 = B_0/2$, or coexistence of two order parameters. By using histograms, even of each value independently, we would see the bimodal distribution and at least suspect that the two order parameters might not be occurring simultaneously during the simulation. To further clarify we could bin the data as a function of both parameters (as opposed to each independently), and we would then see two clusters, each representing the original states we were fluctuating between. In some cases this may also be too data intensive, at which point collecting data on $O_1^2, O_2^2,$ and $O_1 O_2$ would resolve the issue if the parameters were coexisting or not.

It is with these above methods that we analyze each of the models of interest, using each as necessary when they best illustrate the nature of the phases found in each of our system.

1.8 Hopping and the singlet

Often times when discussing Monte Carlo simulations, there is never a strong connection made between hopping and presence (or lack thereof) of singlets in a system. The term "valence bond" is used often, sometimes explicitly referring to the presence of singlets, but often it is not explicitly defined. Here we will attempt to draw a connection between the expectation value of the hopping operator and the presence of a singlet or the fully entangled triplet state on a pair of spins.

There are four properties we measure in simulation that are relevant for two sites i and j: $\langle S_i^z \rangle$, $\langle S_j^z \rangle$, $\langle S_i^z S_j^z \rangle$ and $\langle S_i^+ S_j^- + S_i^i S_j^+ \rangle$. Let us analyze a two site system, and let us assume we analyze it using the following basis

$$|\Psi\rangle = a\,|\uparrow\uparrow\rangle + b\,|\downarrow\downarrow\rangle + \frac{c}{\sqrt{2}}\left[|\uparrow\downarrow\rangle + |\downarrow\uparrow\rangle\right] + \frac{d}{\sqrt{2}}\left[|\uparrow\downarrow\rangle - |\downarrow\uparrow\rangle\right]. \tag{1.40}$$

If we examine the expectation value of the operators on each of the basis states above, we get the relationship

	$\lvert\uparrow\uparrow\rangle$	$\lvert\downarrow\downarrow\rangle$	$\frac{1}{\sqrt{2}}\left[\lvert\uparrow\downarrow\rangle + \lvert\downarrow\uparrow\rangle\right]$	$\frac{1}{\sqrt{2}}\left[\lvert\uparrow\downarrow\rangle - \lvert\downarrow\uparrow\rangle\right]$
$\langle S_i^z \rangle$	$1/2$	$-1/2$	0	0
$\langle S_j^z \rangle$	$1/2$	$-1/2$	0	0
$\langle S_i^z S_j^z \rangle$	$1/4$	$1/4$	$-1/4$	$-1/4$
$\langle S_i^+ S_j^- + S_i^- S_j^+ \rangle$	0	0	1	-1

At this point we should mention that the simulation is capable of simulating both signs of hopping without the sign problem due to the bipartite nature of the lattice. Since the simulation does not change when the sign of the hopping is changed, all the results we have gathered are equally valid for both signs, the only change being the interpretation of the hopping. When we take the opposite sign of hopping, the expectation of hopping is really a measure of $\left\langle -(S_i^+ S_j^- + S_i^- S_j^+) \right\rangle$ instead, flipping the expectation of the third and fourth columns in the table above for the hopping row.

The expectations in the above table are for the eigenstates. If we now imagine a state of the form in Equation (1.40) we can recalculate what the expectation of the various operators would be as a function of the coefficients

$$\begin{aligned}
\langle S_i^z \rangle =& \frac{1}{2}a^2 - \frac{1}{2}b^2 + cd \\
\left\langle S_j^z \right\rangle =& \frac{1}{2}a^2 - \frac{1}{2}b^2 - cd \\
\left\langle S_i^z S_j^z \right\rangle =& \frac{1}{4}a^2 + \frac{1}{4}b^2 - \frac{1}{4}c^2 - \frac{1}{4}d^2 \\
\left\langle S_i^+ S_j^- + S_i^- S_j^+ \right\rangle =& c^2 - d^2 \\
a^2 + b^2 + c^2 + d^2 =& 1.
\end{aligned} \tag{1.41}$$

We see that the expectation of $\left\langle S_i^+ S_j^- + S_i^- S_j^+ \right\rangle$, if close to one, signifies the presence of an entangled pair.

The last complication is that we calculate the above values by Monte Carlo, and so in the worse case the above would be rewritten

$$\begin{aligned}
\langle S_i^z \rangle =& \frac{1}{M}\sum_{i=1}^{M} \frac{1}{2}a_i^2 - \frac{1}{2}b_i^2 + c_i d_i \\
\left\langle S_j^z \right\rangle =& \frac{1}{M}\sum_{i=1}^{M} \frac{1}{2}a_i^2 - \frac{1}{2}b_i^2 - c_i d_i \\
\left\langle S_i^z S_j^z \right\rangle =& \frac{1}{M}\sum_{i=1}^{M} \frac{1}{4}a_i^2 + \frac{1}{4}b_i^2 - \frac{1}{4}c_i^2 - \frac{1}{4}d_i^2 \\
\left\langle S_i^+ S_j^- + S_i^- S_j^+ \right\rangle =& \frac{1}{M}\sum_{i=1}^{M} c_i^2 - d_i^2 \\
a_i^2 + b_i^2 + c_i^2 + d_i^2 =& 1.
\end{aligned} \tag{1.42}$$

In this final form, we want to know if we can put a bound on the coefficients if we know certain properties of the expectation value of the operators above.

Since we are interested in the singlet, let us try to calculate the term d^2 term in the expansion. For simplicity, we will calculate the c^2 term and realize that the d^2 term follows an identical calculation when the sign of the hopping term is inverted in the Hamiltonian. We know the hopping is always positive in our model, and since $\left\langle S_i^+ S_j^- + S_i^- S_j^+ \right\rangle = c^2 - d^2$, it is unlikely we will see any expectation of d^2 unless we flip the sign of the hopping.

Carrying on, we can attempt to isolate c^2

$$\begin{aligned} \frac{1 - 4\left\langle S_i^z S_j^z \right\rangle}{2} &= \frac{1}{M}\sum_{i=1}^{M} c_i^2 + d_i^2, \\ \left\langle S_i^+ S_j^- + S_i^- S_j^+ \right\rangle &= \frac{1}{M}\sum_{i=1}^{M} c_i^2 - d_i^2, \\ \frac{1 - 4\left\langle S_i^z S_j^z \right\rangle}{4} + \frac{\left\langle S_i^+ S_j^- + S_i^- S_j^+ \right\rangle}{2} &= \frac{1}{M}\sum_{i=1}^{M} c_i^2. \end{aligned} \tag{1.43}$$

Since the maximum value for $\left\langle S_i^+ S_j^- + S_i^- S_j^+ \right\rangle$ is 1 and the minimal value for $\left\langle S_i^z S_j^z \right\rangle$ is $-1/4$, we recover that the largest c^2 we can find is 1. In this way, we see that in a perfect singlet neighbors would be antiferromagnetically correlated and the expectation of the hopping operator would be 1. In our 2D models we will never see precisely this, as when many of the bonds would be satisfied by antiferromagnetic arrangement, the singlet will have to share its weight among all of the neighbors where spins can exchange and reduce the systems energy. The above calculation lets us quantitatively determine the weights of particular projections of the wave function on to a two site basis, and thus say without ambiguity the relationship between the singlet and the hopping term of the Hamiltonian.

1.9 Frustrated magnetic systems

Frustrated magnetic systems are those for which all the interactions cannot be simultaneously satisfied. For any plaquette of the system frustration can be created in two general ways, through geometry or through mixing interactions. The prototypical example of geometric frustration is the antiferromagnetic triangular lattice. If we imagine a single plaquette, that is a single triangle of the lattice, it consists of three connected sites. Defining the first spin (spin-1) to be up, the antiferromagnetic interaction would prefer that the next spin we place (spin-2) be oriented down. The problem now is that the third spin (spin-3) is required by spin-1 to down, but required by spin-2 to be spin up. This is shown in Figure 1.5**a**. In this way, the orientation of spin-3 is frustrated since it cannot satisfy all interactions simultaneously.

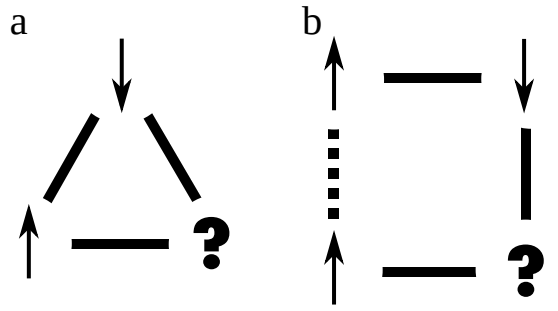

Figure 1.5: Basic frustrated plaquettes. **(a)** Geometric frustration in the triangular antiferromagnet and **(b)** a plaquette of the fully-frustrated square lattice. For a single plaquette of **a**, six of the eight possible configurations are groundstates. Eight of the sixteen configurations are valid groundstates for the plaquette of **b**.

Frustration through interaction is similar, except that it requires a mixing of ferromagnetic and antiferromagnetic interactions. Figure 1.5**b** shows a square lattice with three antiferromagnetic bonds and one ferromagnetic bond. By the same procedure as above, after placing three of the spins in a way that satisfies the interaction, the fourth will be forced to frustrate one of the remaining bonds.

In describing frustrated lattices of the second type it is convenient to define a set of variables that live on the bonds of the lattice. One such representation would be one in which we fix the amplitude of the interaction and let the sign vary.

$$J_{ij} = Je^{iA_{ij}}. \tag{1.44}$$

In such a description the set of A_{ij}'s completely describe the interaction and the frustration for a given lattice. If we imagine a square lattice of bonds randomly chosen to be antiferromagnetic or ferromagnetic, then each plaquette will be frustrated if it satisfies the condition

$$\sum_{\{i,j\}\in p} A_{ij} = (2n+1)\pi, \qquad n \in \{0,1\}. \tag{1.45}$$

Where $\{i,j\} \in p$ describes the set of bonds that belong to a particular plaquette. Such a condition can be extended to a general lattice as well. For any lattice, it is "fully-frustrated" if every plaquette satisfies a condition similar to Equation (1.45), specifically that that the number of antiferromagnetic bonds around every plaquette must be odd. Such a general case covers both geometrically frustrated lattices and those in which we craft the frustration explicitly.

Frustrated systems are interesting to study because they tend to have properties that are unusual in classical systems. Although all frustrated systems cannot satisfy all interactions simultaneously, some of them also have multiple equal energy groundstates, and in rare cases they may have macroscopic degeneracy in the groundstate. Systems that have an extensive entropy at zero temperature often give rise to other peculiar states or transitions when an anisotropy or external perturbation is applied to the system. Frustration can lead to a suppression of "conventional" order and can lead to disordered or spin-liquid groundstates [1], as mentioned earlier in this chapter.

Chapter 2

Classical Fully Frustrated Honeycomb Lattice Ising Model

2.1 Analytical methods for spin models

In the study of spin systems, an approximation that assumes a spin's neighbors take an orientation equal to the average orientation (or "field") of all spins in the system is known as mean field theory. If we were to look at the Ising ferromagnet in mean field with an applied external field, the Hamiltonian would be rewritten as

$$\begin{aligned} H &= -J\sum_{\langle ij\rangle}\sigma_i\sigma_j - \mu B\sum_i \sigma_i \\ &= -\frac{1}{2}Jz\langle\sigma\rangle\sum_i\sigma_i - \mu B\sum_i\sigma_i \\ &= -(\frac{1}{2}Jz\langle\sigma\rangle + \mu B)\sum_i\sigma_i, \end{aligned} \tag{2.1}$$

where z is the number of nearest neighbors and $\langle\sigma\rangle = 1/N\sum_i\sigma_i$ is the mean orientation of any of the spins. The assumptions that we have made here is that each spin is does not fluctuate much from the average value of all spins, which depending on the system can be anywhere from a good to a terrible approximation. Nevertheless, even in this crude approximation we can see that the model undergoes a phase transition from a disordered to an ordered state.

For a given average value of the spin, we can calculate the energy difference between

the two spin configurations for a local spin.

$$\begin{aligned}\Delta\epsilon &= -\mu B\Delta\sigma - Jz\left\langle\sigma\right\rangle\Delta\sigma,\\ &= 2\mu\left(B + \frac{Jz\left\langle\sigma\right\rangle}{\mu}\right),\end{aligned} \tag{2.2}$$

where we take $\Delta\sigma = -2$. As the above form suggests, the average magnetization acts like an external magnetic field for each spin of the lattice. This effective field produced by neighboring spins is usually referred to as the internal or molecular field.

Since we now know the energy difference between the two states, we can use the Boltzmann distribution to find the ratio of up to down spins in equilibrium. The Boltzmann distribution states that in equilibrium we should find

$$\frac{\langle N^-\rangle}{\langle N^+\rangle} = \exp(-2\mu(B' + B)\beta) \tag{2.3}$$

Where $\beta = 1/k_BT$ is the inverse temperature, $B' = Jz\left\langle\sigma\right\rangle/\mu$ is the molecular field and N^+ and N^- represent the total number of up and down spins, respectively. The molecular field B' also explicitly depends on the number of up and down spins, so the above is really a self consistent equation of the form

$$\begin{aligned}\frac{N(\langle\sigma\rangle - 1)/2}{N(\langle\sigma\rangle + 1)/2} &= \exp(-2\mu(\frac{Jz\left\langle\sigma\right\rangle}{\mu} + B)\beta),\\ \frac{\langle\sigma\rangle - 1}{\langle\sigma\rangle + 1} &= \exp(-2\mu(\frac{Jz\left\langle\sigma\right\rangle}{\mu} + B)\beta),\\ \frac{1}{2}\ln\left(\frac{\langle\sigma\rangle + 1}{\langle\sigma\rangle - 1}\right) &= \beta(Jz\left\langle\sigma\right\rangle + \mu B),\\ \tanh^-1(\langle\sigma\rangle) &= \beta(Jz\left\langle\sigma\right\rangle + \mu B),\\ \langle\sigma\rangle &= \tanh\left(\beta(Jz\left\langle\sigma\right\rangle + \mu B)\right),\end{aligned} \tag{2.4}$$

where now the self consistent form is very apparent. If we lump the terms $\beta' = \beta Jz$ and set the external field to zero, we can plot both left and right side together and find solutions where they cross. In Figure 2.1 we see that there is always one solution at $\langle\sigma\rangle = 0$ for any β', but as we take larger and larger β' (corresponding to lower and lower temperature) there is a point at which two more solutions develop. This point at which we have non-zero solutions for the magnetization is known as the mean field critical temperature T_c. For example, if we were considering the 2D Ising model on a square lattice, then $k_BT_c = 4J$. It is important to note that as long as we can make β' large enough, the system will always order. This implies that for any positive z value an Ising system will order at a low enough temperature, while more advanced approximations or Monte Carlo simulation show that

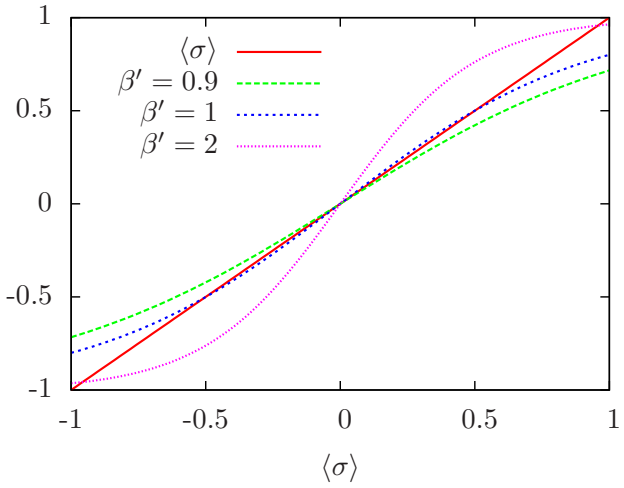

Figure 2.1: The self consistent mean field theory magnetization. The graph shows the intersections of the self consistent relationship in Equation (2.4). When β' is below 1, there is only one solution at $\langle\sigma\rangle = 0$. If β' is greater than 1, than two additional symmetric non-zero solutions develop.

although classical 2D models do order, the classical 1D Ising model does not order all the way down to $T = 0$ [7]. Extending this to the honeycomb ferromagnet, where $z = 3$, we find that the critical temperature is predicted to be $T_c = 3J$ in mean-field theory.

In one dimension the exact solution to the Ising model was derived by Ising himself [7], where he found there was no phase transition all the way down to absolute zero, but incorrectly concluded that there was no finite temperature transition for any number of dimensions. For the two dimensional Ising model the exact solution was derived by Onsager [17], but the derivation is more mathematically challenging than the above and not necessary for our discussion of this work. Beyond two dimensions there are various other methods, but the mean field approximation above also becomes more and more accurate, becoming exact as we go above the upper critical dimension [18].

The next relevant model that we can treat analytically is the quantum XY model. in this model we assume a Hamiltonian of the form

$$H = -J \sum_{\langle ij \rangle} S_i^x S_j^x + S_i^y S_j^y. \tag{2.5}$$

If we rotate the basis so the y direction now points along the z axis, and expand the S^x

operators into raising and lowering operators for the S^z basis we get

$$H = -J \sum_{\langle ij \rangle} S_i^z S_j^z + \frac{1}{4}(S_i^+ + S_i^-)(S_j^+ + S_j^-), \tag{2.6}$$

after which we can apply the Holstein-Primakoff transformation. The Holstein-Primakoff transformation [19] starts from an ordered groundstate "guess" and calculates corrections as perturbations from this guess. In it we define the quantity S representing the magnitude of the spins on the lattice, in this case $\frac{1}{2}$. Here we will perform what is known as linear spin-wave theory, in which we will find the lowest excitations are gapless non-interacting magnons.

Applying the transform to the above Hamiltonian we get

$$\begin{aligned} H = &- J \sum_{\langle ij \rangle} (S - a_i^\dagger a_i)(S - a_j^\dagger a_j) + \\ &\frac{S}{2} \left[\left(1 - \frac{a_i^\dagger a_i}{2S}\right)^{1/2} a_i \left(1 - \frac{a_j^\dagger a_j}{2S}\right)^{1/2} a_j + \left(1 - \frac{a_i^\dagger a_i}{2S}\right)^{1/2} a_i a_j^\dagger \left(1 - \frac{a_j^\dagger a_j}{2S}\right)^{1/2} + \right. \\ &\left. a_i^\dagger \left(1 - \frac{a_i^\dagger a_i}{2S}\right)^{1/2} \left(1 - \frac{a_j^\dagger a_j}{2S}\right)^{1/2} a_j + a_i^\dagger \left(1 - \frac{a_i^\dagger a_i}{2S}\right)^{1/2} a_j^\dagger \left(1 - \frac{a_j^\dagger a_j}{2S}\right)^{1/2} \right]. \end{aligned} \tag{2.7}$$

Expanding the square root in each term and only keeping terms of order $1/S$ we get

$$\begin{aligned} H = &- J \sum_{\langle ij \rangle} (S - a_i^\dagger a_i)(S - a_j^\dagger a_j) + \\ &\frac{S}{2} \left[\left(1 - \frac{a_i^\dagger a_i}{4S}\right) a_i \left(1 - \frac{a_j^\dagger a_j}{4S}\right) a_j + \left(1 - \frac{a_i^\dagger a_i}{4S}\right) a_i a_j^\dagger \left(1 - \frac{a_j^\dagger a_j}{4S}\right) + \right. \\ &\left. a_i^\dagger \left(1 - \frac{a_i^\dagger a_i}{4S}\right) \left(1 - \frac{a_j^\dagger a_j}{4S}\right) a_j + a_i^\dagger \left(1 - \frac{a_i^\dagger a_i}{4S}\right) a_j^\dagger \left(1 - \frac{a_j^\dagger a_j}{4S}\right) \right]. \end{aligned} \tag{2.8}$$

We take this form and Fourier transform the creation and annihilation operators, keeping only quadratic terms. Defining L as the linear dimension of some finite $L \times L$ lattice, we

get

$$H = -J\sum_{\langle mn\rangle}\left[\left(S-\frac{1}{L}\sum_{k_1}\sum_{k_2}e^{i(k_1-k_2)m}b^\dagger_{k_1}b_{k_2}\right)\left(S-\frac{1}{L}\sum_{k_1}\sum_{k_2}e^{i(k_1-k_2)n}b^\dagger_{k_1}b_{k_2}\right)+\right.$$
$$\frac{S}{2L}\left(\sum_{k_1}e^{-ik_1m}b_{k_1}\sum_{k_2}e^{-ik_2n}b_{k_2}+\sum_{k_1}e^{-ik_1m}b_{k_1}\sum_{k_2}e^{ik_2n}b^\dagger_{k_2}+\right. \tag{2.9}$$
$$\left.\left.\sum_{k_1}e^{ik_1m}b^\dagger_{k_1}\sum_{k_2}e^{-ik_2n}b_{k_2}+\sum_{k_1}e^{ik_1m}b^\dagger_{k_1}\sum_{k_2}e^{ik_2n}b^\dagger_{k_2}\right)\right].$$

Changing the sum to one explicitly over nearest neighbors, δ, we get

$$H = -\frac{J}{2}\sum_{m}\sum_{\delta}\left[\left(S-\frac{1}{L}\sum_{k_1}\sum_{k_2}e^{i(k_1-k_2)m}b^\dagger_{k_1}b_{k_2}\right)\left(S-\frac{1}{L}\sum_{k_1}\sum_{k_2}e^{i(k_1-k_2)(m+\delta)}b^\dagger_{k_1}b_{k_2}\right)+\right.$$
$$\frac{S}{2L}\left(\sum_{k_1}e^{-ik_1m}b_{k_1}\sum_{k_2}e^{-ik_2(m+\delta)}b_{k_2}+\sum_{k_1}e^{-ik_1m}b_{k_1}\sum_{k_2}e^{ik_2(m+\delta)}b^\dagger_{k_2}+\right.$$
$$\left.\left.\sum_{k_1}e^{ik_1m}b^\dagger_{k_1}\sum_{k_2}e^{-ik_2(m+\delta)}b_{k_2}+\sum_{k_1}e^{ik_1m}b^\dagger_{k_1}\sum_{k_2}e^{ik_2(m+\delta)}b^\dagger_{k_2}\right)\right]. \tag{2.10}$$

We can now perform the sum over all m explicitly to get the form

$$H = -\frac{JL}{2}\sum_{\delta}\left[\left(S-\frac{1}{L}\sum_{k}b^\dagger_k b_k\right)\left(S-\frac{1}{L}\sum_{k}b^\dagger_k b_k\right)+\right.$$
$$\frac{S}{2L}\left(\sum_{k}e^{ik\delta}b_kb_{-k}+\sum_{k}e^{-ik\delta}b_kb^\dagger_k+\right. \tag{2.11}$$
$$\left.\left.\sum_{k}e^{ik\delta}b^\dagger_kb_k+\sum_{k}e^{-ik\delta}b^\dagger_kb^\dagger_{-k}\right)\right].$$

Performing the sum over δ then gives us the form

$$H = -\frac{JLz}{2}\sum_{\delta}\left[\left(S-\frac{1}{L}\sum_{k}b^\dagger_k b_k\right)\left(S-\frac{1}{L}\sum_{k}b^\dagger_k b_k\right)+\right.$$
$$\frac{S}{2L}\left(\sum_{k}\gamma_kb_kb_{-k}+\sum_{k}\gamma_{-k}b_kb^\dagger_k+\right. \tag{2.12}$$
$$\left.\left.\sum_{k}\gamma_kb^\dagger_kb_k+\sum_{k}\gamma_{-k}b^\dagger_kb^\dagger_{-k}\right)\right],$$

where z is the number of nearest neighbors and we define

$$\gamma_k = \frac{1}{z}\sum_{\delta} e^{ik\delta}. \tag{2.13}$$

After making this transformation the Hamiltonian has the form

$$\begin{aligned} H &= -\frac{JS^2Lz}{2} + \frac{JSz}{4}\sum_k (4-2\gamma_k)\, b_k^\dagger b_k - \gamma_k \left(b_k b_{-k} b_k^\dagger b_{-k}^\dagger\right), \\ H &= -\frac{JS^2Lz}{2} + \frac{JSz}{4} H_k. \end{aligned} \tag{2.14}$$

From here if we can diagonalize H_k we will have diagonalized the problem.

If we use a Bogoliubov transformation [19] of the following form

$$\begin{aligned} \alpha_k =& u_k b_k - v_k b_{-k}^\dagger \\ \alpha_{-k}^\dagger =& u_k b_{-k}^\dagger - v_k b_k \\ \left[\alpha_k, \alpha_k^\dagger\right] =& 1 = u_k^2 - v_k^2, \end{aligned} \tag{2.15}$$

we find that to have the set of α_k behave with proper boson statistics, we have a restriction on the coefficients u and v. If we insist that this new set of variables is diagonal with respect to the Hamiltonian, we get a further set of restrictions on the coefficients

$$\begin{aligned} [\alpha_k, H_k] =& \alpha_k \lambda_k, \\ \lambda_k u_k =& \left[u_k(4-2\gamma_k) - 2v_k\gamma_k\right], \\ \lambda_k v_k =& \left[-v_k(4-2\gamma_k) + 2u_k\gamma_k\right]. \end{aligned} \tag{2.16}$$

This gives us the system of equations

$$\begin{pmatrix} -(4-2\gamma_k-\lambda_k) & 2\gamma_k \\ 2\gamma_k & -(4-2\gamma_k+\lambda_k) \end{pmatrix} \begin{pmatrix} u_k \\ v_k \end{pmatrix} = \begin{pmatrix} 0 \\ 0 \end{pmatrix}. \tag{2.17}$$

Solving this gives this constraint

$$\lambda_k^2 = (4-2\gamma_k)^2 - 4\gamma_k^2. \tag{2.18}$$

If we substitute this back into H_k and then collect all the terms from the original Hamiltonian, we finally get the diagonalized form

$$H = -\frac{JLzS(S+1)}{2} + \frac{JzS}{2}\sum_k \left(\alpha_k\alpha_k^\dagger + \frac{1}{2}\right)\sqrt{(2-\gamma_k)^2 - \gamma_k^2}. \tag{2.19}$$

In this form we can explicitly calculate the reduction of the groundstate energy from the maximal energy per interaction—that being if every site could be in a singlet with every other site of the lattice. We can also calculate the reduction in magnetization at zero temperature due to quantum fluctuations from this Hamiltonian.

For the honeycomb model, the γ_k must be averaged over the two sublattice contributions, and we get the form

$$\begin{aligned}\gamma_k =& \frac{\gamma_{k_1} + \gamma_{k_2}}{2}, \\ =& \frac{1}{6}\left(e^{ik_x} + e^{-ik_x} + e^{i(\frac{k_x}{2}+\sqrt{3}\frac{k_y}{2})} + e^{-i(\frac{k_x}{2}+\sqrt{3}\frac{k_y}{2})} + e^{i(\frac{-k_x}{2}+\sqrt{3}\frac{k_y}{2})} + e^{-i(\frac{-k_x}{2}+\sqrt{3}\frac{k_y}{2})}\right), \\ =& \frac{1}{3}\left(\cos(k_x) + \cos(\frac{k_x}{2} + \sqrt{3}\frac{k_y}{2}) + \cos(\frac{-k_x}{2} + \sqrt{3}\frac{k_y}{2})\right).\end{aligned} \tag{2.20}$$

Plugging the above energy into Equation (2.19) and simplifying we find a groundstate energy of

$$H_0 = -\frac{3}{2}JSL(S + 1 - 0.6947). \tag{2.21}$$

To compare, the classical antiferromagnet has an energy of $-3/2JSL(S)$, so the addition of quantum terms reduces the energy from this classical limit.

We can also calculate the expectation of the spin stiffness in this approximation. The spin stiffness is defined as

$$\frac{1}{2}\rho_s\phi^2 = \frac{\langle H(\phi)\rangle}{N} - \frac{\langle H(0)\rangle}{N}, \tag{2.22}$$

where $\langle H(\phi)\rangle$ is the energy of the twisted Hamiltonian—that is the internal energy when we assume the system has a twist enforced between neighboring spins of the lattice. Enforcing the twisted condition give us a Hamiltonian of the form

$$H(\phi) = -J\sum_{\langle ij\rangle}\left(S_i^x S_j^x + S_i^y S_j^y\right)\cos(\phi) + \left(S_i^x S_j^y - S_i^y S_j^x\right)\sin(\phi). \tag{2.23}$$

Taylor expanding the above in terms of ϕ and matching up with Equation (2.22) we get

$$H(\phi) = (1 - \frac{\phi^2}{2})H_0, \tag{2.24}$$

$$\rho_s = 0.6039J, \tag{2.25}$$

for the spin-$\frac{1}{2}$ honeycomb lattice. This is the same value that is obtained during quantum Monte Carlo calculations performed on the XXZ model when $J/t = 0$, which is effectively the XY model.

2.2 Hamiltonian and gauge choice

The classical fully-frustrated honeycomb lattice is an instance of the Ising model. The general Hamiltonian we consider takes the form

$$\hat{H} = J \sum_{\langle ij \rangle} e^{-iA_{ij}} S_i^z S_j^z, \qquad A_{ij} \in 0, \pi, \tag{2.26}$$

where the fully-frustrated requirement is satisfied by

$$\forall p \quad \sum_{ij \in p} A_{ij} = (2n+1)\,\pi, \qquad n \in \{0, 1, 2\}, \tag{2.27}$$

where each p is a plaquette of the lattice. In our model, A_{ij} is only allowed to take on the value zero or π. This means for each bond it is satisfied, while J^z is positive, if the spins are parallel when A_{ij} is π, or anti-parallel when A_{ij} is zero. For each plaquette the above restriction is equivalent to requiring that an odd number of bonds have $A_{ij} = \pi$. In this way the A_{ij} variables can be seen as a gauge choice, as there are many ways to satisfy this constraint.

The reason for using the term "gauge" can be examined by looking at the fully-frustrated constraint of the system and how it can be manipulated. If we examine the condition in Equation (2.27) it is fairly clear that there is more than one unique way to generate the fully-frustrated condition. Using the variables on the bonds, we can define a lattice curl as

$$\nabla_p = \sum_{ij \in p} A_{ij}, \tag{2.28}$$

where every bond can only takes values that are multiple of π. Using this definition, the fully-frustrated requirement can be recast as enforcing the curl on every plaquette to be equal to π modulo 2π. Such gauge language was developed to understand the problem of random bond models and transform them in a way that allowed analytical progress [20], and it is similar enough conceptually that we use it here as well.

With this in mind, we can now suggest more concretely why a choice of frustration is similar to a choice in gauge. If we take a particular choice of frustration, we may add an arbitrary pattern to the bonds, as long as it satisfies

$$\forall p \quad \nabla_p \equiv 0 \pmod{2\pi}. \tag{2.29}$$

Using this transformation, we may transform from any frustration choice to any other frustration choice. In this way, it is similar to the gauge freedom in electrodynamics where the electric potential and vector potential can be changed by

$$\begin{aligned} V &\to V + \nabla\phi, \\ A &\to A - \frac{\partial \phi}{\partial t}, \end{aligned} \tag{2.30}$$

causing no change in the the electric and magnetic field, the only measurable effect of these potentials.

If we consider the relevant variables of the fully-frustrated honeycomb model to be the location of the frustrated bonds, then changing the gauge by the above transform simply changes the particular spin configuration. The dynamics of the system are only dependent on the energy, and without an external magnetic field the energy is only dependent on frustrated bonds. In this way, transforming the gauge cannot affect the dynamics of the classical simulation, and in effect only transforms the particular spin configuration for a particular choice of frustration. In the classical system, the choice of frustration truly acts as a gauge freedom which aside from the particular spin configuration, does not affect the simulation.

When we move to the quantum system the two signs of the interaction are fundamentally different, as with the addition of the hopping term the two signs of the interaction are no longer effectively identical. The hopping term acts similar to an external field in that the first prefers spins to pair anti-aligned and the second prefers a particular spin orientation—both cases breaking the symmetry between up and down spins. Either of these qualities destroys the symmetry that allows this gauge transformation to truly be a gauge freedom, but for the sake of using conventional terminology we refer to the particular way in which the bonds are frustrated as our gauge choice.

The first approach when looking at such a problem is to attempt an analytical solution. Here such an approach is to solve the interaction matrix of a unit cell of the problem to see what the ordering wave vectors are. The interaction matrix relaxes the constraint that the spins must be strictly up or down and lets them take continuous values. This is done by taking the state of the system to be a classical vector of dimension n, where n is the number of spins in the system. If this is done we can then take the Hamiltonian to be a matrix with non-zero elements wherever spins interact with other spins, with a complex factor between cells to allow for rotating all of the spins from one cell to another, to further reduce the energy. The constraint that we have relaxed in this process is requiring that all the spins point up and down—now the values of the eigenvector, which we normalize so they are all less than one, may take on any real values. In this sense, we solve a similar problem to the one we were interested in and hope to gain insight from that solution.

The interaction matrix is generated by first indexing all the spins in the unit cell with a number. If there are n spins, then we build the $n \times n$ interaction matrix I. I_{ij} is defined directly from the Hamiltonian: if i and j are in the same unit cell, then it is simply the sign and strength of the interaction between the two spins (zero if they do not interact), which we can call J_{ij}. If i and j are on different unit cells, then the matrix element is of the form

$$I_{ij} = J_{ij} e^{-i\vec{r}_{ab}\cdot\vec{q}}, \tag{2.31}$$

where J_{ij} is the same as defined above and $\vec{r}_{ab}$ is the vector between unit cell a and b, where spin i is taken to be in unit cell a, and spin j is taken to be in unit cell b. The vector $\vec{q}$ allows us the freedom to assume that the spin configurations are the same in each unit cell, except that spins in adjacent cells are allowed to change phase corresponding to a factor $e^{-i\vec{r}_{ab}\cdot\vec{q}}$. Such a vector is physical to real problems as it corresponds to some sort of long range ordered state of the kind that could be detected through an appropriate scattering measurement [21].

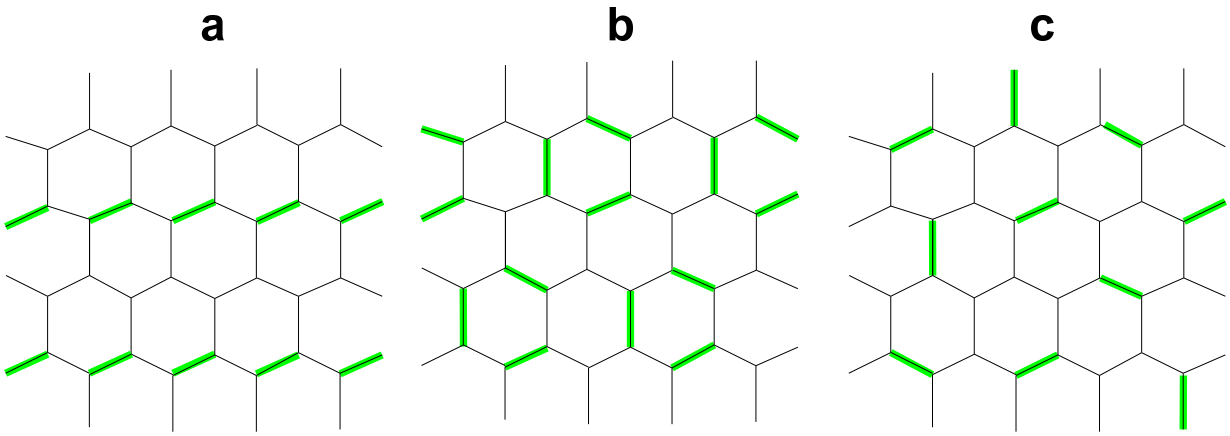

Figure 2.2: Pictures of the different gauge choices considered in this thesis. The highlighted bonds show where $A_{ij} = \pi$. Similar gauges can be constructed by flipping the overall sign of J. **(a)** shows the discrete translationally symmetric (DTS) gauge choice, while **(b)** shows the discrete rotationally symmetric (DRS) gauge choice. **(c)** is an example using a random process to fulfill the fully-frustrated requirement.

For other models the interaction matrix approximation can be very informative. In the case of the triangular model the peaks in **q**-space of the eigenvalues of the interaction matrix correspond to the peaks in the real system when quantum perturbations are added [22], while in the Kagome case the spectrum is completely flat even with quantum effects [4], and the quantum case does not order [23].

We can construct the interaction matrix for the fully-frustrated honeycomb using any of the gauges shown in Figure 2.2 that have a unit cell, that is the discrete translationally symmetric (DTS) gauge or the discrete rotationally symmetric (DRS) gauge. For the DTS

Model	Extensive Entropy	Correlations	Interaction Matrix Result
Triangular	0.323 k_B [4]	$\frac{1}{\sqrt{r}}$ [4]	minima at $\vec{q} = [\frac{4\pi}{3}, 0]$ [22]
Kagome	0.502 k_B [4]	$e^{-r/\xi}$ [4]	flat spectrum [4]
FF-honeycomb	0.214 k_B [12]	$e^{-r/\xi}$ [4]	minima at $\vec{q} = [\frac{\pi}{6}, \frac{2\pi}{6}]$

Figure 2.3: Results for the interaction matrix for different systems. In the triangular and Kagome lattices the interaction matrix relates to the ordering or lack of ordering of the systems, and hence the correlations. In the fully-frustrated honeycomb lattice it fails to predict the lack of order and hence type of correlations.

gauge we get an interaction matrix of the form

$$J \begin{pmatrix} 0 & 1 & 0 & I_{1,4} \\ 1 & 0 & I_{2,3} & 0 \\ 0 & I^*_{2,3} & 0 & 1 \\ I^*_{1,4} & 0 & 1 & 0 \end{pmatrix} \tag{2.32}$$

$$\text{where: } I_{1,4} = -e^{-i\vec{a_2}\cdot\vec{q}} + e^{i(\vec{a_1}-\vec{a_2})\cdot\vec{q}}$$

$$I_{2,3} = 1 + e^{-i\vec{a_1}\cdot\vec{q}}$$

where we use a 4×4 matrix of a unit cell of four spins to simplify calculations. The minimal eigenvalue of this matrix (assuming $r_{AB} = n_1\vec{a_1} + n_2\vec{a_2}$ and $\vec{a_1} = \hat{i}$ and $\vec{a_2} = 2\hat{j}$) is found when $\vec{q} = (\frac{\pi}{6}, \frac{2\pi}{6})$. The minimal eigenvalue's value at this point is $\lambda_{min} = -2.449J$.

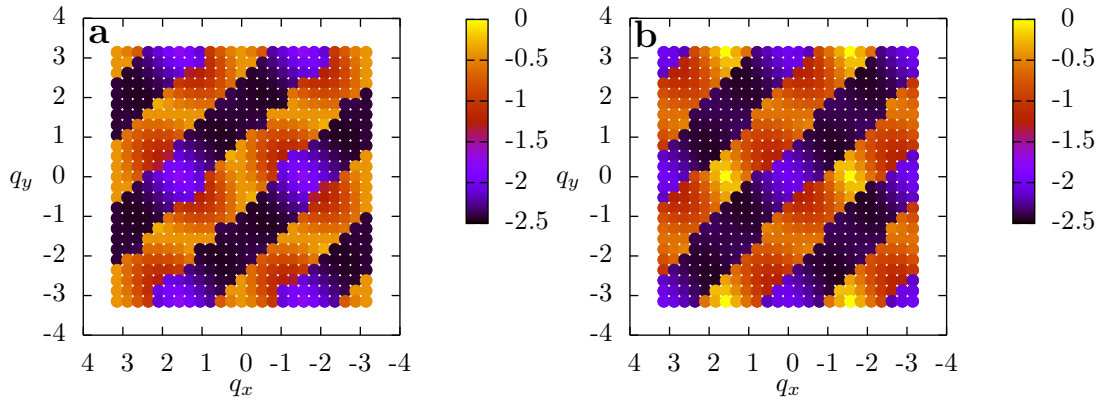

Figure 2.4: The lowest eigenvalue of the interaction matrix for the **(a)** DTS gauge and the **(b)** DRS gauge over the first Brillouin Zone. The square Brillouin zone and basis vectors are chosen in such a way such that these results are directly comparable to the structure factor results presented in later sections.

Using the DRS gauge we need a larger unit cell, but we can construct the interaction matrix in the same way. Using that unit cell we get

$$J\begin{pmatrix} 0 & 1 & 0 & 0 & 0 & I_{1,6} & 0 & I_{1,8} \\ 1 & 0 & 0 & 0 & 1 & 0 & I_{2,7} & 0 \\ 0 & 0 & 0 & 1 & 0 & I_{3,6} & 0 & I_{3,8} \\ 0 & 0 & 1 & 0 & -1 & 0 & 1 & 0 \\ 0 & 1 & 0 & -1 & 0 & 1 & 0 & 0 \\ I^*_{1,6} & 0 & I^*_{3,6} & 0 & 1 & 0 & 0 & 0 \\ 0 & I^*_{2,7} & 0 & 1 & 0 & 0 & 0 & -1 \\ I^*_{1,8} & 0 & I^*_{3,8} & 0 & 0 & 0 & -1 & 0 \end{pmatrix} \tag{2.33}$$

where: $I_{1,6} = -e^{-i\vec{a_2}\cdot\vec{q}}$

$I_{1,8} = e^{-i\vec{a_2}\cdot\vec{q}}$

$I_{2,7} = e^{-i\vec{a_1}\cdot\vec{q}}$

$I_{3,6} = e^{i(\vec{a_1}-\vec{a_2})\cdot\vec{q}}$

$I_{3,8} = e^{-i\vec{a_2}\cdot\vec{q}}$

The minimal eigenvector of this matrix takes the form (assuming $r_{AB} = n_1\vec{a_1} + n_2\vec{a_2}$ and $\vec{a_1} = 2\hat{i}$ and $\vec{a_2} = 2\hat{j}$) is found when $\vec{q} = (\frac{5\pi}{12}, -\frac{2\pi}{12})$. The eigenvalue at this point is again $\lambda_{min} = -2.449J$.

In both cases the eigenvalue spectra have minima corresponding to a unique configuration and **q**-vector that minimizes the energy. Although we know that this classical Hamiltonian retains a disordered degenerate groundstate, one may ask whether the momentum-space location of these minima will correspond to an ordering wave vector when quantum fluctuations are added to this model.

The presence of mixed bonds adds something unique to the fully-frustrated honeycomb model. As mentioned earlier we have a choice of gauge in the A_{ij} variables. What was not immediately clear is that classically any valid choice of the A_{ij} (those that satisfy the constraint in Equation (2.27)) will produce a similar groundstate. By similar we mean that many of the thermodynamic properties, aside from specific spin configurations, are the same. Further discussion of the groundstate can be found in Section 2.3.

2.3 Results from classical Monte Carlo

As mentioned in the section describing classical Monte Carlo algorithms, the fully-frustrated honeycomb lattice takes a bit more work to simulate due to its frustrated nature. When a simple Monte Carlo algorithm is implemented, the system would take a long time to

find the true groundstate of the system, often because it would get stuck in local minima. Figure 2.5 shows the slow decay of the energy as the Monte Carlo algorithm iterates. Although it is easy to construct a particular ground state of the classical fully-frustrated honeycomb model, it is somewhat more difficult to imagine all of the allowed states analytically (although, this was done in [12]). Instead, it is more productive to examine the type of simple moves that take us from one allowed groundstate to another. Single spin flips are always guaranteed to cost energy when we are in the groundstate, so the only way to create moves that do not cost energy is to engineer a move that flips at least two spins. The realization of this cluster move for the case of the classical fully-frustrated honeycomb model is called the chain move.

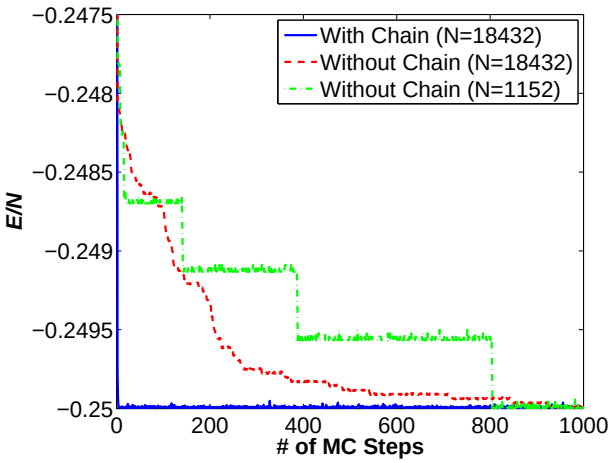

Figure 2.5: This graph shows the energy of the system as a function of the number of Monte Carlo steps with and without chain moves. Without the moves the system becomes stuck in local minima and takes much longer to find the groundstate energy, while with chain moves it is able to find the groundstate energy very quickly. Figure reprinted from [12] with permission from authors.

To simulate the classical fully-frustrated honeycomb Ising model properly, the chain move was designed in such a way that it would either take the system between degenerate groundstates or fix a defect. The chain is constructed by starting on one of the frustrated bonds of the lattice and flipping a tree of spins that only ends upon being connected to another frustrated bond [12]. In this way, the chain guarantees that it takes the system to an equal energy configuration in the absence of anisotropy or an external field. This is important since the equivalent set of single spin flips that would be required to move between these states require going through intermediate states of energy at least $E_0 + J$ and are hence are suppressed in the Monte Carlo algorithm by a factor of $e^{-\beta J}$.

If we look at the restriction of the groundstate, we find that one of the bonds on each plaquette must be unsatisfied. One bond being unsatisfied per plaquette is the exact groundstate independent of any gauge choice. If we looked only at the position of the frustrated bonds and their dynamics in the classical Monte Carlo, we would be unable to differentiate between different gauge choices. Whether each bond is frustrated or not also entirely determines the energy and hence the dynamics of the system. Given a particular state of all the bonds of the system, it is entirely possible to perform the classical Monte Carlo simulation without knowing the precise spins. We can do this because we know the effect of flipping a single spin regardless of the type of bonds it is connected to or the initial orientation of the spin. If one can perform the full simulation without knowing the type of bonds or spins, then they cannot be relevant to the dynamics of the problem, although they remain relevant to observables that depend on the details of the spin configuration, such as total magnetization.

Additionally, one can lift the extensive degeneracy by applying a small uniform magnetic field or by creating one weak bond per hexagon. By changing the problem in the latter way, the groundstate becomes unique (up to spin-inversion) and now the problem of finding the unique groundstate is impossible without the use of the above mentioned loops. When the loops move between non-equal energy states, we use the normal detailed balance condition to decide on accepting a move between the two states. Since the chain is deterministic given a starting spin, the selection probability for moving from one configuration to a valid final configuration after a chain is equal, and we again only need to compare the energies of the two states. When the anisotropy is small, normal single spin flips will not find the global minimum state, but the chains will continue to work at the low temperatures where the anisotropy becomes important. If the anisotropy is large, then even single spin flips will be able to approach the groundstate configuration—although if the anisotropy is large enough then a *new* chain move may be necessary to take one between near degenerate groundstates of the perturbed Hamiltonian. Using the chain moves, the recovery of entropy, implying a unique groundstate, and realization of the lowest energy configuration in the perturbed model are both explicitly found for the classical fully-frustrated honeycomb lattice [12].

When a small field is applied, the extensive degeneracy breaks and we find ourself in a regime where the groundstate entropy scales with the square root of the number of spins in the system. When the field reaches the same strength as the interaction energy, $h/J = 1$, the systems again has an extensive entropy. Figure 2.6 shows the specific heat as a function of temperature, with a soft peak and a second sharp peak, representing partial ordering. We are able to calculate the specific heat using the equation

$$\frac{S(T_2) - S(T_1)}{N} = \int_{T_1}^{T_2} \frac{c_v}{T'} dT'. \tag{2.34}$$

Although the extensive entropy is less than the ground state without a magnetic field, Figure 2.7 shows that it still scales to a non-zero value. For fields larger than $h/J = 1$ the

system loses its extensive entropy and the number of ground states scales with the linear length of the system [12]. At the special field value of $h/J = 3/2$ The system reaches a special symmetric point where the entropy becomes extensive again, and scale to a larger value than in the case of $h/J = 1$, as shown in Figure 2.7

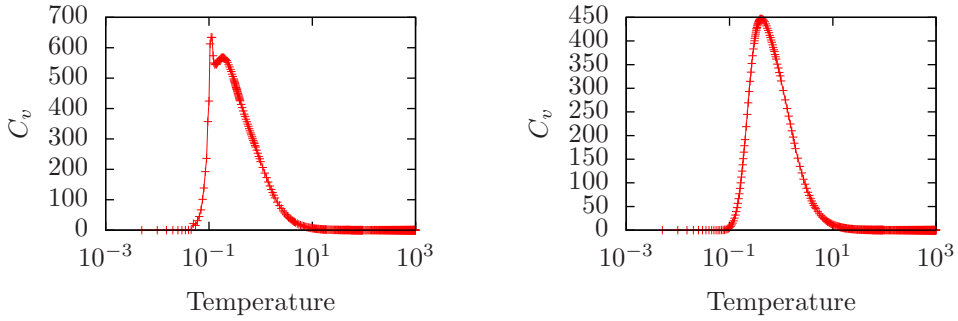

Figure 2.6: The specific heat of the classical fully-frustrated honeycomb when $h/J = 1$ (left) and $h/J = 3/2$ (right), where h is the strength of the external field. Notice the spike at low temperature indicating a second ordering transition when $h/J = 1$ while there is no bump for $h/J = 3/2$.

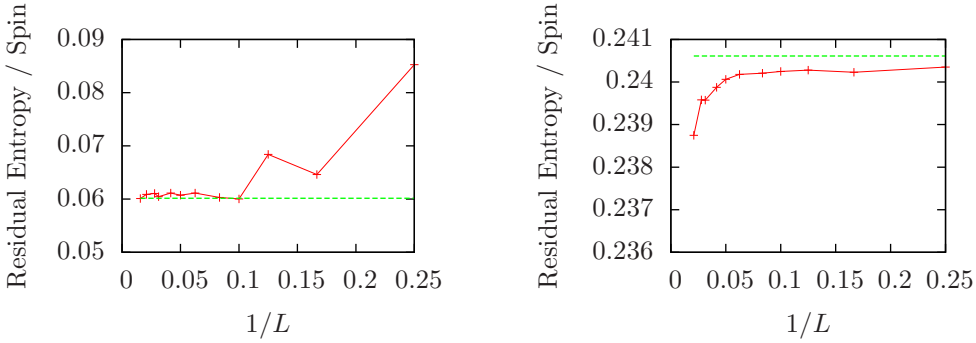

Figure 2.7: The size scaling of the residual entropy of the classical fully-frustrated honeycomb when $h/J = 1$ (left) and $h/J = 3/2$ (right). Both scale to a residual value that is extensive in the number of spins in the system. The dashed green lines show the analytical results from combinatorics in the large L limit.

The results of this classical study at a field was also complimented by a study of all possible ground state configurations using combinatorics. This combinatoric analysis allowed prediction of the extensive entropy and non-extensive entropy for all values of the

external field. For $h/J = 1$ we find the extensive entropy is

$$\frac{S}{N} = \frac{\ln 2}{2L^2} + \frac{1}{8L} + \frac{1}{8}\ln\phi, \tag{2.35}$$

where ϕ is the golden ratio, or $\frac{1+\sqrt{5}}{2}$, and L is the length of the system. In the limit of large L, we find $\frac{S}{N} \approx 0.06015$ [12]. In the case where $h/J = 3/2$ we find the equation of the limiting case is

$$\frac{S}{N} = \frac{1}{4L}\ln\left(\frac{5+3\sqrt{5}}{10}\right) + \frac{1}{2}\ln\phi, \tag{2.36}$$

and we find in the limit of large L that we get a residual entropy of $\frac{S}{N} \approx 0.24061$ [12]. In this way the ground state of the classical fully-frustrated honeycomb Ising model is very well understood, not only in terms of the appropriate simulation needed to explore the manifold of degenerate groundstates but also in terms of the microscopic description of the frustrated manifold and the number of ways it can be rearranged. Note that Figure 2.7 the Monte Carlo results do not exactly converge to the predicted results from the combinatorics method within the bounds of error, suggesting there may be subtle corrections not accounted for or that the Monte Carlo results need to be pushed to even larger sizes.

The fully-frustrated honeycomb is also an interesting problem because the groundstate can be mapped to the groundstate of a hard core dimer problem on a triangular lattice. The hard core dimer problem assumes we have a dual lattice and each site belongs to exactly one dimer, and in this context a dimer is simply an object that connects two nearest neighbor sites on a lattice. The mapping from the fully-frustrated honeycomb is done by first constructing the dual lattice, which is triangular, and then on the dual lattice each bond crosses one bond of the original lattice. Figure 2.8 shows how the frustrated bonds of the fully-frustrated honeycomb model map to the dimers of the hard core dimer model. Where a dual lattice bond crosses a frustrated original bond, we place a dimer. Every plaquette has only one frustrated bond in the groundstate, so for each node at the center of a plaquette it has only one dimer connecting to it. Exactly every node having only one dimer connect to it is precisely the condition of the hard core dimer model, and as long as we are in a groundstate of the fully-frustrated honeycomb the mapping is good.

In the Hamiltonian we have shown so far, the residual entropy of the groundstate was measured to be $S \approx 0.214$ per spin [12]. In the classical hard core dimer model, the residual entropy has also been calculated—in that case it is also known to be the same value [24], suggesting that this mapping allows one to sample all the same relevant configurations in the dual model, up to a constant non-extensive factor.

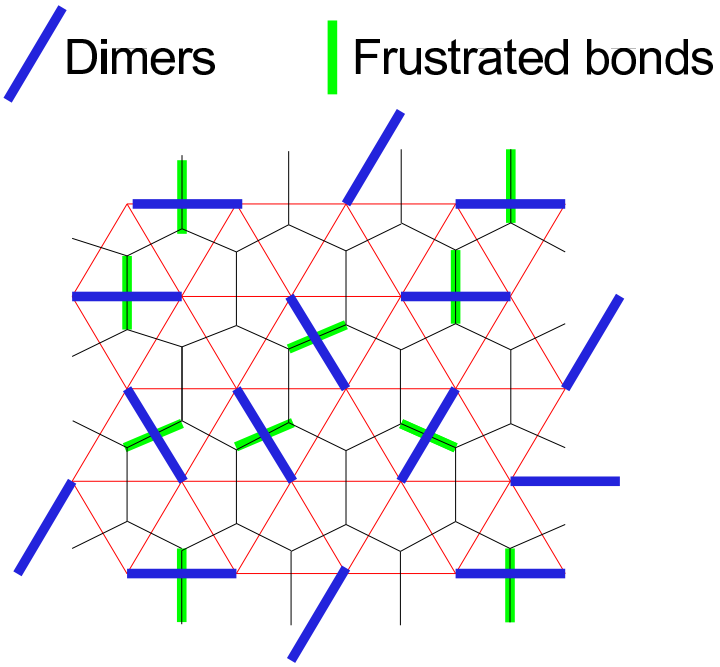

Figure 2.8: The duality mapping of the fully-frustrated honeycomb model to the hard core dimer model on the triangular lattice. Everywhere there is a frustrated bond of the honeycomb model, we insert a dimer on the triangular lattice bond it crosses. In this way, every groundstate of the fully-frustrated honeycomb model has an analogue in the hard core dimer model on the triangular lattice.

Chapter 3

Quantum Monte Carlo Results

3.1 Quantum XXZ Hamiltonian

One extension to the classical Hamiltonian described so far is to add a hopping term to the spins to see the effect on the degenerate groundstate. The new Hamiltonian takes the form

$$\hat{H} = J \sum_{\langle ij \rangle} e^{-iA_{ij}} S_i^z S_j^z - \frac{t}{2} \sum_{\langle ij \rangle} S_i^+ S_j^- + S_i^- S_j^+, \tag{3.1}$$

or the so-called XXZ model. The $\frac{t}{2}$ term can also be written as $S_i^x S_j^x + S_i^z S_j^z$ without the factor of $\frac{1}{2}$. Normally when quantum fluctuations of this sort are introduced they disorder a system. This can be noted by the fact that if we look at the above Hamiltonian in the limit where $J/t \to 0$ we are left with the uniform XY model on the honeycomb lattice. The uniform XY model on a honeycomb lattice is defined by having an off-diagonal order parameter, $\langle S_x \rangle \neq 0$ at $T = 0$, and a non-zero spin stiffness at low temperature [25]. The effect of a disordering interaction on a system which is already highly disordered is then one of interest for this work.

Firstly, we test our method by comparing the energy of the groundstate in the SSE method to that from Lanczos method. The Lanczos method is one where we use the Hamiltonian to iteratively generate an orthogonal set of states, and within this set of states we find are able to find the minimal energy [26, 27, 28]. The method works by taking a random state and applying the Hamiltonian to generate a new state. This new state is then made orthogonal to the states generate so far, and the procedure continues to generate more and more states. This is efficient to do because the nature of the generating method for Lanczos ensures that the expectation of two states sandwiching the

Hamiltonian, $\langle\psi_i| H |\psi_j\rangle$, only has non zero expectation value for a small number of pairs i, j.

If we start with a random state $|f_0\rangle$ we generate new states by applying the Hamiltonian and requiring orthogonality to previous states. This is achieved by

$$|f_1\rangle = H |f_0\rangle - a_0 |f_0\rangle \tag{3.2}$$

where

$$a_m = H_{mm}/N_m, N_m = \langle f_m|f_m\rangle , H_{mm} = \langle f_m| H |f_m\rangle . \tag{3.3}$$

Equation (3.2) guarantees the second state is orthogonal to the first state. We can now attempt to generate the next state in a similar way. For the second state, we can generate it by

$$|f_2\rangle = H |f_1\rangle - a_1 |f_1\rangle - b_0 |f_0\rangle \tag{3.4}$$

where

$$b_{m-1} = N_m/N_{m-1}. \tag{3.5}$$

If we look at the overlap of $|f_2\rangle$ with the previous two states, we get

$$\langle f_2|f_1\rangle = H_{11} - a_1 N_1, \langle f_2|f_0\rangle = N_1 - b_0 N_0, \tag{3.6}$$

which by definition, is zero for both states by construction. We can now define the general equation for new Lanczos states as

$$|f_{m+1}\rangle = H |f_m\rangle - a_m |f_m\rangle - b_{m-1} |f_{m-1}\rangle , \tag{3.7}$$

and the orthogonality with all earlier states is guaranteed by the construction [29]. As a small note, when performing this construction numerically states can become non-orthogonal due to numerical imprecision present in a computer. In these cases it is possible the states are no longer orthogonal, causing obvious problems in the algorithm. This can be fixed by re-orthogonalizing the system every so often.

In the typical Lanczos method, the matrix of expectation values of the Hamiltonian is tridiagonal. Using this set of states we can calculate the expectation of the Hamiltonian for every pair of states and hence are able to calculate the eigenvalues of the system, corresponding to the energies of the reduced basis we are working in. If properly implemented, the minimal energy (or eigenvalue) of the Lanczos method very quickly converges to the exact groundstate energy for the finite system at zero temperature [26, 28].

Figure 3.1 shows how the energy in SSE converges towards the groundstate energy as the temperature is decreased. The fact that for particular parameters the system converges faster or slower should not be seen as an error in the simulation technique, rather this likely reflects the real physics of the system at a finite temperature. Although Lanczos is

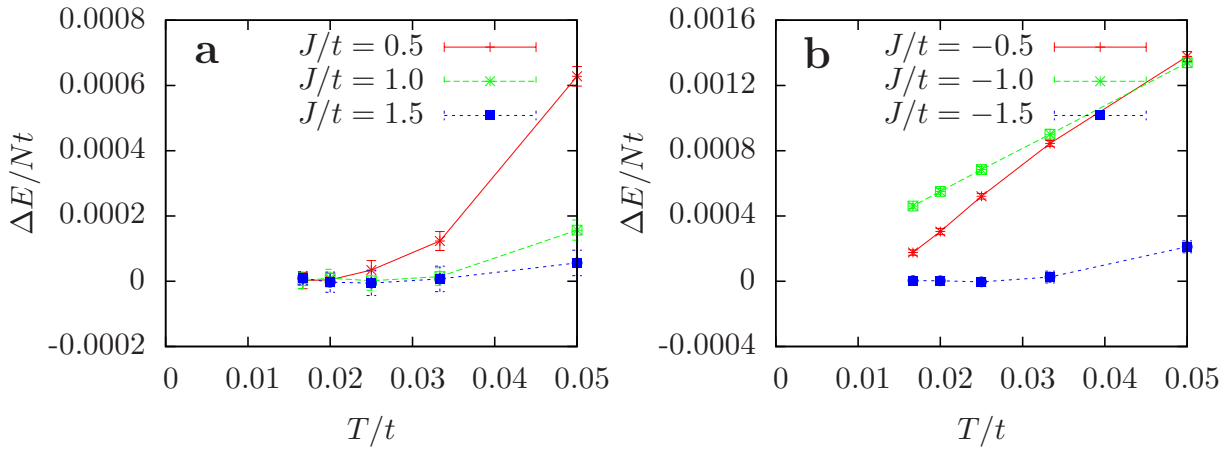

Figure 3.1: The energy of the Monte Carlo simulation with the groundstate energy from Lanczos subtracted on a $3 \times 3 \times 2$ sized system. **a)** shows the system for which $J < 0$ and **b)** shows the system in which $J > 0$. $\Delta E = \langle E_{QMC} \rangle - E_{Lanczos}$.

an efficient method for calculating groundstate properties, it scaled poorly and in general cannot be used to study very large systems. For this reason Lanczos cannot be used to directly study the large lattice sizes needed to extract interesting physics in this model, and a small $3 \times 3 \times 2$ system was used to test the SSE. Beyond this particular implementation, there are many other previous implementations of the SSE, many of which have established the method's ability to reproduce known results [15, 16, 25].

In the sections that follow we will discuss the results for the three gauges, shown in Figure 2.2.

3.2 Discrete Translationally Symmetric gauge

The quantum Monte Carlo performed in this section uses the DTS gauge to satisfy the fully-frustrated requirement. Simulations are run as a single quenched simulation at modestly low temperature, $\beta t = 5$ is first used, to examine properties of the system.

We qualify the general phase diagram of the fully-frustrated honeycomb XXZ model by examining the spin stiffness as a function of J/t. In the limit of $J/t \to \infty$ the model is exactly the classical fully-frustrated honeycomb Ising model, for which the phase diagram is well understood. In the limit of $J/t \to 0$ the model becomes the XY model on the honeycomb lattice—a model we discussed in the earlier section of this thesis, and for which the spin-wave description is fairly accurate. In Figure 3.2 we see that the spin stiffness

is very close to the classical prediction of spin-wave theory from Equation (2.25). The simplest way to examine the intermediate region is to look at the behavior of simple order parameters as a function of the J/t parameter. We use the spin stiffness as the parameter of interest to examine the general behavior over the range of J/t.

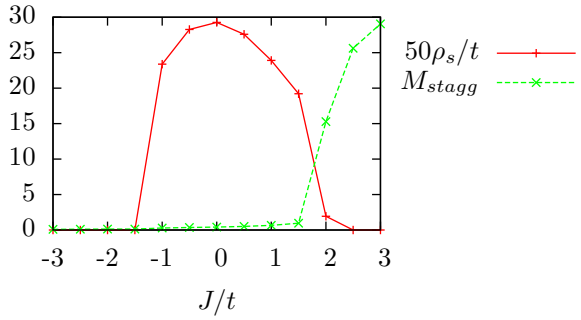

Figure 3.2: The spin stiffness of the DTS gauge as we vary J/t with $L = 24$ and $\beta = 10$. Notice the spin stiffness is a maximum at the point where the model is equivalent to the XY-model, and decays reaching zero by $|J/t| > 2$.

Figure 3.2 shows that in this gauge choice it is easy to see the transition from a phase with non-zero spin stiffness to one with sublattice order as $J/t \gtrsim 1.75$. At this point the spin stiffness quickly drops and the sublattice magnetization turns on. Initial work on this system shows that the transition from the phase where the spin stiffness parameter is non-zero to the phase where the sublattice magnetization is non-zero becomes sharper as system size is increased and temperature decreased. In this sense we expect that there is no value of J/t for which a non-zero sublattice magnetization and non-zero spin stiffness would survive in the thermodynamic limit of an infinite lattice at zero temperature.

Considering that we know the behavior of the system in the limits of very large or very small J/t, the question is then what occurs for intermediate regimes. Of particular interest is the phase where there is no spin stiffness, but also non-trivial quantum fluctuations. We believe that this phase is the one that best represents a classical disordered groundstate perturbed by quantum fluctuations. With this in mind, most of the properties we discuss are studies of the system with $J/t = \pm 3$. Simulations are performed for larger values of J/t, but the SSE uses the off-diagonal operators of the Hamiltonian to sample configuration space. If the off-diagonal operators only make up a small fraction of the Hamiltonian this sampling is inefficient and new algorithms would need to be introduced to restore the ergodicity of the algorithm.

For large simulations ($24 \times 24 \times 2$ sites, 24 unit cells in the x and y directions, and two spins per unit cell) the DTS gauge with $J < 0$ has difficulty finding the exact groundstate, as shown in Figure 3.3. After understanding the problem through analyzing the lattice

spin configuration, we chose to use an annealing algorithm to remove the defects of the lattice.

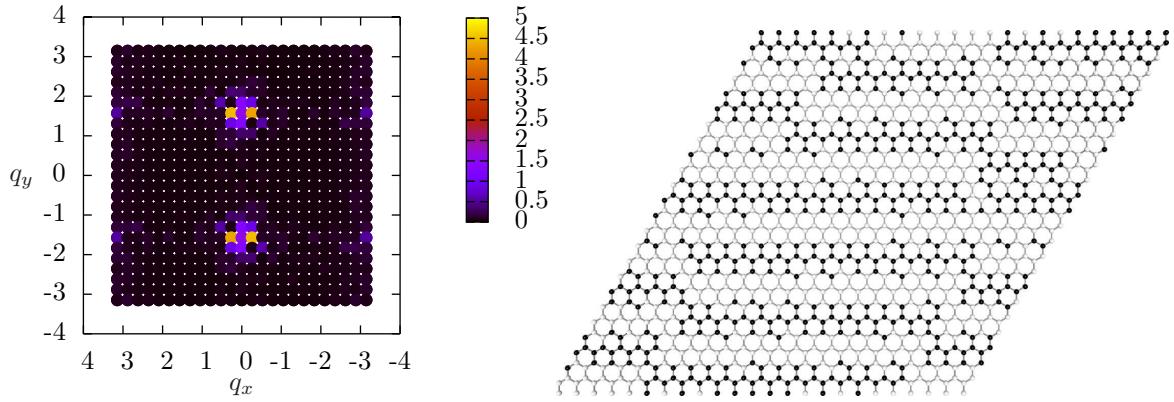

Figure 3.3: (left) The structure factor of the DTS gauge when $J < 0$. For this picture the system was not annealed and found to contain a defect that can be seen in the real-space snapshot of $|\alpha_0\rangle$ at the end of the simulation (right). The defect can be seen as a kink in the layers of white (spin up) and black (spin down) particles on the lattice, and if often referred to as a screw dislocation [30].

The annealing algorithm is quite simple, and more complicated schemes are available to implement if this scheme had failed. We start the system at a high temperature and run Monte Carlo steps until the system reaches equilibrium. We then use the configuration, corresponding to a particular choice of $|\alpha_0\rangle$ and a valid choice of operator list S_M, and use this as the initial configuration for a simulation at a lower temperature. The process of re-equilibration and changing temperature is repeated until the target temperature is reached. Using this process, the structure factors in Figure 3.4 are generated. With proper annealing both peaks signify strong order, and the peak values scale with the number of spins, indicating Bragg peaks.

Later analysis uses the real-space image of the lattice to verify the type of order that the strong peaks corresponded to. Initial attempts to visualize the lattice simply mapped the current step of the simulation, $|\alpha_0\rangle$, directly to up and down spins on the lattice. This is an interesting method, but in the SSE formalism, any random $|\alpha_i\rangle$ carries no particular meaning, except that averaging diagonal operator expectation values over the set $\{\alpha\}$ gives the expectation of that operator. With this understanding we then collected statistics, notably $\langle S_i^z \rangle$ and $\left\langle S_i^+ S_j^- + S_i^- S_j^+ \right\rangle$, to generate images. In this way, the image truly represented the real-space version of the data that was being Fourier transformed to generate the sublattice structure factors. Any patterns visible in the structure factor should also be visible in the real-space image. Patterns for the two structure factors in

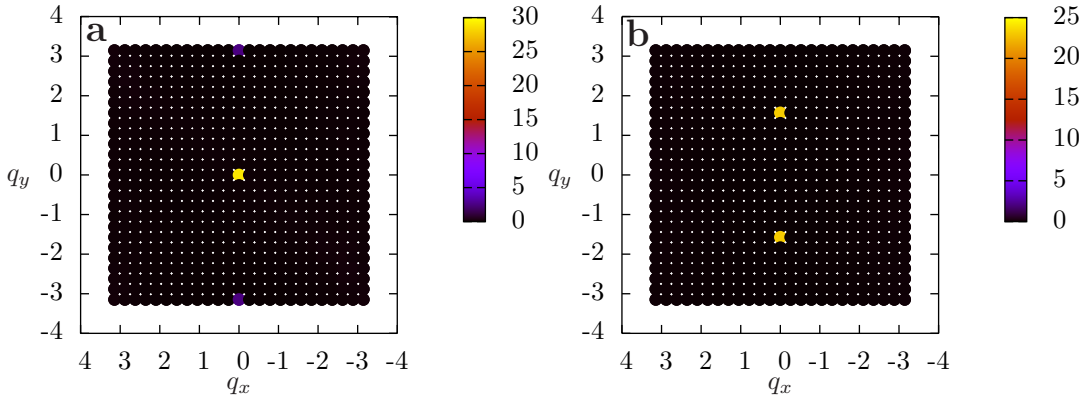

Figure 3.4: The sublattice structure factor of the spin-spin correlation function of the DTS gauge when **(a)** $J > 0$ and **(b)** $J < 0$ using annealing. Compare the sharp peaks found in this case to the double peaks found without annealing in Figure 3.3.

Figure 3.4 are shown in Figures 3.5,3.6.

Let us now turn to the real-space images of the lattice and confirm that sublattice structure factors correspond to the order observed in them. In the case where $J > 0$, the order is primarily antiferromagnetic, with spins on each sublattice pointing opposite to spins on the other sublattice. For the honeycomb lattice a sublattice structure factor was often used rather than the full structure factor. This is because when decomposing the lattice as a Bravais lattice with a basis, the calculations remain simple if we only consider one species per unit cell. Examining the sublattice structure factor allows us a simple interpretation of the results along the lines of the basic results presented earlier. If we examine the sublattice structure factor, it should have a $\mathbf{q} = (0, 0)$ peak, corresponding to a sublattice magnetization. The structure factor has one other subtle feature—two small symmetric peaks at $\mathbf{q} = (0, \pi)$ and $\mathbf{q} = (0, -\pi)$. These two peaks refer to the same order and suggest that in addition to the sublattice magnetization, spins vertical to one another (on the same sublattice) are weakly anti-parallel. Looking more closely at the real-space image, spins connected to bonds where $A_{ij} = \pi$ are reduced in magnetization, and occur every second layer. This reduction every second layer is picked up by the structure factor as the smaller signatures. A final important point is that all the peaks in the structure factor occur for $q_x = 0$, implying translational symmetry in the x-direction of the lattice. Examining the visualization this translational symmetry is easily spotted.

With the above measures we can now describe the nature of the groundstate. First of all, the strong peaks in the spin-spin structure factor suggest that the material is crystalline, in so far that the spins are primarily localized. In both cases local fluctuations persist, but as the phase diagram in Figure 3.2 shows, the system has no spin stiffness despite these

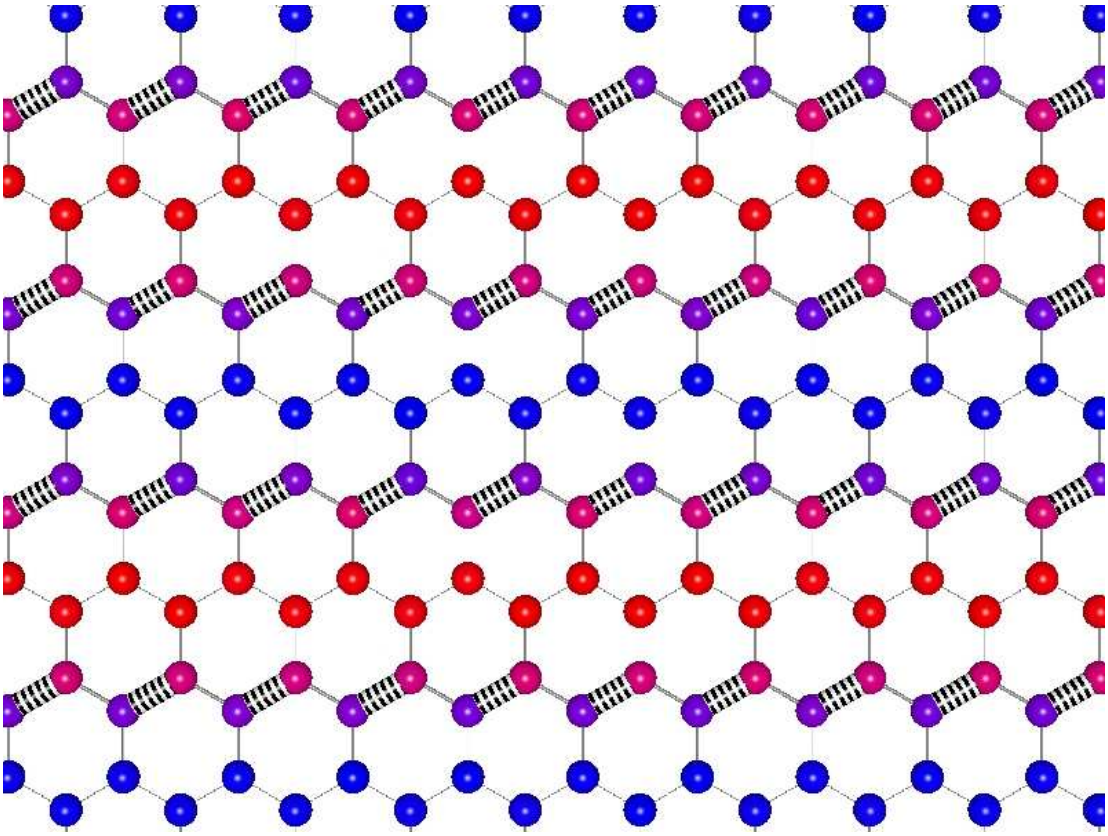

Figure 3.5: The real-space image of the DTS gauge when $J < 0$. The variables represented are in the image are $\langle S_i^z \rangle$ (color of the spins) and $\left\langle S_i^+ S_j^- + S_i^- S_j^+ \right\rangle$ (thickness of the bonds). The spins range from blue ($\langle S_i^z \rangle = -0.5$) to red ($\langle S_i^z \rangle = 0.5$) with purple representing a site that spends equal time up and down ($\langle S_i^z \rangle = 0$). All of the bond thicknesses are normalized such that the thickest bond's diameter is 80% the diameter of the spheres.

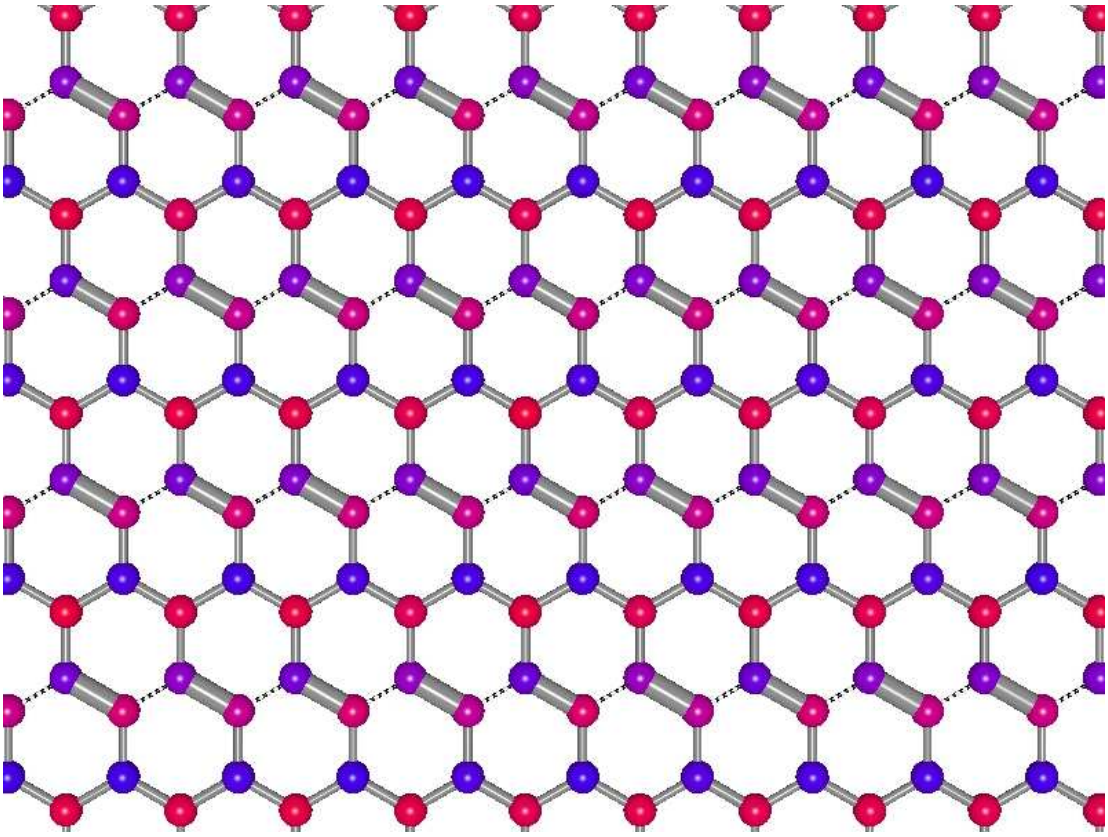

Figure 3.6: The real-space image of the DTS gauge when $J > 0$. The variables represented are in the image are $\langle S_i^z \rangle$ (color of the spins) and $\left\langle S_i^+ S_j^- + S_i^- S_j^+ \right\rangle$ (thickness of the bonds). The spins range from blue ($\langle S_i^z \rangle = -0.5$) to red ($\langle S_i^z \rangle = 0.5$) with purple representing a site that spends equal time up and down ($\langle S_i^z \rangle = 0$). All of the bond thicknesses are normalized such that the thickest bond's diameter is 80% the diameter of the spheres.

fluctuations. A lack of spin stiffness implies that the spins are never transported around the boundary when sampling valid operator expansions S_M. This is because there is a close relation between the winding of spins around the boundary and the spin stiffness. The spin stiffness is related to the winding of spins across the boundary by the equation, derived in [31, 32],

$$\rho_\alpha^W = \frac{1}{\beta} \left\langle W_\alpha^2 \right\rangle, \quad \alpha \in \{x, y\} \tag{3.8}$$

where W is the number of (signed) number of spins that wind around the boundary of the system in the expansion S_M. Consequently, this implies that the fluctuations only move the spins short distances.

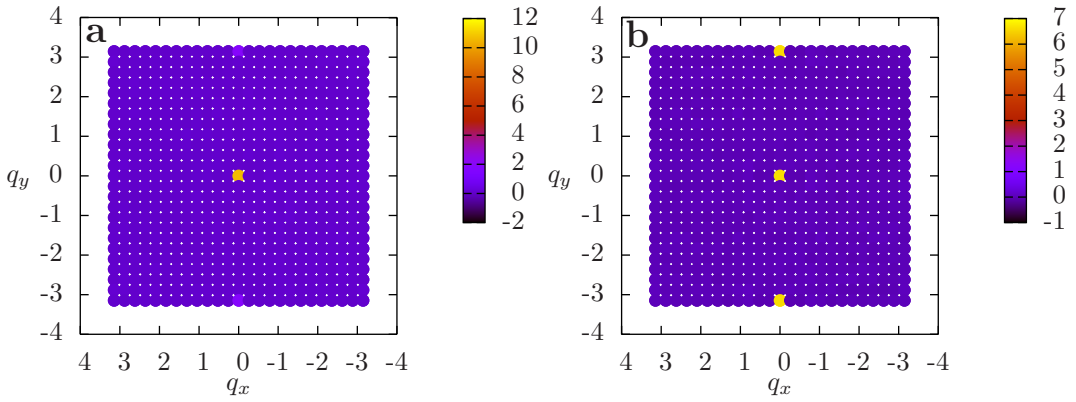

Figure 3.7: The sublattice structure factor of the bond-bond correlation function of the DTS gauge for the sublattice of bonds with the largest value of $\left\langle S_i^+ S_j^- + S_i^- S_j^+ \right\rangle$ when **(a)** the $J > 0$ and **(b)** $J < 0$ using annealing. Notice the central peaks indicating a non-zero value of the bond parameter and a fairly flat spectrum otherwise. The peaks at $\mathbf{q} = (0, \pm\pi)$ (more prominent in **(b)** but also present in **(a)**) show that in addition to the overall order, there is vertical modulation.

If we look where the fluctuations occur, there is a preferred bond for both signs of J/t that fluctuates more than the rest. This time we can use our real-space image to predict that there should be peaks in the bond-bond structure factor. Considering that we have invariance in the x-direction in both system, we expect any peaks (if they exist) should occur for $q_x = 0$, and the two layer vertical modulation in the system (from thick to thin bonds on the same sublattice) suggests peaks should occur at $q_y = \pm\pi$. The structure factor of the bond-bond correlation function in Figure 3.7 shows that this is indeed the case. With long range order in the bonds for both cases, we could describe the system as a partial valence bond crystal (often called a valence bond solid) in addition to a spin crystal. We use partial here to distinguish from the case where every spin is part of a valence bond,

which is not the case of this groundstate. This phase has been found in other works, and has also been referred to as a CDW-VB (charge density wave valence bond) phase [33].

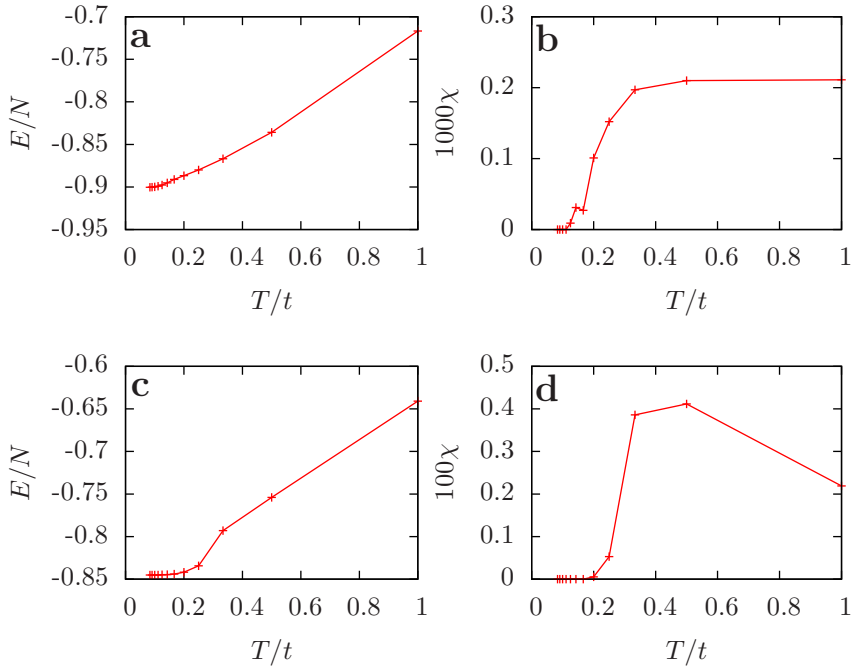

Figure 3.8: The low temperature thermodynamic properties of the DTS gauge. The **(a)** $J > 0$ energy levels off and the **(b)** magnetic susceptibility drops to zero by $T/t \approx 0.1$, showing that the groundstate does not permit single spin flips, but potentially allows moves that conserve the total number of spin up and spin down. For the case where $J < 0$ the **(c)** energy and **(d)** magnetic susceptibility flatten out and go to zero, respectively, by about $T/t \approx 0.2$. Notice the difference in scale for the case when $J < 0$ for the magnetic susceptibility, likely due to the $J < 0$ case allowing large clusters of spins to flip since it prefers spins to be aligned where $A_{ij} = 0$.

Thermodynamic properties of the groundstates for both signs of J are shown in Figure 3.8. In both cases the energy decreases with temperature and saturates by $T/t \approx 0.2$ when $J > 0$ and $T/t \approx 0.1$ when $J < 0$. Similarly, the magnetic susceptibility remains finite but sharply decreases to zero at these same points. For this reason, we describe the groundstate as zero magnetic susceptibility phases, ones in which the total number of spins is fixed with strong order in the spins where they are localized. The localization can be seen through the lack of spin-stiffness, which only exists when spins wind around the lattice. When the spins do fluctuate, they usually do it in a very confined region to reduce the kinetic energy of the system, but motion on the length scale of the system is highly suppressed.

In examining the low energy manifold we lower the temperature to the point that single spin flips no longer occur. At this temperature, the system chooses one of the symmetry broken groundstates and is unable to fluctuate to the other symmetry broken state. We can see this by examining the expectation of $\langle S_i^z \rangle$ for each spin and noticing that when the magnetization fluctuates away from zero, the groundstate samples both symmetry broken groundstate when $J > 0$. Once such magnetization fluctuations stop, the system is no longer able to sample the spin inverted state. In the case where $J < 0$ the system tends not to fluctuate between the two sectors until higher temperatures, likely due to the ferromagnetic spin clusters costing a large amount of energy to break. The only moves allowed at this temperature are the swapping of two spins to minimize the kinetic energy of the system.

If we imagine the quantum term as a perturbation to the classical Hamiltonian, keeping in mind that the groundstate of the classical Hamiltonian is extensively degenerate, we would suspect that the quantum terms would choose a superposition of classical configurations that minimize their energy. In this light, we examine the groundstate configurations of the model presented above. There are two points to note that arise naturally from the nature of the groundstate restriction. The first is that the hopping must occur on a satisfied bond with $Je^{A_{ij}} = |J|$, or a bond that is satisfied when the spins on it take opposite sign. The second restriction is that two of the four legs connecting the pair must be frustrated in the initial configuration to ensure that if we are in a valid classical configuration before the flip, we remain in a valid classical configuration after the flip. Figure 3.9 shows a cartoon of one of the local configurations that when flipped keeps one within the classical manifold of states.

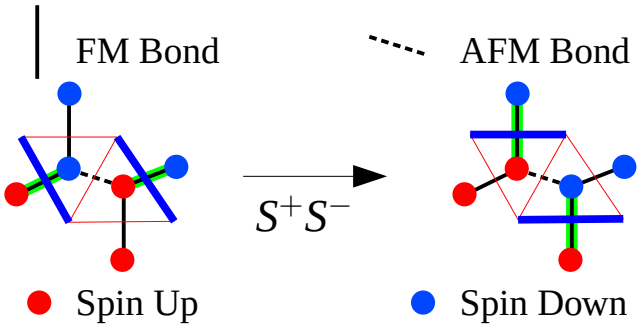

Figure 3.9: A cartoon of the action of the $(S_i^+ S_j^- + S_i^- S_j^+)$ element of the Hamiltonian on a local configuration of spins. Notice that the number of frustrated bonds does not change, nor does the number of frustrated bonds per hexagon. If the initial configuration is part of a valid classical groundstate, so if the final configuration.

Using this cartoon picture we see that configurations satisfying Figure 3.9 minimize

kinetic energy without costing classical energy. If we extend this to the full lattice and keep in mind that the groundstate minimizes the sum of the kinetic and classical energy, then the configurations that allow the most satisfying configurations while also being a valid groundstate of the classical Hamiltonian should minimize the quantum Hamiltonian. If we extend this to the full lattice and keep in mind that the groundstate minimizes the sum of the kinetic and classical energy, then the groundstate Examining the state we extract through Monte Carlo we find that the thick bonds occur precisely where exchanging two spins causes no change to the classical energy. Looking more closely at Figures 3.5,3.6, there are 1-dimensional chains of spins that although highly fluctuating, have a preferential orientation. If we imagine starting from the configuration described by each spin in the orientation that it spends most of the time in, we see now that any of the spins may be swapped along the large chains to minimize kinetic energy without costing classical energy. The second result from this thought experiment is that we see that flipping one spin in a chain precludes both of its neighbors from flipping. If this scenario is correct, we should be able to see a signature of this repulsion in the bond-bond correlation function. Indeed, Figure 3.10 shows how within a layer there are short range correlations, but bonds on differing layers interact weakly if at all.

3.3 Discrete Rotationally Symmetric gauge

In the DTS system the addition of quantum terms to the Hamiltonian changes the groundstate from a massively degenerate set of classical configurations to some quantum superposition of them that breaks translational symmetry. This is perhaps unsurprising, as the nature of the quantum term is very sensitive to the sign of the classical interaction between two spins. The DRS gauge is constructed in such a way as to minimize additional symmetry breaking, although it requires quadrupling the unit cell from 2 to 8 spins. The super-cell has a reduced rotational symmetry when compared to the original lattice—it must be rotated by $2\pi/3$ about one of the hexagons with $\sum_{ij} A_{ij} = 3\pi$ to recover the same lattice. By comparison, a general honeycomb lattice only requires being rotated by $\pi/3$ about any hexagon to return to the same lattice, as shown in Figure 3.11.

As before, the first thing to examine is the spin stiffness as a function of J/t, to see where the model transitions to an zero spin stiffness phase and becomes more interesting to study. Unlike the DTS gauge, this system never exhibits sublattice magnetization for either sign of J. The phase diagram for this choice of gauge can be seen in Figure 3.12, and it carries the same general characteristics that the DTS system did. Due to the similar phase diagram, we chose to study this system at $J/t = \pm 3$ as well. Like in the previous case, the two limits of this model, $J/t = 0$ and $J/t = \pm\infty$, are the known XY-model honeycomb and classical fully-frustrated honeycomb Ising model.

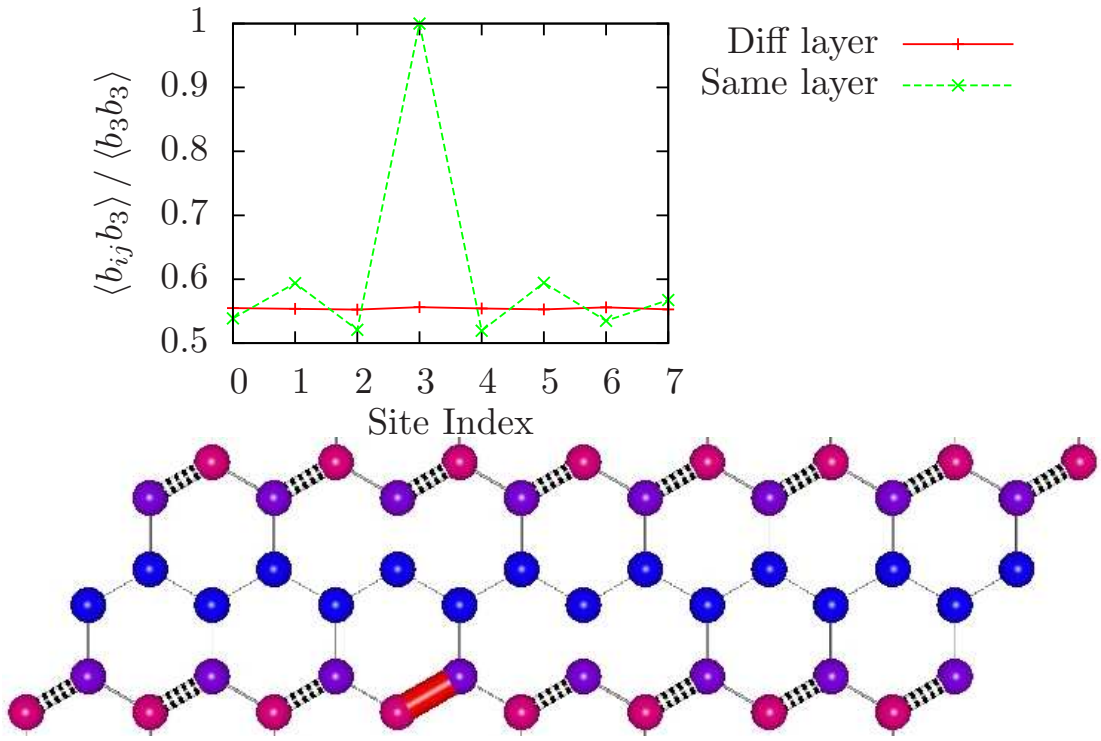

Figure 3.10: The (left) sublattice bond-bond correlation function and (right) the real-space image of the bond-bond correlation function, both using the third bond (marked in red) as a reference. Notice the slight anti-correlation of nearest neighbors when compared to differing layers, for which only interactions between fluctuations are much weaker.

Although this gauge likely leads to a different quantum groundstate, the classical manifold of allowed states is very similar to that from the DTS gauge. If we ignore specific spin configurations and think only in terms of patterns of frustrated bonds, the DRS gauge has the same set of classical configurations when compared to the DTS gauge. In this perspective, we may get some similar properties when examining how quantum fluctuations change the system. One difference we might expect is that the number of groundstates is larger due to the different symmetry of the system. In the case of the DTS the second symmetry broken state can only be reached by overall spin-inversion. For the DRS gauge there should exist spin-inversion symmetry and perhaps rotational symmetry (if the groundstate breaks rotational symmetry) meaning we can expect as many as six symmetry breaking groundstates.

As with the DTS gauge we studied a $24\times24\times2$ lattice at low temperature to examine the groundstate properties. The structure factor of the sublattice spin-spin correlation function

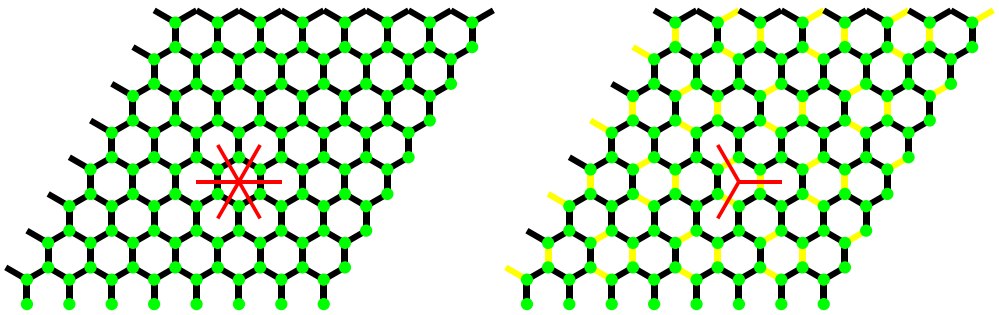

Figure 3.11: Rotational symmetry of the DRS gauge. The red lines show far the system must be rotated to return to the original lattice for the normal honeycomb (left) and DRS gauge (right). There is also reduced translational symmetry. Green dots represent sites, while black lines represent normal bonds and yellow lines bonds where $A_{ij} = \pi$.

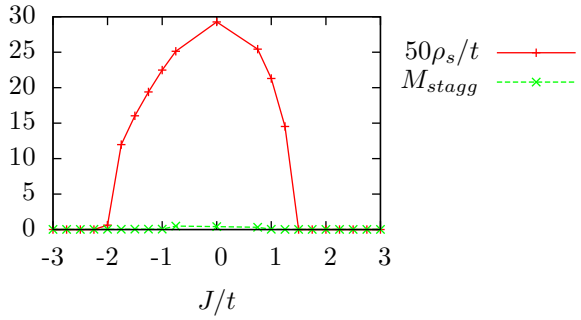

Figure 3.12: The spin stiffness of the DRS gauge as we vary J/t. The points where the spin stiffness goes to zero are very similar to the DTS gauge (figure 3.2) on both sides, suggesting that the number of bonds where $A_{ij} = \pi$ may be the leading factor in the transition.

is shown in Figure 3.13. These structure factors have peaks that scale with the number of spins in the system, indicating long range order. The weaker peaks indicate a more subtle order that exists along side the primary Bragg peaks. In the case of Figure 3.13**a** the main peaks suggest that within each layer moving over two cells will result in landing on a spin of opposite orientation. The fact that the peaks have $q_y = 0$ describe translational symmetry in the y-direction. The smaller peaks at $q_y = \pm\pi$ suggest an anti-symmetry between adjacent layers which can can be seen more clearly in Figure 3.15. For the other choice of J the strong peaks are at $q_x = \pm\pi$ and all peaks lie on $q_y = \pm\pi/2$. Such strong peaks in this case indicate moving in the x-direction one cell and in the y-direction two cells, one ends up on a spin of the opposite orientation from the one started at. The weaker

peaks at $q_x = 0$ signify a weak sublattice magnetization between vertical rows. All of these strong and weak peaks can be seen in the visualization of each site's average magnetization.

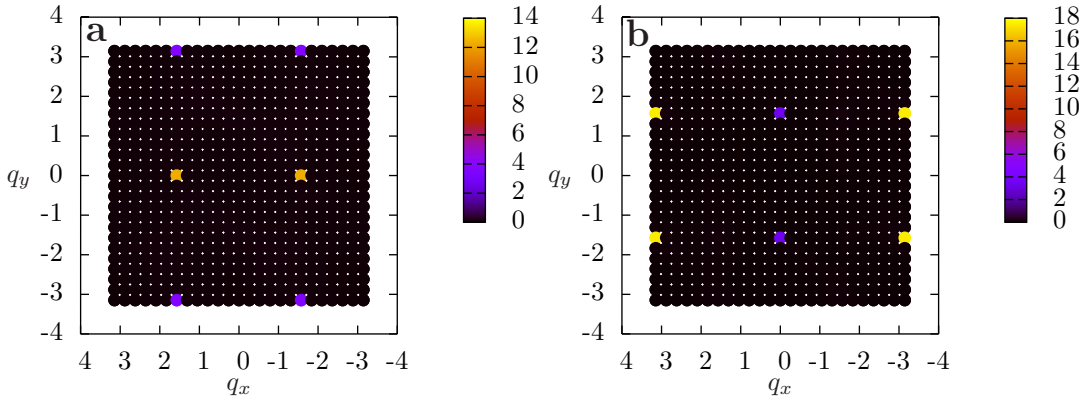

Figure 3.13: Sublattice structure factors of the DRS gauge for one of their six symmetry broken states when **a)** $J > 0$ and **b)** $J < 0$. The other three states correspond to rotations of the above configuration, keeping in mind that the underlying symmetry is triangular rather than square.

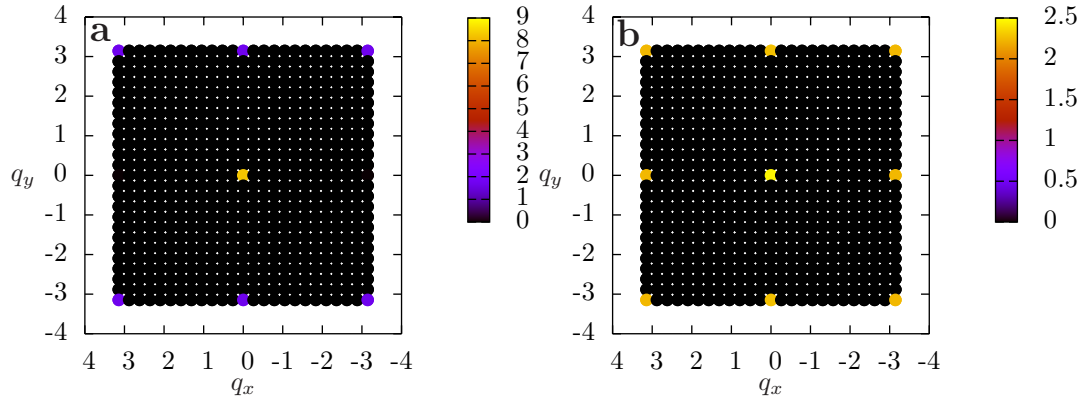

Figure 3.14: The bond-bond structure factor for the DRS gauge for **(a)** $J > 0$ and **(b)** $J < 0$. In both cases the sublattice containing the thick bonds has been selected to show their order. In both cases we have strong central peaks, with different edge behavior due to the fluctuations on the non-thick bonds. When $J > 0$ these bonds have an expectation of the hopping operator comparable to the highly fluctuating bond, while when $J < 0$ these bonds have a very small expectation value.

The main different between the DTS gauge and the DRS gauge is that in the case of the latter, the highly fluctuating bonds have no preferential spin configuration. In the

case of the DTS gauge one of the two spins spends more time up than down, and the other spends more time down than up. This is because for the neighbors to fluctuate, that configuration is required on the neighboring pair. In the case of the DRS gauge the nearest similar configuration is far enough away that each highly fluctuating bond can be in either configuration equally and not affect the fluctuations of the other highly fluctuating bonds. In addition to this, the higher symmetry of the lattice causes the the thick bonds to form a triangular lattice like pattern as opposed to simply stripes as in the DTS gauge.

Figure 3.14 shows the long range sublattice order in the bonds. The bond ordering and spin ordering are both reflected in the real-space pictures of the lattice shown in Figures 3.15,3.16. The long range order in both structure factors lead us to classify this groundstate as a crystalline state, similar to the DTS gauge. We again have locally fluctuating pairs, but the bulk of the lattice has long range order that does not fluctuate in the groundstate. Due to the ordering of the fluctuating bonds, it would also be appropriate to call this groundstate a partial valence bond crystal or in the CDW-VB phase. We use "partial" here again is to distinguish from the picture of a valence bond solid, where every spin is in an a valence bond.

The low temperature thermodynamic properties of the system also suggest a solid phase. Figure 3.17 shows we have similar behavior to the DTS gauge case where fluctuations in the total number of spins are frozen out when the temperature is reduced below $0.1t$. The long range order and lack of overall spin fluctuation further suggest this groundstate as a solid phase with only local fluctuations.

Examining the quantum term as a perturbation from the classical manifold again, we can look for configurations that satisfy Figure 3.9 to see if our previous reasoning still applies. If we examine the highly fluctuating bonds, for either orientation of an up and down spin on each pair the classical energy cost is identical, and minimal. To first order, each pair can fluctuate independently to minimize the energy of the quantum Hamiltonian. In the case where $J < 0$, most of the bonds tend not to fluctuate. Those that do fluctuate do so at a very reduced scale, as aside from the thick bonds such fluctuations will cost classical energy. The case where $J > 0$ is more interesting, as more of the bonds can potentially fluctuate. Examining the pattern carefully, the bonds on the same sublattice as the thick bonds tend to have more hopping than the other sublattices. We could look at this as two different 1-dimensional chains competing for order to minimize the quantum energy. The reason there are not three competing directions is that in the third direction, the sublattice contains bonds where $A_{ij} = \pi$ and hence hopping on these bonds does not occur within the classical manifold of states.

In longer simulations, the DRS gauge is able to sample three rotationally symmetric groundstates without leaving the zero magnetization sector. This can be seen in Figure 3.18 by the purple background color of the spins. One thing to check is whether the true groundstate is one of three distinct groundstates or a superposition of all three. To do this,

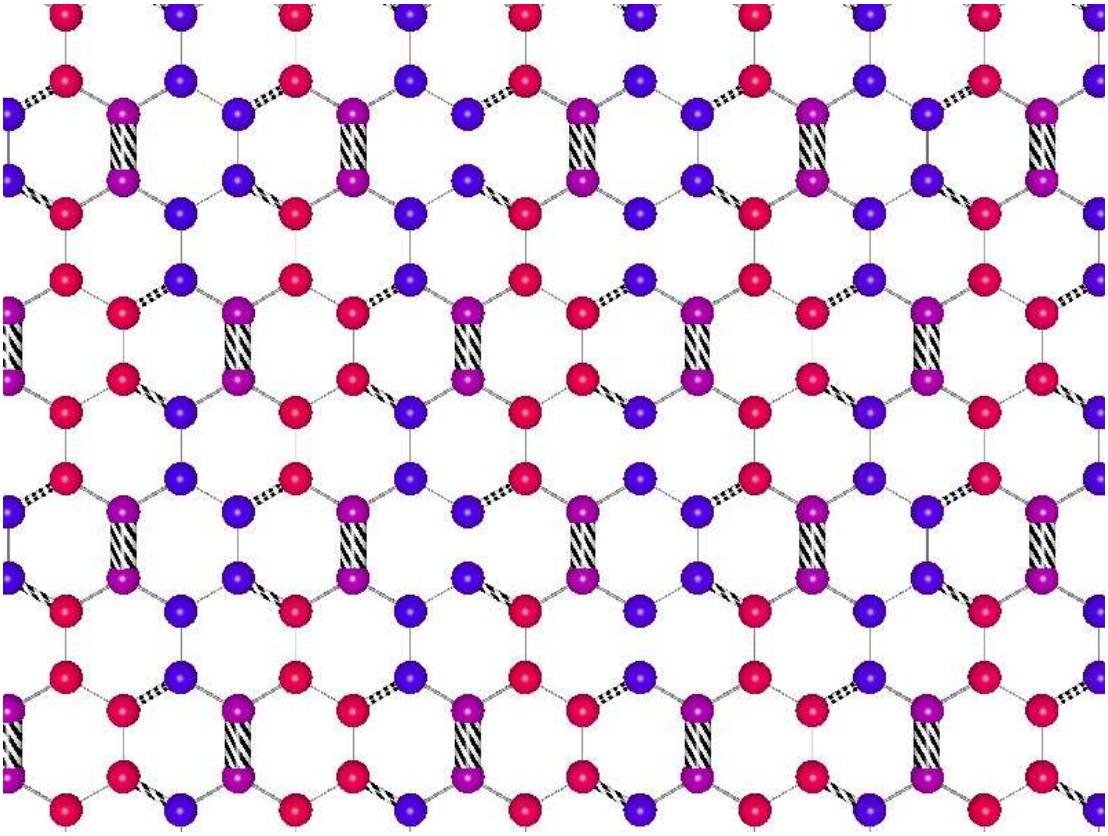

Figure 3.15: The real-space image of the DRS gauge when $J < 0$. The variables represented are in the image are $\langle S_i^z \rangle$ (color of the spins) and $\left\langle S_i^+ S_j^- + S_i^- S_j^+ \right\rangle$ (thickness of the bonds). The spins range from blue ($\langle S_i^z \rangle = -0.5$) to red ($\langle S_i^z \rangle = 0.5$) with purple representing a site that spends equal time up and down ($\langle S_i^z \rangle = 0$). All of the bond thicknesses are normalized such that the thickest bond's diameter is 80% the diameter of the spheres. Notice the pattern of very thick bonds forms a triangular lattice.

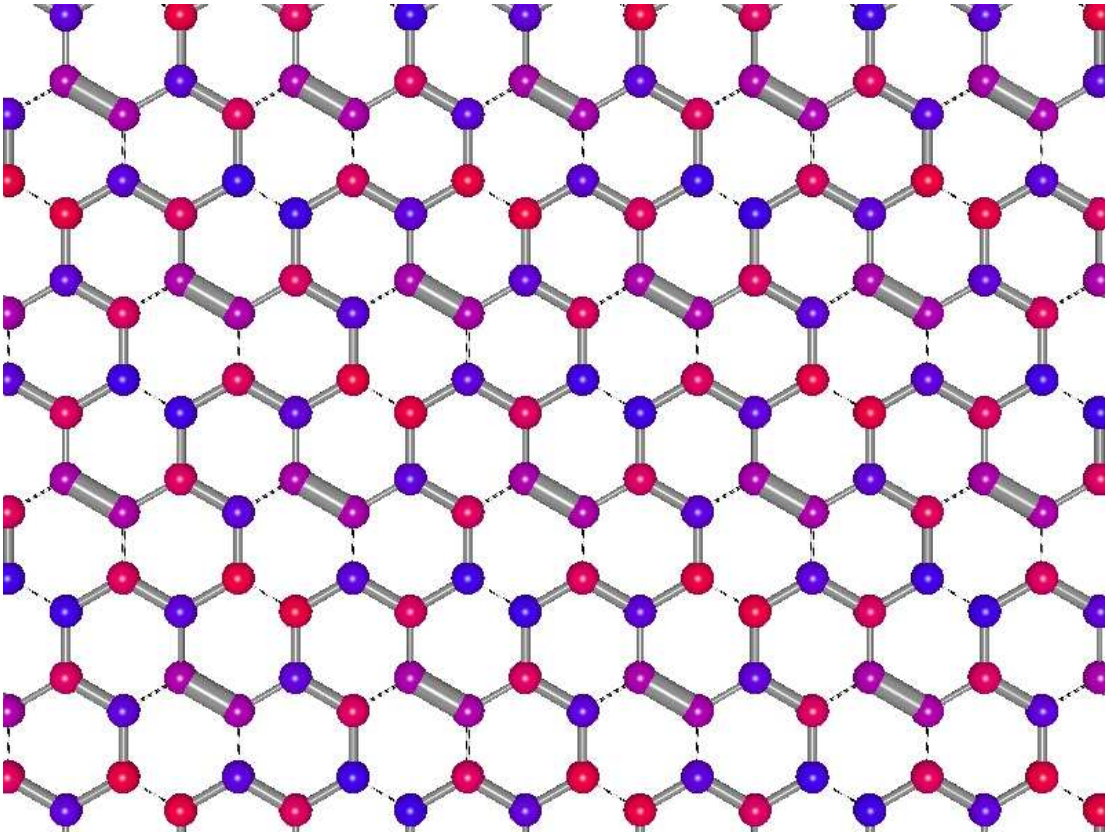

Figure 3.16: The real-space image of the DRS gauge when $J > 0$. The variables represented are in the image are $\langle S_i^z \rangle$ (color of the spins) and $\left\langle S_i^+ S_j^- + S_i^- S_j^+ \right\rangle$ (thickness of the bonds). The spins range from blue ($\langle S_i^z \rangle = -0.5$) to red ($\langle S_i^z \rangle = 0.5$) with purple representing a site that spends equal time up and down ($\langle S_i^z \rangle = 0$). All of the bond thicknesses are normalized such that the thickest bond's diameter is 80% the diameter of the spheres. Notice the pattern of very thick bonds forms a triangular lattice.

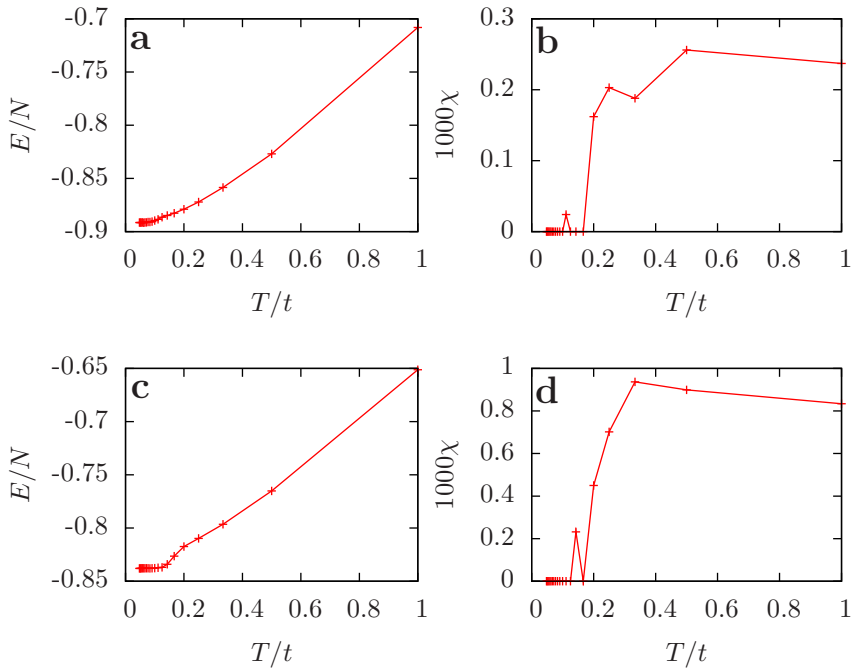

Figure 3.17: The low temperature thermodynamic properties of the DRS gauge. The **a)** $J > 0$ energy levels off and the **b** magnetic susceptibility drops to zero by $T/t \approx 0.1$. This behavior is identical to the DTS case where the groundstate did no allow single spin flips. For the case where $J < 0$ the **c)** energy and **d)** magnetic susceptibility flatten out and go to zero, respectively, by about $T/t \approx 0.1$. We again have a difference in scale between the $J < 0$ and $J > 0$ case, with the $J < 0$ case having a larger magnetic susceptibility.

we look at $\langle S_{A_i} S_{A_j} \rangle$, where each S_{A_i} corresponds to the structure factor for a particular groundstate. When $i = j$ we extract information about the magnitude of each ordered state, while when $i \neq j$ we see if the two order parameters ever coexist, something that should occur if the groundstate is a superposition of the symmetry broken groundstates. If we compare the ratio of the correlation order parameters, we find $\langle S_{A_i} S_{A_i} \rangle \,/\, \langle S_{A_i} S_{A_j} \rangle \approx 8$ for a system of $L = 8$. Such a large value suggests that these phases do not coexist, and rather that the system spontaneously fluctuates between each of them, existing in the transition phase for only a short period of time.

Although the DRS gauge is able to fluctuate between groundstate sectors, we have shown that the system primarily exists in one of the symmetry broken sectors at any given time. In this way we are convinced that although there is no excitations involving the addition of spin required to move from one state to another, there may be excitations in the hopping that are required to move between these different groundstates. The lower

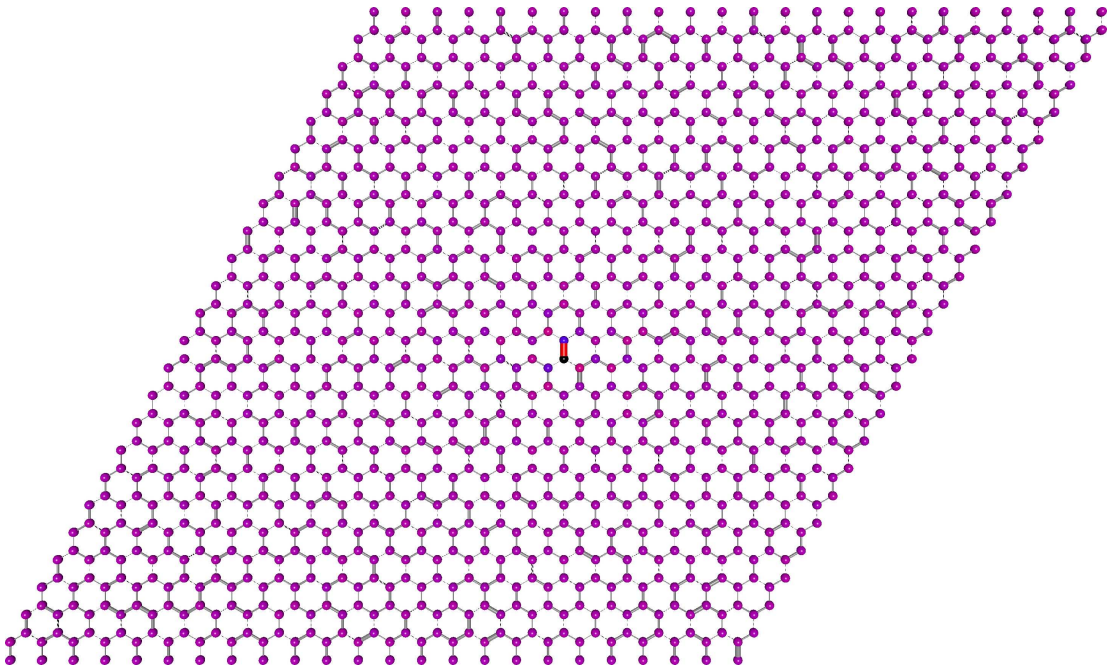

Figure 3.18: The real-space picture of the lattice generated using a slice of the spin-spin and bond-bond correlation functions over a very long simulation. The purple background of spins indicates that relative to the black spin, each spin spends equal time in the up and down configurations. What is not immediately clear is if this is due to random fluctuations or by accessing three different groundstates that when averaged have spin-spin correlations that are zero between every spin.

energy would allow the system to access all the sectors without changing magnetization, but would also explain why the system spends less time in that transition phase than in any of the ordered phases. If we assume that each of the ordered phases represent a possible groundstate of the system, then apart from the particular configuration (and possibly excitations), the system is very similar to the DTS gauge. That is, it is a crystalline system that has zero magnetic susceptibility.

3.4 Random gauge

The final system we studied was the case where we used a random configuration of frustration to fulfill the fully-frustrated requirement. Any sort of regular scheme of placing the bonds would likely result in a pattern that had a unit cell or would not fit using periodic boundary conditions. To overcome this problem, the original classical Monte Carlo code was used to randomly generate the locations where $A_{ij} = \pi$. If we imagine the set of possible groundstates of the classical Hamiltonian from Section 2.3, the only restriction is that one bond per hexagon be frustrated. We generate the random pattern of frustration by mapping the frustrated bonds from the final configuration of a classical Monte Carlo to the bonds where $A_{ij} = \pi$ for the quantum Monte Carlo. Since the classical system has no bias towards any particular configuration within the degenerate groundstate, the pattern of bonds in the quantum Monte Carlo should be equally random and without bias.

Although in theory each configuration generated is an entirely unique system with a cell the size of the full lattice, our simulations have shown that many random instances of the set of such models tend to have similar behavior. This would suggest that the ordered cases, or cases with a small unit cell, are the special cases. Therefore if the random gauge fails to develop any order it is reasonable to believe that if we had a very large system that lacked any long range order in the gauge choice, that it would behave similarly. That is to say if we averaged over all possible configurations of frustration, we would expect that any long range ordered cases would only lead to $1/N$ contributions to Bragg peak intensity, where N is the number of possible choices of the frustration. From the results of the classical fully-frustrated honeycomb Ising model the number of choices of frustration is, by mapping frustrated bonds to a choice of frustration, extensive in the number of spins. The systems with unit cells containing 4 and 8 spins, for the DTS and DRS gauges, respectively, ordered in patterns that could be represented using the same number of spins and an ordering wave vector. This is another way in which the random gauge can be viewed as a system where the unit cell is the size of the entire lattice.

As one might expect from examining a random system, there are an extensive number of such random configurations for any given system size. In initial studies we examined a small set of instances of the random gauge, but for each sample the average properties were

always very similar. This suggested to us that the qualities of the random gauge did not rely on examining the disorder average properties of the system, but rather that for a large enough system the properties of all system, except in rare cases, converged to the same set of properties. The rare cases where the properties are not similar can be thought of as the case where the instance of the random gauge gives a system that is ordered, as such cases are allowed by construction within the random gauge. In the case where there is order we have results showing that such systems behave differently, but such configurations are a small fraction of all possible random configurations, and so in the general case we should be able to ignore them when examining the disordered system as a whole.

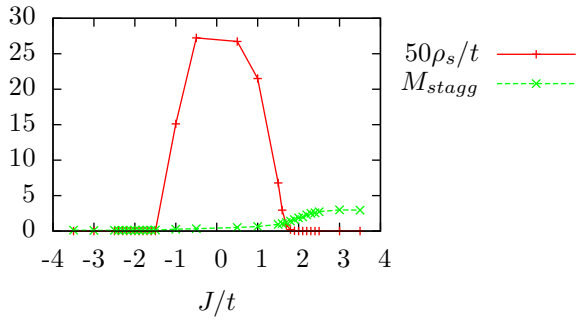

Figure 3.19: The spin stiffness for one realization of the the random gauge. In the random gauge the spin stiffness is forced to zero faster than in the either the DTS or DRS gauges. There is also a subtle staggered magnetization that turns on in the zero spin stiffness phase, but it does not scale with system size and is not consistent among different realizations.

As before, classifying the groundstate within these phases is the main objective of this work. Figure 3.19 shows that the system transitions from a system with non-zero spin stiffness by $|J/t| > 2$, similar to the previous two cases. Despite the random nature of this gauge, in the limiting cases of $|J/t| \to 0$ or $|J/t| \to \infty$ the random nature of the fully frustrating bonds does not change either groundstate. In the case of only classical interactions, the groundstate still maps to the classical fully-frustrated honeycomb lattice as long as we restrict ourselves to look at where the frustrated bonds occur and ignore specific spin configurations. The case of only quantum terms in the Hamiltonian the sign of the classical term is non-existent, and we have the XY-model which is classified by $\langle S^x \rangle \neq 0$.

As before, most of the simulation was done on a system of 24×24 unit cells containing 2 spins each. Initial results showed two very different behaviors depending on the sign of J. When $J < 0$ the system formed large domains of aligned spins that possibly formed boundaries around places where $A_{ij} = \pi$. When $J > 0$ the system was unable to order, and we were unable to find a typical order parameter to classify the phase.

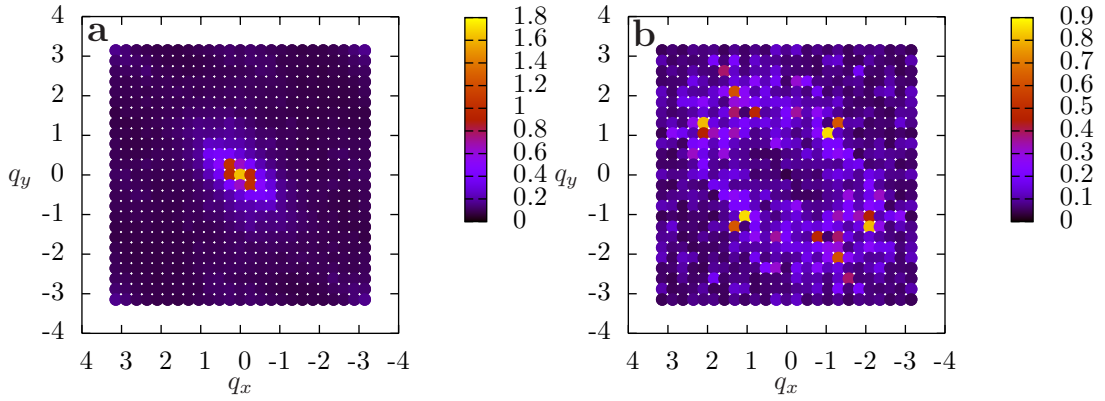

Figure 3.20: The Fourier transform of the spin-spin correlation functions. **(a)** shows the transform when $J > 0$ and has a smooth transform with a non-Bragg peak (one that does not scale with the number of spins) at $\mathbf{q} = (0, 0)$. **(b)** shows the transform when $J < 0$ that has a low intensity Fourier transform, indicating weak ordering. Different simulations show inconsistent behavior in the transform of **(b)**, aside from the low intensity.

Using the same analysis methods as before, we examined the sublattice structure factors of the system using the same parameters as the previous models. Figure 3.20 shows that when $J < 0$ the structure factor of the system is random and of a low intensity, suggesting a disordered state. When most of the interactions are antiferromagnetic there is a slight sublattice magnetization, but this does not scale with the number of spins in such a way to suggest an ordered phase in the thermodynamic limit. From these two pictures it is difficult to understand these states in a way that distinguishes them from high temperature disordered states or the states with off-diagonal order when J/t is small. As before, we look at the real-space pictures to see if they illuminate the nature of the groundstate at all.

This time the real-space show something qualitatively different than the other gauges, and perhaps lend insight to the structure factors found. When $J < 0$, the system appears as a disordered but well defined "solid". There are large regions of up and down spins with fluctuating spins occurring on the interface between each region. In some sense this is very similar to what we saw in the DTS gauge where bulk layers were formed with fluctuations strongly isolated to the region between layers. The major difference in this case is that regions of spins is not obvious in the random gauge case. We examined one instance of the random gauge, using a set of simulations all using different random seeds, to see if the cluster boundaries were defined by the instance of the random gauge or dynamic. Each simulation found the same or very similar clusters, but the particular spin orientation and relative spin orientation of each cluster was not consistent. This suggests a similar picture

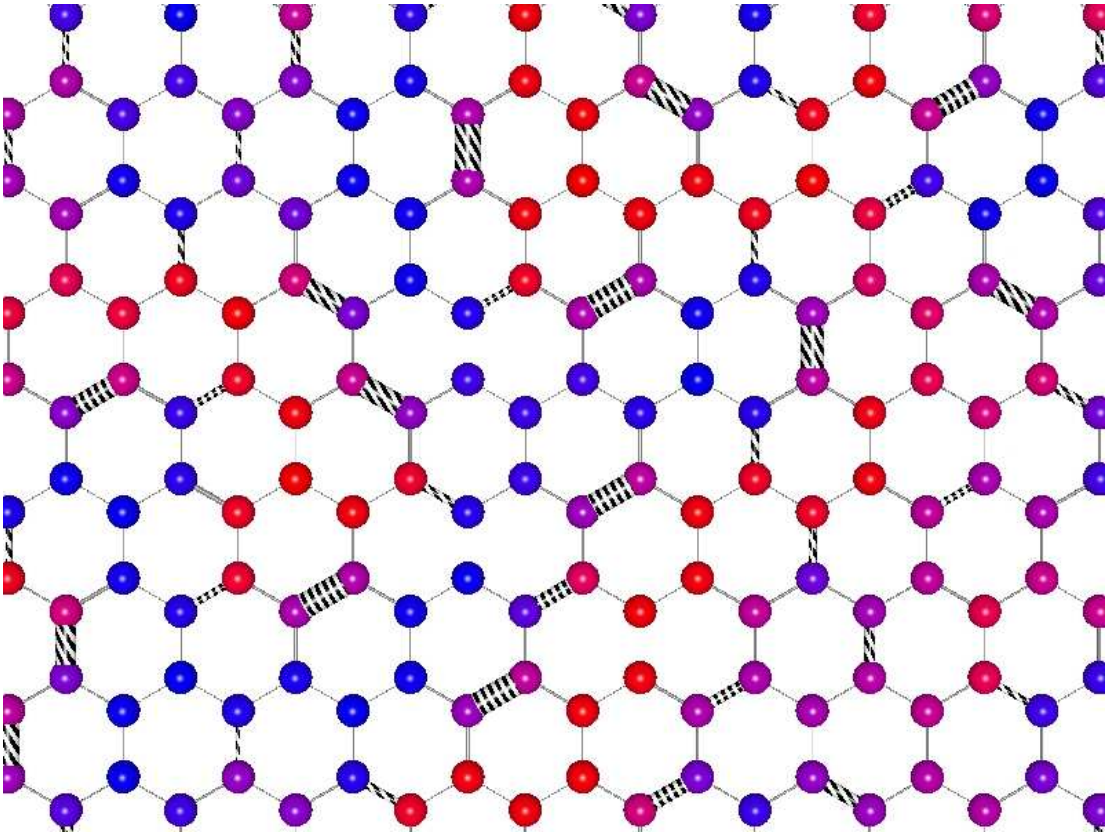

Figure 3.21: The real-space image of the random gauge when $J < 0$. The variables represented are in the image are $\langle S_i^z \rangle$ (color of the spins) and $\left\langle S_i^+ S_j^- + S_i^- S_j^+ \right\rangle$ (thickness of the bonds). The spins range from blue ($\langle S_i^z \rangle = -0.5$) to red ($\langle S_i^z \rangle = 0.5$) with purple representing a site that spends equal time up and down ($\langle S_i^z \rangle = 0$). All of the bond thicknesses are normalized such that the thickest bond's diameter is 80% the diameter of the spheres. Notice that the system appears as a disordered solid when $J < 0$.

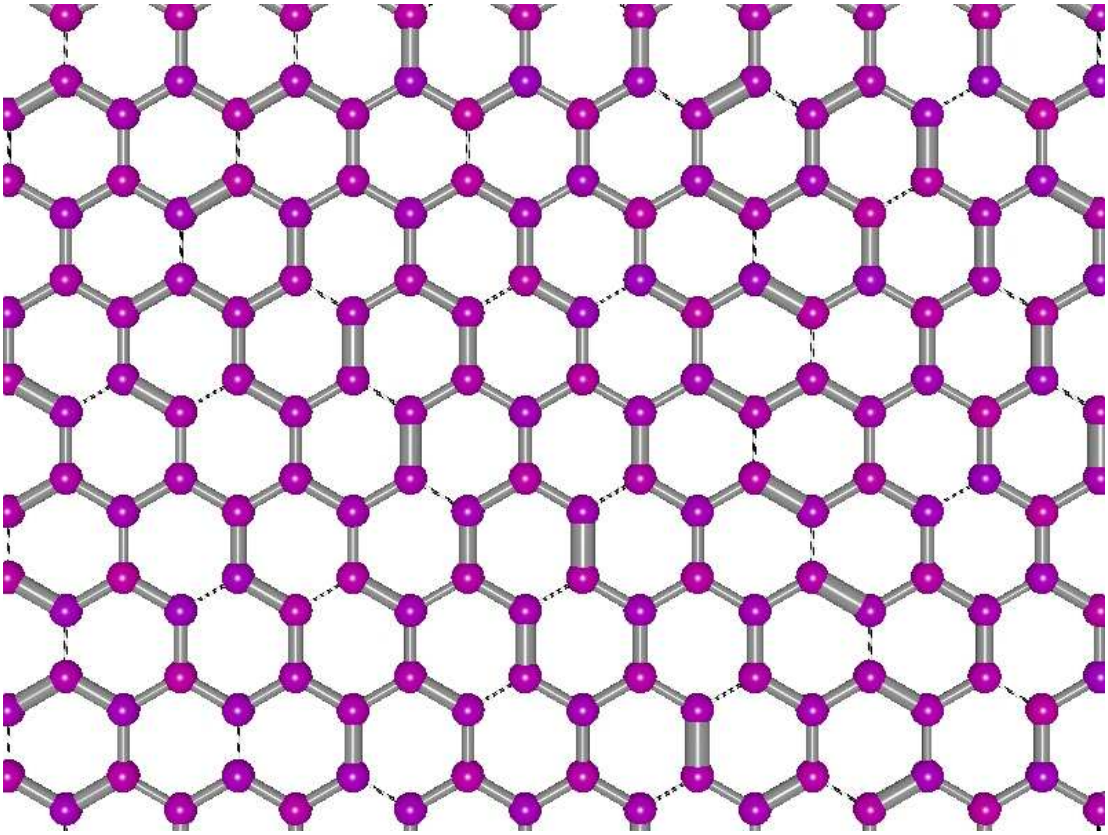

Figure 3.22: The real-space image of the random gauge when $J > 0$. The variables represented are in the image are $\langle S_i^z \rangle$ (color of the spins) and $\left\langle S_i^+ S_j^- + S_i^- S_j^+ \right\rangle$ (thickness of the bonds). The spins range from blue ($\langle S_i^z \rangle = -0.5$) to red ($\langle S_i^z \rangle = 0.5$) with purple representing a site that spends equal time up and down ($\langle S_i^z \rangle = 0$). All of the bond thicknesses are normalized such that the thickest bond's diameter is 80% the diameter of the spheres. Notice how $\langle S_i^z \rangle \approx 0 \quad \forall i$ when $J > 0$.

to the DTS gauge as mentioned earlier, although where in the non-random case it is easy to identify a defect, such distinctions are less clear in the random gauge without explicitly examining the energy. In the case where $J > 0$, we find a phase very different than the previous cases. When examining the expectation value of each spin, the system fluctuates in such a way that every spin tends to spend equal time up and down. Although such a pattern could occur if the system were fluctuating between only two spin-inverted states, such a situation would be resolved by examining the spin-spin correlation function.

If we define the matrix $SS_{ij} = \left\langle S_i^z S_j^z \right\rangle$ then the real-space image in Figure 3.23 is generated by using a slice of the matrix SS. This allows us the view the spin-spin correlation function directly on the lattice. If the system were fluctuation between the two spin-inverted states, or even had well defined clusters that stayed flipped with respect to one another, we would expect to see these clusters through the matrix SS. The only case in which we might not see them is in the case where the average over all symmetry breaking gives a matrix SS that is zero. Although it was not mentioned explicitly, this was the case in the DRS gauge case, which is why looking at the structure factors and their correlation is a better way to analyze that groundstate. In this case there is no reason for the different groundstates to have such a careful symmetry that would cause the average of the SS matrix over all groundstates to be zero. For that reason the matrix elements of SS for spins separated by a large distance being close to zero suggests that the groundstate itself is only correlated on the short length scale.

The random gauge also differs in the uniform magnetic susceptibility. Figure 3.24 shows the magnetic susceptibility for the random gauge when $J > 0$. Notice the smooth transition and tail that eventually goes to zero. Such a transition (as opposed to a sharp transition) suggests that a large range of energy scales exist rather than a small set as in the cases with well ordered groundstates. The main reason for examining these properties of the system were to determine if the groundstate were glass like or liquid like. In the case of $J < 0$ we are fairly certain the groundstate is a disordered solid—fluctuations are limited to the boundary between domains and each domain has a high energy to flip similar to the groundstate of DTS. We might expect that $J > 0$ gives us a state similar to the $J > 0$ case of DTS as well, but in that case the symmetry of bonds where $A_{ij} = \pi$ is such that there is a particular classical configuration one can perturb around to minimize the energy in each cell while satisfying the boundary conditions with the neighboring cell. When there is no well defined unit cell, there are many local configurations that might allow the most hopping, but any choice will necessarily frustrate the allowed fluctuations of the neighbors, and it will affect each neighbor in a different way depending on the orientation bonds where $A_{ij} = \pi$. If the energy cost to move between different classical configurations were high, we would expect a random disordered groundstate for different random seeds of the Monte Carlo simulation. If the energy cost were low between the different states, we open the possibility for the groundstate to explore the entire constrained manifold of states and find

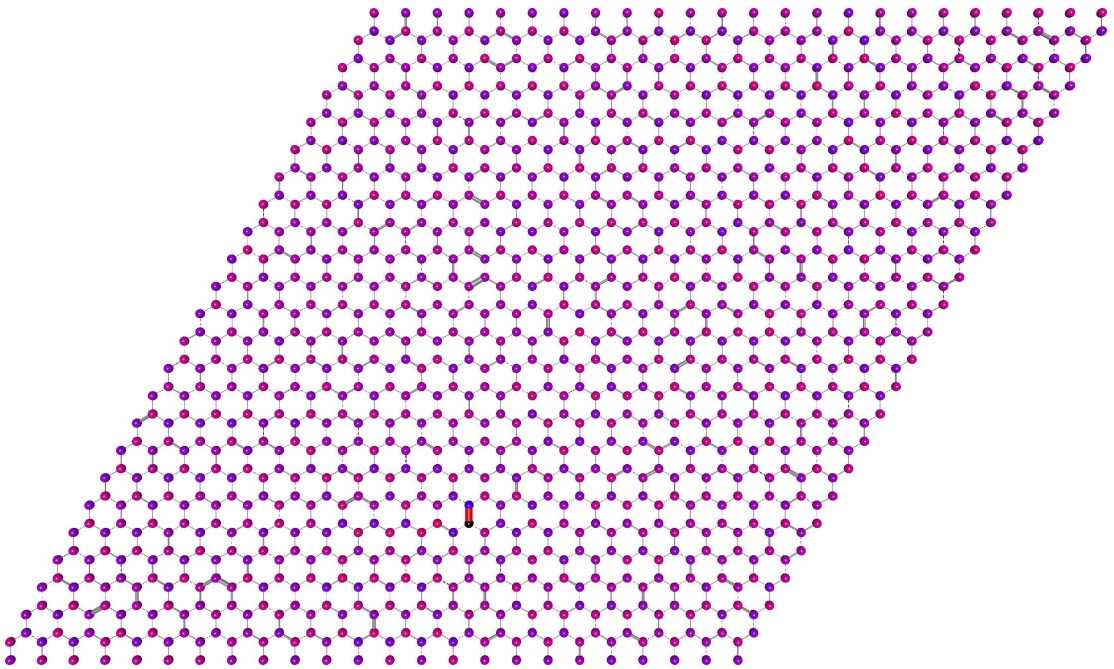

Figure 3.23: The real-space lattice of the random gauge, generated using the spin-spin correlation function ($\langle S_a^z S_i^z \rangle$) and the bond-bond correlation function ($\left\langle (S_{a_1}^+ S_{a_2}^- + S_{a_1}^- S_{a_2}^+)(S_i^+ S_j^- + S_i^- S_j^+) \right\rangle$) , with the black spin and red bond as the reference. Notice that most spins remain purple except for one of the spins directly neighboring the black spin. From this and the previous figure, we see that not only does every spin fluctuate, but it fluctuates with respect to every other spin up to short range correlations. The bond statistics are noisy as its takes much longer simulations to generate good statistics on the bond-bond correlation function.

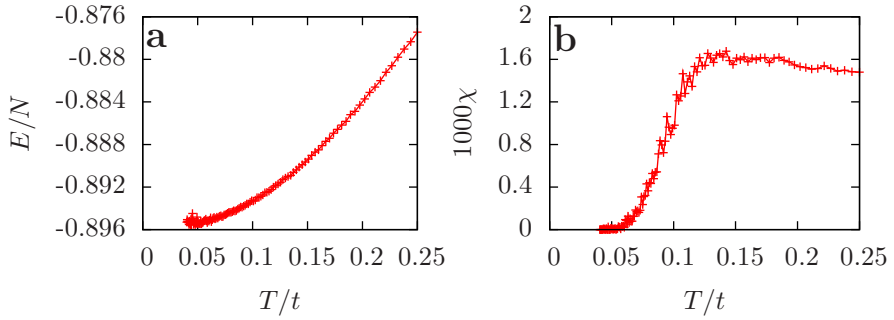

Figure 3.24: The low temperature thermodynamic properties of the random gauge. The **(a)** $J > 0$ energy levels off and the **b** magnetic susceptibility drops to zero by $T/t \approx 0.05$, lower than the temperature for the DTS gauge and the DRS gauge by a factor of 2. The magnetic susceptibility drops off much more smoothly in this case, as unlike the cases with small unit cells, there are many energy scales for the insertion of a single spin. This also sets the energy scale for simulations, since the Hamiltonian commutes with total magnetization, it must be fixed for any state at the very least.

the state that maximizes hopping.

In the classical fully-frustrated honeycomb Ising model we describe the groundstate as an extensively degenerate manifold, but one could equally define such a manifold as a liquid like state. By liquid we mean that although the system lacks in long range correlations, it is not entirely paramagnetic like a gaseous state, but rather only has correlations corresponding in this case to the minimum energy constraint. In light of recent interest in the quantum version of such liquid states [1], we attempted to examine properties of this state to see in what aspects it satisfied or did not satisfy the qualities of a quantum spin liquid state. The difficulty with Stochastic Series Expansion quantum Monte Carlo is that it samples from the thermal ensemble and is limited in the types of observables that one is able to measure.

A quantum spin liquid is fairly well defined as a state, but even experimentally there is great difficulty in determining a definitive measure that would quantify a state as one of the quantum spin liquids. The one quality that all quantum spin liquids (and classical spin liquids) have in common is that in the ideal models, they do not order at zero temperature. This is already something which tends to be uncommon in most materials, as even in frustrated systems it is possible that the extensively degenerate groundstates may be unstable to small perturbations which exist in a more complete treatment of a system. In addition to the extensive degeneracy, theoretical work [1] suggests that a quantum spin liquid should have exotic excitations. One such excitation all quantum spin liquids should have is a spinon like excitation, most well known in the 1D Heisenberg model where such

excitations occur at the boundaries of a defect. In 1D such the region between the defects, sometimes called a string, is tensionless, which is another way of saying that the energy cost of the intermediate region is independent of its length. If we took the groundstate of a triangular lattice antiferromagnet in 2D, we would find that similar excitation to the 1D case do still exist, but now the "string" has an energy cost proportional to its length. If the groundstate were some quantum superposition of singlets instead of some classical configuration, then it would be possible for the string to be tensionless, as moving the ends of the string around would simply cause a rearrangement of the singlets. Beyond this case there are also more exotic properties that some quantum spin liquids may have, such as the presence of vison excitations [34].

In the end the only qualities of the random gauge that we can say for certain is that it is spin liquid with quantum fluctuations, but if this falls under the strict definition of a quantum spin liquid as defined in [1] is less clear. If it is a quantum spin liquid, it is unclear if the two-spin excitation corresponds to the low energy excitations that quantum spin liquids are required to have. Considering the model can be cast in a way that lacks the sign problem, it may be worth continued study in examining the further character of the system to quantify all the qualities of the state. The only remaining difficulty would be if there was need to do sampling over realizations of the random gauge, which would increase the complexity and run time of any further simulation work.

3.5 Two spin excitations

In an attempt to understand the low energy physics of the system, we added an uniform external field to the system to promote excitations where the magnetization is not zero. From a classical perspective, the smallest excitation that can exist is one where a single spin is flipped on a site connected to one frustrated bond. This creates two frustrated bonds and raises the energy by J. The classical Hamiltonian also allows moves that involve flipping two spins that do not cost classical energy. Since none of the elements in the quantum Hamiltonian change the total number of up or down spins, the total magnetization of the system is a good quantum number. Taken together, this means that different magnetizations correspond to eigenstates of the quantum Hamiltonian that may have different expectations of the hopping term over the lattice. In the limit of $t << J$ this means that states with magnetization $+2$ (as in two spin-$\frac{1}{2}$ spins flipped) greater than the ground state correspond to low energy excitations.

In the Hamiltonian, there are only terms that swap two neighboring spins of opposite orientation, meaning that the total magnetization within the groundstate is conserved. This means that within a particular list of operator S_M and the associated layers, $|\alpha_0\rangle, |\alpha_1\rangle, \ldots, |\alpha_M\rangle$, in the SSE representation, all of them have the same total magnetiza-

tion. To change the total magnetization requires the off-diagonal update using the directed loop algorithm. Since there is no off-diagonal operator that takes two down spins to two up spins, or vice-versa, the winding of the loop update can only change one spin per wind around through the operator list. In this way, to change the total spin of the system by two requires passing through the configuration with one extra spin during the update.

If we recall the fully-frustrated honeycomb Ising model in the classical limit, then one can imagine that flipping any single spin from the groundstate will either cost $3J$ or J energy compared to the groundstate. This is because in the groundstate, every spin is connected to 3 other spins but at most one of the connections is frustrated, meaning that 2 or 3 bonds will be classically frustrated in the new configuration. Despite this fact, there are moves that involve flipping two spins that preserve the classical energy. Such move must represent a new state, as the total magnetization is a good quantum number for the XXZ Hamiltonian. An example of such a move is shown in Figure 3.25, that shows the addition of two spins while keeping the total number of frustrated bonds unchanged, while both the left and right states are valid configurations in part of a larger classically allowed groundstate.

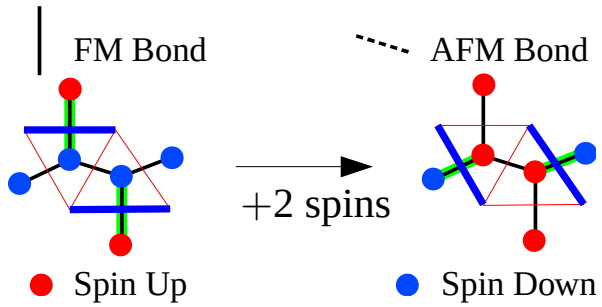

Figure 3.25: A move that does not exist in the Hamiltonian that takes us from one classically allowed state to another by two spin flips. In the simulation to get from the left configuration to the right configuration requires passing through an intermediate configuration where there is one more spin than the left configuration. This intermediate state costs energy on the scale of J, and hence is a large energy barrier between two states that have the same classical cost. It should be noted that the above move requires the presence of a bond that prefers the spins to be ferromagnetically aligned to proceed, while the bonds connected to the ferromagnetic bond can be of any type.

This strange double spin insertion was found by examining the effect of quenching in the presence of a weak field. If we binned the magnetization, we often found large bins for zero magnetization and +2 magnetization aligned with the field. The +1 magnetization bins were always very small, and if we examined the time evolution we found that the

system transitioned from zero to +1, stayed in the +1 sector for a few steps, then jumped to the +2 sector and was fixed in that sector. This is precisely the behavior we would expect if the +1 magnetization sector were an energy barrier that the system was passing through between two low lying energy states. The field was necessary to bring the +1 and +2 magnetization sectors closer to the groundstate in energy, and bias the system to transition to those states in fewer Monte Carlo steps so we could examine the behavior of the system away from zero magnetization.

Chapter 4

Conclusions

Through this work on the quantum fully-frustrated honeycomb model we have explored the effect of quantum fluctuations on a classically disordered system. As was somewhat expected, the quantum terms in the Hamiltonian cause the system to be sensitive to how the fully-frustrated requirement is satisfied. Since the number of possible ways to arrange the frustration on a large lattice is extensive, we started by using simple patterns that could be easily tiled to arbitrary sizes. For each model, the simplest quantities to measure were those involving the spins or the expectation of hopping, or higher order correlations of these operators. Using these two measures and the fact that all the phases of interest lack spin stiffness, we can coarsely classify each of the phases based on these two measures.

The simplest quality to check in each system is if the structure factor of the spin-spin correlation function has Bragg peaks signifying long range order, or not. In this case we would classify the resulting system as a (spin) crystal. Any peaks in the sublattice structure factor indicates the system breaks symmetry in a way that persists over the simulation. If we consider the normal definition of a crystal as an object which breaks continuous symmetry then in a lattice system where the variable on the sites breaks the symmetry of the lattice, we would call this a crystal. In this sense we describe the system as a fixed choice of one of the available symmetry broken groundstates, and in such a state an extensive number of the spins contribute to the "solidness" of the system. This diagonal long range order does not deny other properties such as the existence of spin stiffness in the supersolid or superglass phases [35], but it qualifies one aspect of the phase.

Still examining the spins, we can look at the low temperature uniform magnetic susceptibility of the system. At low temperature we expect the magnetic susceptibility to go to zero if the system is gapped to single spin flips at low temperature. If the magnetic susceptibility converges to a constant value this implies that the system is gapless to single spin excitations. Gapless spin excitations imply that an infinitesimal field will polarize the system, giving rise to a bulk magnetization. Being gapped to spin excitations at low

temperature is associated with the system being difficult to perturb, as a small potential applied to the system does not cause it to change significantly. When a system has zero magnetic susceptibility away from a fully polarized state, this may be due to the system being in a "spin crystal", or a regular modulation of spin arrangement on the lattice.

We then chose to examine the expectation of the hopping, or $\left(S_i^+ S_j^- + S_i^- S_j^+\right)$, also called the expectation of the "kinetic energy". This quantity has no classical analogue, but we examined it in the same way as the S^z component of the spins. If we look at the sublattice structure factor of the hopping, peaks that scale with the system size again correspond to long range order. Long range order in valence bonds would be referred to as a valence bond crystal, while we can similarly designate a disordered solid phase if we have a fixed bond distribution that lacks long range order. Since the expectation of the hopping can only be positive, a liquid like phase would have the quality of a uniform and featureless distribution. As was shown earlier, the hopping relates to either the singlet or the maximally entangled triplet. Although the exact relation also depends on the spin-spin correlation function, the weight of the singlet (or entangled triplet) increases linearly with expectation of hopping.

The first such model used the same frustration choice that was used during a recent classical study of the fully-frustrated honeycomb lattice Ising model [12, 36]. This choice of the variables A_{ij} was referred to here as the DTS gauge, and lead to a groundstate we understand as a perturbation from a particular classical groundstate. For either sign of J, we find that the system forms a crystal in both the spins and the bonds. The spin order is a perturbed antiferromagnet when $J > 0$ and forms ferromagnetic strips when $J < 0$. In both cases a layer of strong bonds forms that is isotropic in nature and has a short range repulsive interaction, something that we can understand through perturbation theory. As temperature is decreased the system becomes gapped to spin excitations and is unable to fluctuate between its different symmetry broken sectors without fluctuating total spin. The combination of all these qualities lead us to describe the system as a crystal, both when viewed from the point of view of the spins and the bonds. In addition to be a crystal it is has zero magnetic susceptibility at low temperature. The quantum fluctuations can be seen as ordering what was a classically disordered phase, and the ordering is to a dominantly solid phase that maximizes local fluctuations that themselves only act locally.

In the DRS gauge we again find similar properties for both signs of J. When $J > 0$ we again realize a pattern that looks somewhat like a honeycomb antiferromagnet, but the pattern never realizes a sublattice magnetization. This is realized through regular defects in the global antiferromagnetic pattern that disallow the possibility for sublattice magnetization. Ever without the sublattice magnetization, this system still realizes a structure factor in both the spins and the bonds. The local fluctuations are different than in the previous case, as the strongly fluctuating bonds spend equal time in each of the two possible configurations and the strongly fluctuating bonds are twice as far apart than

the first case. Similar to the DTS gauge, single spin excitations are frozen out at low temperature, and the spin susceptibility reduces to zero. When $J < 0$ the model freezes into a particular groundstate sector and is unable to fluctuate to the other groundstates. When $J > 0$ the system chooses a particular groundstate, but in long simulations it is found that it is able to sample the different groundstates while staying at zero magnetization. To ensure that the true groundstate is not some overlap of these various groundstates, we examined the order parameters for each and compared the self correlation and cross correlation of these parameters over the simulation. By examining these, we find that only one parameter is ever active at a time, implying that although transitions occur from one state to another, the simulation never exhibits coexistence of the different groundstates. This leads us to classify the groundstate as any of the symmetry broken states, and again as a crystal phase with fluctuations that remain local.

The random gauge is the first to have very different behavior depending on the sign of J. When $J < 0$, the system was shown to form a set of domains, each containing either up or down spins. Since it was possible that the choice of domains might not be unique, we quenched the system at low temperature using different random seeds and found that the shape of the domain was consistent, but the orientation of spins within each domain was not. In this way the conceptual picture for this model should be that it is similar to the DTS gauge when $J < 0$. Here there may be a true groundstate configuration, up to spin inversion, but unlike the DTS gauge the cost of a defect, either choosing the domains incorrectly or choosing the relative orientation of domains incorrectly, is likely to be different for each particular defect. Like all other systems, the spin susceptibility vanishes at low temperature.

When the random gauge is simulated with $J > 0$, we get a system that seems to exhibit physics very different in nature to the essentially solid states that we have seen previously. Snapshots of the system show configurations that appear predominantly antiferromagnetic—this makes sense as we expect to be within the classical manifold where there is only on frustrated bond per hexagon, and 5 of 6 of the bonds on each hexagon prefer spins to anti-align. As the temperature is decreased we find that the spin susceptibility reduces to zero, although at a lower temperature than in either of the cases with a well defined unit cell. If we examine the expectation of the single spin density at each site, $\langle S_i^z \rangle$, we find that this expectation value converges to zero as the simulation is allowed to continue to run. Convergence takes longer at lower temperatures, but it does continue to occur down to the lowest temperatures we were able to simulate. The structure factor of the spin-spin correlation function is also flat, indicating no long range order. Examining the real space version of the spin-spin correlation function, we find that although there are nearest neighbor antiferromagnetic or ferromagnetic correlations depending on the type of bond present, these correlations do not persist beyond one or two sites, and quickly decay to that of being uncorrelated. If we look at the bond distribution, $\left\langle S_i^+ S_j^- + S_i^- S_j^+ \right\rangle$, we find that

the behavior is somewhat disordered at lower temperatures. By disordered we mean that there is a spatial distribution to the hopping that does not converge to isotropic hopping with an increasing number of Monte Carlo steps. Taking all of these qualities together the system seems to be a liquid when examining the spins, although we cannot yet comment on the quantum or classical nature of this liquid, while also exhibiting disordered solid behavior in the bonds.

Within the framework of Stochastic Series Expansion we were able to explore large enough systems with enough detail to reveal the basic nature of this previously unstudied family of lattices. In the simple cases, the results show two consistent aspects—collapse of the extensive degeneracy to a crystalline state with local fluctuations. In the one case which is not entirely resolved, the random gauge with $J > 0$, we have shows the results of the fundamental variables. Fully understanding and qualifying this state may require examining more complicated measures of the state, may require examining the excitations from this state or may required simulations over many realizations of disorder, all of which SSE is not well suited. The required properties of quantum spin liquid ground states, as discussed in [1], are:

- no order in the spins, and
- deconfined spinon excitations.

There are other properties that quantum spin liquids might have, but here are the only universal ones. In our random gauge we have found that we indeed have no order in the spins for every instance of the random gauge studied. We however were unable to confirm or deny the nature of magnetic excitations, as the costs an energy $\Delta E = J$ which is quite large, and SSE QMC is not well suited to studying such excited states. We made several attempts to analyze these aspects of the excited states using an external magnetic field to attempt to promote states with magnetization, but after some analysis we found the lowest spin excitations (in all gauges) were two spin excitations, which would necessarily be different eigenstates, as total magnetization commutes with the Hamiltonian. Further work, guided by certain properties of classical or quantum spin liquids, might shed light on other characters of this state. Different numerical methods might allow measurement of different observables, and with such measurements it might be easier to discern the true nature of the random gauge, and whether it is simply an novel type of featureless spin system with zero magnetic susceptibility, a class of quantum spin liquid, or something else.

Bibliography

[1] L. Balents. Spin liquids in frustrated magnets. *Nature*, 464(7286):199–208, 2010. 1, 2, 3, 26, 71, 72, 78

[2] Patrick A Lee. From high temperature superconductivity to quantum spin liquid: progress in strong correlation physics. *Reports on Progress in Physics*, 71(1):012501, 2008. 1

[3] T. Itou, A. Oyamada, S. Maegawa, and R. Kato. Instability of a quantum spin liquid in an organic triangular-lattice antiferromagnet. *Nat Phys*, 6(9):673–676, 09 2010. 1

[4] R. Moessner and S. L. Sondhi. Ising models of quantum frustration. *Phys. Rev. B*, 63(22):224401, May 2001. 1, 36, 37

[5] R. Moessner and S. L. Sondhi. Resonating valence bond phase in the triangular lattice quantum dimer model. *Phys. Rev. Lett.*, 86(9):1881–1884, Feb 2001. 2

[6] B. Hayes. The world in a spin. *American Scientist*, 88(5):384–389, 2000. 4

[7] E. Ising. Beitrag zur theorie des ferromagnetismus. *Zeitschrift für Physik A Hadrons and Nuclei*, 31(1):253–258, 1925. 4, 29

[8] N. D. Mermin and H. Wagner. Absence of ferromagnetism or antiferromagnetism in one- or two-dimensional isotropic Heisenberg models. *Phys. Rev. Lett.*, 17(22):1133–1136, Nov 1966. 5

[9] W. K. Hastings. Monte Carlo sampling methods using Markov chains and their applications. *Biometrika*, 57(1):97–109, 1970. 6

[10] Ulli Wolff. Collective Monte Carlo updating for spin systems. *Phys. Rev. Lett.*, 62(4):361–364, Jan 1989. 8

[11] Robert H. Swendsen and Jian-Sheng Wang. Nonuniversal critical dynamics in monte carlo simulations. *Phys. Rev. Lett.*, 58(2):86–88, Jan 1987. 8

[12] Shawn Andrews, Hans De Sterck, Stephen Inglis, and Roger G. Melko. Monte Carlo study of degenerate ground states and residual entropy in a frustrated honeycomb lattice Ising model. *Phys. Rev. E*, 79(4):041127, Apr 2009. 8, 37, 39, 40, 41, 42, 76

[13] David Griffiths. *Introduction to Quantum Mechanics*. 2nd edition edition, 2005. 8

[14] Olav F. Syljuåsen and Anders W. Sandvik. Quantum Monte Carlo with directed loops. *Phys. Rev. E*, 66(4):046701, Oct 2002. 9, 12

[15] Anders W. Sandvik. Stochastic series expansion method for quantum Ising models with arbitrary interactions. *Phys. Rev. E*, 68(5):056701, Nov 2003. 9, 46

[16] Anders W. Sandvik. Stochastic series expansion method with operator-loop update. *Phys. Rev. B*, 59(22):R14157–R14160, Jun 1999. 9, 10, 46

[17] Lars Onsager. Crystal statistics. i. a two-dimensional model with an order-disorder transition. *Phys. Rev.*, 65(3-4):117–149, Feb 1944. 29

[18] R. K. Pathria. *Statistical mechanics / R.K. Pathria*. Butterworth-Heinemann, Oxford ; Boston :, 2nd ed. edition, 1996. 29

[19] Assa Auerbach. *Interacting Electrons and Quantum Magnetism*. Springer-Verlag, 1994. 30, 32

[20] Hidetoshi Nishimori. Internal energy, specific heat and correlation function of the bond-random Ising model. *Progress of Theoretical Physics*, 66(4):1169–1181, 1981. 34

[21] Clifford G. Shull. Early development of neutron scattering. *Rev. Mod. Phys.*, 67(4):753–757, Oct 1995. 36

[22] R. G. Melko, A. Paramekanti, A. A. Burkov, A. Vishwanath, D. N. Sheng, and L. Balents. Supersolid order from disorder: Hard-core bosons on the triangular lattice. *Phys. Rev. Lett.*, 95(12):127207, Sep 2005. 36, 37

[23] S. V. Isakov, S. Wessel, R. G. Melko, K. Sengupta, and Yong Baek Kim. Hard-core bosons on the kagome lattice: Valence-bond solids and their quantum melting. *Phys. Rev. Lett.*, 97(14):147202, Oct 2006. 36

[24] P. Fendley, R. Moessner, and S. L. Sondhi. Classical dimers on the triangular lattice. *Phys. Rev. B*, 66(21):214513, Dec 2002. 42

[25] Anders W. Sandvik and Chris J. Hamer. Ground-state parameters, finite-size scaling, and low-temperature properties of the two-dimensional $s = 12$ xy model. *Phys. Rev. B*, 60(9):6588–6593, Sep 1999. 44, 46

[26] C. Lanczos. An iteration method for the solution of the eigenvalue problem of linear differential and integral operators. *J. Res. Nat. Bur. Standards*, 45(4):255–282, 1950. 44, 45

[27] J.K. Cullum and R.A. Willoughby. *Lanczos Algorithms for Large Symmetric Eigenvalue Computations*. Society for Industrial Mathematics, 2002. 44

[28] Y. Saad. *Numerical methods for large eigenvalue problems*. Algorithms and architectures for advanced scientific computing. 1992. 44, 45

[29] Anders Sandvik. Lecture notes for quantum spin simulations. http://physics.bu.edu/ sandvik/perimeter/index.html, 2010. 45

[30] P. M. Chaikin and T. C. Lubensky. *Principles of Condensed Matter Physics*. Cambridge University Press, 1st edition, October 2000. 48

[31] R. G. Melko, A. W. Sandvik, and D. J. Scalapino. Aspect-ratio dependence of the spin stiffness of a two-dimensional *xy* model. *Phys. Rev. B*, 69(1):014509, Jan 2004. 52

[32] E. L. Pollock and D. M. Ceperley. Path-integral computation of superfluid densities. *Phys. Rev. B*, 36(16):8343–8352, Dec 1987. 52

[33] Y. Chen and J. Ye. Quantum phases, Supersolids and quantum phase transitions of interacting bosons in frustrated lattices. *ArXiv Condensed Matter e-prints*, November 2006. 53

[34] T. Senthil and Matthew P. A. Fisher. Fractionalization in the cuprates: Detecting the topological order. *Phys. Rev. Lett.*, 86(2):292–295, Jan 2001. 72

[35] Ka-Ming Tam, Scott Geraedts, Stephen Inglis, Michel J. P. Gingras, and Roger G. Melko. Superglass phase of interacting bosons. *Phys. Rev. Lett.*, 104(21):215301, May 2010. 75

[36] R. Moessner, S. L. Sondhi, and P. Chandra. Two-dimensional periodic frustrated Ising models in a transverse field. *Phys. Rev. Lett.*, 84(19):4457–4460, May 2000. 76